Measurement of the distributions of event-by-event flow harmonics in lead-lead collisions at $\sqrt{s_{NN}} = 2.76$ TeV with the ATLAS detector at the LHC

The ATLAS collaboration

E-mail: atlas.publications@cern.ch

ABSTRACT: The distributions of event-by-event harmonic flow coefficients v_n for $n = 2$–4 are measured in $\sqrt{s_{NN}} = 2.76$ TeV Pb+Pb collisions using the ATLAS detector at the LHC. The measurements are performed using charged particles with transverse momentum $p_T > 0.5$ GeV and in the pseudorapidity range $|\eta| < 2.5$ in a dataset of approximately $7\,\mu b^{-1}$ recorded in 2010. The shapes of the v_n distributions suggest that the associated flow vectors are described by a two-dimensional Gaussian function in central collisions for v_2 and over most of the measured centrality range for v_3 and v_4. Significant deviations from this function are observed for v_2 in mid-central and peripheral collisions, and a small deviation is observed for v_3 in mid-central collisions. In order to be sensitive to these deviations, it is shown that the commonly used multi-particle cumulants, involving four particles or more, need to be measured with a precision better than a few percent. The v_n distributions are also measured independently for charged particles with $0.5 < p_T < 1$ GeV and $p_T > 1$ GeV. When these distributions are rescaled to the same mean values, the adjusted shapes are found to be nearly the same for these two p_T ranges. The v_n distributions are compared with the eccentricity distributions from two models for the initial collision geometry: a Glauber model and a model that includes corrections to the initial geometry due to gluon saturation effects. Both models fail to describe the experimental data consistently over most of the measured centrality range.

KEYWORDS: Heavy-ion collision, harmonic flow, event-by-event fluctuation, unfolding, Hadron-Hadron Scattering

Contents

1 Introduction

Heavy ion collisions at the Relativistic Heavy Ion Collider (RHIC) and the Large Hadron Collider (LHC) create hot, dense matter that is thought to be composed of strongly interacting quarks and gluons. A useful tool to study the properties of this matter is the azimuthal anisotropy of particle emission in the transverse plane [1, 2]. This anisotropy has been interpreted as a result of pressure-driven anisotropic expansion (referred to as "flow") of the created matter, and is described by a Fourier expansion of the particle distribution in azimuthal angle ϕ, around the beam direction:

$$\frac{\mathrm{d}N}{\mathrm{d}\phi} \propto 1 + 2\sum_{n=1}^{\infty} v_n \cos n(\phi - \Phi_n) , \qquad (1.1)$$

where v_n and Φ_n represent the magnitude and phase of the nth-order anisotropy of a given event in the momentum space. These quantities can also be conveniently represented by the per-particle "flow vector" [2]: $\vec{v}_n = (v_n \cos n\Phi_n, v_n \sin n\Phi_n)$. The angles Φ_n are commonly referred to as the event plane (EP) angles.

In typical non-central [2] heavy ion collisions, the large and dominating v_2 coefficient is associated mainly with the "elliptic" shape of the nuclear overlap. However, v_2 in

central (head-on) collisions and the other v_n coefficients in general are related to various shape components of the initial state arising from fluctuations of the nucleon positions in the overlap region [3]. The amplitudes of these shape components, characterized by eccentricities ϵ_n, can be estimated via a simple Glauber model from the transverse positions (r, ϕ) of the participating nucleons relative to their centre of mass [4, 5]:

$$\epsilon_n = \frac{\sqrt{\langle r^n \cos n\phi \rangle^2 + \langle r^n \sin n\phi \rangle^2}}{\langle r^n \rangle} \ . \tag{1.2}$$

The large pressure gradients and ensuing hydrodynamic evolution can convert these shape components into v_n coefficients in momentum space. Calculations based on viscous hydrodynamics suggest that v_n scales nearly linearly with ϵ_n, for $n < 4$ [6]. The proportionality constant is found to be sensitive to properties of the matter such as the equation of state and the ratio of shear viscosity to entropy density [7, 8]. In particular, the proportionality constant is predicted to decrease quickly with increasing shear viscosity [9]. Hence detailed measurements of v_n coefficients and comparisons with ϵ_n may shed light on the collision geometry of the initial state and transport properties of the created matter [10, 11].

Significant v_n coefficients have been observed for $n \leq 6$ at RHIC and the LHC [12–18]. These observations are consistent with small values for the ratio of shear viscosity to entropy density, and the existence of sizable fluctuations in the initial state. Most of these measurements estimate v_n from the distribution of particles relative to the event plane, accumulated over many events. This event-averaged v_n mainly reflects the hydrodynamic response of the created matter to the average collision geometry in the initial state. More information, however, can be obtained by measuring $\vec{v}_n$ or v_n on an event-by-event (EbyE) basis.

Some properties of the v_n distributions, such as the mean $\langle v_n \rangle$, the standard deviation (hereafter referred to as "width") σ_{v_n}, the relative fluctuation $\sigma_{v_n}/\langle v_n \rangle$, and the root-mean-square $\sqrt{\langle v_n^2 \rangle} \equiv \sqrt{\langle v_n \rangle^2 + \sigma_{v_n}^2}$, were previously estimated from a Monte Carlo template fit method [19], or two- and four-particle cumulant methods [20–22]. The value of $\sigma_{v_2}/\langle v_2 \rangle$ was measured to be 0.3–0.7 in different centrality bins. However, these methods are reliable only for $\sigma_{v_n} \ll \langle v_n \rangle$, and are subject to significant systematic uncertainties. In contrast, $\langle v_n \rangle$, σ_{v_n} and higher-order moments can be calculated directly from the full v_n distributions.

The EbyE distributions of $\vec{v}_n$ or v_n also provide direct insight into the fluctuations in the initial geometry [23]. If fluctuations of $\vec{v}_n$ relative to the underlying flow vector associated with the average geometry, $\vec{v}_n^{\mathrm{RP}}$, in the reaction plane[1] (RP) [23, 24] are described by a two-dimensional (2D) Gaussian function in the transverse plane, then the probability density of $\vec{v}_n$ can be expressed as:

$$p(\vec{v}_n) = \frac{1}{2\pi\delta_{v_n}^2} e^{-\left(\vec{v}_n - \vec{v}_n^{\mathrm{RP}}\right)^2 / \left(2\delta_{v_n}^2\right)} \ . \tag{1.3}$$

Model calculations show that this approximation works well for central and mid-central collisions [23, 25]. Integration of this 2D Gaussian over the azimuthal angle gives the

---

[1]The reaction plane is defined by the impact parameter vector and the beam axis.

one-dimensional (1D) probability density of $v_n = |\vec{v}_n|$ in the form of the Bessel-Gaussian function [7, 26]:

$$p(v_n) = \frac{v_n}{\delta^2_{v_n}} e^{-\frac{(v_n)^2 + (v_n^{\mathrm{RP}})^2}{2\delta^2_{v_n}}} I_0\left(\frac{v_n^{\mathrm{RP}} v_n}{\delta^2_{v_n}}\right) , \qquad (1.4)$$

where I_0 is the modified Bessel function of the first kind. Additional smearing to eq. (1.3) also arises from effects of the finite number of particles produced in the collision. If it is Gaussian, this smearing is expected to increase the observed δ_{v_n} value, but the value of v_n^{RP} should be stable.

The parameters v_n^{RP} and δ_{v_n} in eq. (1.4) are related to $\langle v_n \rangle$ and σ_{v_n}, and can be estimated directly from a fit of the measured $p(v_n)$ distribution with eq. (1.4). For small fluctuations $\delta_{v_n} \ll v_n^{\mathrm{RP}}$ [23]:

$$\delta_{v_n} \approx \sigma_{v_n}, \quad \left(v_n^{\mathrm{RP}}\right)^2 \approx \langle v_n \rangle^2 - \delta^2_{v_n} . \qquad (1.5)$$

For large fluctuations $\delta_{v_n} \gg v_n^{\mathrm{RP}}$ (e.g. in central collisions), eqs. (1.3) and (1.4) can be approximated by:

$$p(\vec{v}_n) = \frac{1}{2\pi\delta^2_{v_n}} e^{-\vec{v}_n^2/\left(2\delta^2_{v_n}\right)}, \ p(v_n) = \frac{v_n}{\delta^2_{v_n}} e^{-v_n^2/\left(2\delta^2_{v_n}\right)}, \qquad (1.6)$$

which is equivalent to the "fluctuation-only" scenario, i.e. $v_n^{\mathrm{RP}} = 0$. In this case, both the mean and the width are controlled by δ_{v_n} [27]:

$$\langle v_n \rangle = \sqrt{\frac{\pi}{2}}\, \delta_{v_n}, \ \sigma_{v_n} = \sqrt{2 - \frac{\pi}{2}}\, \delta_{v_n}, \qquad (1.7)$$

and hence:

$$\frac{\sigma_{v_n}}{\langle v_n \rangle} = \sqrt{\frac{4}{\pi} - 1} = 0.523, \ \sqrt{\langle v_n^2 \rangle} = \frac{2}{\sqrt{\pi}}\langle v_n \rangle = 1.13\langle v_n \rangle . \qquad (1.8)$$

In the intermediate case, $\delta_{v_n} \approx v_n^{\mathrm{RP}}$, a more general approximation to eq. (1.4) can be used via a Taylor expansion of the Bessel function, $I_0(x) = e^{x^2/4}\left[1 - x^4/64 + O(x^6)\right]$:

$$p(v_n) \approx \frac{v_n}{\delta'^2_{v_n}} e^{-v_n^2/\left(2\delta'^2_{v_n}\right)}\left[1 - \left(\frac{v_n^{\mathrm{RP}} v_n}{\delta^2_{v_n}}\right)^4/64\right], \qquad (1.9)$$

$$\delta'^2_{v_n} = \delta^2_{v_n}\left(1 - \frac{(v_n^{\mathrm{RP}})^2}{2\delta^2_{v_n}}\right)^{-1} \approx \delta^2_{v_n} + (v_n^{\mathrm{RP}})^2/2 . \qquad (1.10)$$

Defining $\alpha \equiv \delta_{v_n}/v_n^{\mathrm{RP}}$, eqs. (1.9) and (1.10) imply that for $v_n \ll 2\sqrt{2}\delta_{v_n}\alpha$, the shape of the distribution is very close to that of eq. 1.6, except for a redefinition of the width. For example, the deviation from the fluctuation-only scenario is expected to be less than 10% over the range $v_n < 1.6\delta_{v_n}\alpha$. Hence the reliable extraction of v_n^{RP} requires precise determination of the tails of the v_n distributions, especially when v_n^{RP} is smaller than δ_{v_n}.

This is especially important for the study of the v_3 and v_4 distributions, which are expected to be dominated by δ_{v_n}.

Each quantity mentioned above, $\langle v_n \rangle$, σ_{v_n}, $\sqrt{\langle v_n^2 \rangle}$, $\sigma_{v_n}/\langle v_n \rangle$, v_n^{RP} and δ_{v_n}, has been the subject of extensive studies both experimentally [19, 22, 25] and in theoretical models [23, 24, 28]. Experimental measurement of the EbyE v_n distributions can elucidate the relations between these quantities, as well as clarify the connections between various experimental methods. In particular, previous measurements based on multi-particle cumulant methods suggest that the v_2 distributions are consistent with the Bessel-Gaussian function [29, 30]. However, this consistency is inferred indirectly from agreement among four-, six- and eight-particle cumulants: the measurement of the EbyE v_n distributions can directly quantify whether the Bessel-Gaussian function is the correct description of the data.

This paper presents the measurement of the EbyE distribution of v_2, v_3 and v_4 over a broad range of centrality in lead-lead (Pb+Pb) collisions at $\sqrt{s_{NN}} = 2.76\,\mathrm{TeV}$ with the ATLAS detector at the LHC. The observed v_n distributions are measured using charged particles in the pseudorapidity range $|\eta| < 2.5$ and the transverse momentum range $p_{\mathrm{T}} > 0.5\,\mathrm{GeV}$, which are then unfolded to estimate the true v_n distributions. The key issue in the unfolding is to construct a response function via a data-driven method, which maps the true v_n distribution to the observed v_n distribution. This response function corrects mainly for the smearing due to the effect of finite charged particle multiplicity in an event, but it also suppresses possible non-flow effects from short-range correlations [31], such as resonance decays, Bose-Einstein correlations and jets [7].

The paper is organized as follows. Sections 2 and 3 give a brief overview of the ATLAS detector, trigger, and selection criteria for events and tracks. Section 4 discusses the details of the single-particle method and the two-particle correlation method used to obtain the observed v_n values, the Bayesian unfolding method used to estimate the true distributions of v_n, and the performance of the unfolding procedure and systematic uncertainties of the measurement. The results are presented in section 5, and a summary is given in section 6.

2 The ATLAS detector and trigger

The ATLAS detector [32] provides nearly full solid-angle coverage around the collision point with tracking detectors, calorimeters and muon chambers, which are well suited for measurements of azimuthal anisotropies over a large pseudorapidity range.[2] This analysis uses primarily two subsystems: the inner detector (ID) and the forward calorimeter (FCal). The ID is immersed in the 2 T axial field of a superconducting solenoid magnet, and measures the trajectories of charged particles in the pseudorapidity range $|\eta| < 2.5$ and over the full azimuthal range. A charged particle passing through the ID traverses typically three modules of the silicon pixel detector (Pixel), four double-sided silicon strip modules of

---

[2]ATLAS uses a right-handed coordinate system with its origin at the nominal interaction point (IP) in the centre of the detector and the z-axis along the beam pipe. The x-axis points from the IP to the centre of the LHC ring, and the y-axis points upward. Cylindrical coordinates (r, ϕ) are used in the transverse plane, ϕ being the azimuthal angle around the beam pipe. The pseudorapidity is defined in terms of the polar angle θ as $\eta = -\ln \tan(\theta/2)$.

the semiconductor tracker (SCT) and, for $|\eta| < 2$, a transition radiation tracker composed of straw tubes. The FCal covers the range $3.1 < |\eta| < 4.9$ and is composed of symmetric modules at positive and negative η. The FCal modules are composed of either tungsten or copper absorbers with liquid argon as the active medium, which together provide ten interaction lengths of material. In heavy ion collisions, the FCal is used mainly to measure the event centrality and event plane angles [15, 16].

The minimum-bias Level-1 trigger used for this analysis requires signals in two zero-degree calorimeters (ZDC) or either of the two minimum-bias trigger scintillator (MBTS) counters. The ZDCs are positioned at 140 m from the collision point, detecting neutrons and photons with $|\eta| > 8.3$, and the MBTS covers $2.1 < |\eta| < 3.9$ on each side of the nominal interaction point. The ZDC Level-1 trigger thresholds on each side are set below the peak corresponding to a single neutron. A Level-2 timing requirement based on signals from each side of the MBTS is imposed to remove beam-induced backgrounds.

3 Event and track selections

This paper is based on approximately 7 μb^{-1} of Pb+Pb collisions collected in 2010 at the LHC with a nucleon-nucleon centre-of-mass energy $\sqrt{s_{NN}} = 2.76\,\text{TeV}$. An offline event selection requires a time difference $|\Delta t| < 3$ ns between the MBTS trigger counters on either side of the interaction point to suppress non-collision backgrounds. A coincidence between the ZDCs at forward and backward pseudorapidity is required to reject a variety of background processes, while maintaining high efficiency for non-Coulomb processes. Events satisfying these conditions are required to have a reconstructed primary vertex with z_{vtx} within 150 mm of the nominal centre of the ATLAS detector. About 48 million events pass the requirements for the analysis.

The Pb+Pb event centrality is characterized using the total transverse energy (ΣE_{T}) deposited in the FCal over the pseudorapidity range $3.2 < |\eta| < 4.9$ measured at the electromagnetic energy scale [33]. A larger ΣE_{T} value corresponds to a more central collision. From an analysis of the ΣE_{T} distribution after all trigger and event selections, the sampled fraction of the total inelastic cross section is estimated to be $(98\pm2)\%$ [34]. The uncertainty associated with the centrality definition is evaluated by varying the effect of the trigger, event selection and background rejection requirements in the most peripheral FCal ΣE_{T} interval [34]. The FCal ΣE_{T} distribution is divided into a set of 5%-wide percentile bins, together with five 1%-wide bins for the most central 5% of the events. A centrality interval refers to a percentile range, starting at 0% for the most central collisions. Thus the 0-1% centrality interval corresponds to the most central 1% of the events; the 95-100% centrality interval corresponds to the least central (i.e. most peripheral) 5% of the events. A standard Glauber model Monte Carlo analysis is used to estimate the average number of participating nucleons, $\langle N_{\text{part}}\rangle$, for each centrality interval [34, 35]. These numbers are summarized in table 1.

The v_n coefficients are measured using tracks reconstructed in the ID that have $p_{\text{T}} > 0.5\,\text{GeV}$ and $|\eta| < 2.5$. To improve the robustness of track reconstruction in the high-multiplicity environment of heavy ion collisions, more stringent requirements on track

Centrality	0–1%	1–2%	2–3%	3–4%	4–5%
$\langle N_{\mathrm{part}} \rangle$	400.6 ± 1.3	392.6 ± 1.8	383.2 ± 2.1	372.6 ± 2.3	361.8 ± 2.5
Centrality	0–5%	5–10%	10–15%	15–20%	20–25%
$\langle N_{\mathrm{part}} \rangle$	382.2 ± 2.0	330.3 ± 3.0	281.9 ± 3.5	239.5 ± 3.8	202.6 ± 3.9
Centrality	25–30%	30–35%	35–40%	40–45%	45–50%
$\langle N_{\mathrm{part}} \rangle$	170.2 ± 4.0	141.7 ± 3.9	116.8 ± 3.8	95.0 ± 3.7	76.1 ± 3.5
Centrality	50–55%	55–60%	60–65%	65–70%	
$\langle N_{\mathrm{part}} \rangle$	59.9 ± 3.3	46.1 ± 3.0	34.7 ± 2.7	25.4 ± 2.3	

Table 1. The relationship between centrality intervals used in this paper and $\langle N_{\mathrm{part}} \rangle$ estimated from the Glauber model [34].

quality, compared to those defined for proton-proton collisions [36], are used. At least 9 hits in the silicon detectors (compared to a typical value of 11) are required for each track, with no missing Pixel hits and not more than 1 missing SCT hit, after taking into account the known non-operational modules. In addition, at its point of closest approach the track is required to be within 1 mm of the primary vertex in both the transverse and longitudinal directions [15].

The efficiency, $\epsilon(p_{\mathrm{T}}, \eta)$, of the track reconstruction and track selection cuts is evaluated using Pb+Pb Monte Carlo events produced with the HIJING event generator [37]. The generated particles in each event are rotated in azimuthal angle according to the procedure described in ref. [38] to give harmonic flow consistent with previous ATLAS measurements [15, 16]. The response of the detector is simulated using GEANT4 [39] and the resulting events are reconstructed with the same algorithms as applied to the data. The absolute efficiency increases with p_{T} by 7% between 0.5 GeV and 0.8 GeV, and varies only weakly for $p_{\mathrm{T}} > 0.8$ GeV. However, the efficiency varies more strongly with η and event multiplicity [40]. For $p_{\mathrm{T}} > 0.8$ GeV, it ranges from 72% at $\eta = 0$ to 51% for $|\eta| > 2$ in peripheral collisions, while it ranges from 72% at $\eta = 0$ to about 42% for $|\eta| > 2$ in central collisions. The fractional change of efficiency from most central to most peripheral collisions, when integrated over η and p_{T}, is about 13%. Contributions of fake tracks from random combinations of hits are generally negligible, reaching only 0.1% for $|\eta| < 1$ for the highest multiplicity events. This rate increases slightly at large $|\eta|$.

4 Method and data analysis

To illustrate the level of EbyE fluctuations in the data, the top panels of figure 1 show the azimuthal distribution of charged particle tracks with $p_{\mathrm{T}} > 0.5$ GeV for three typical events in the 0-5% centrality interval. The corresponding track-pair $\Delta\phi$ distributions from the same events are shown in the bottom panels. For each pair of particles two $\Delta\phi$ entries, $|\phi_1 - \phi_2|$ and $-|\phi_1 - \phi_2|$, are made each with a weight of 1/2, and then folded into the $[-0.5\pi, 1.5\pi]$ interval. Rich EbyE patterns, beyond the structures in the event-averaged
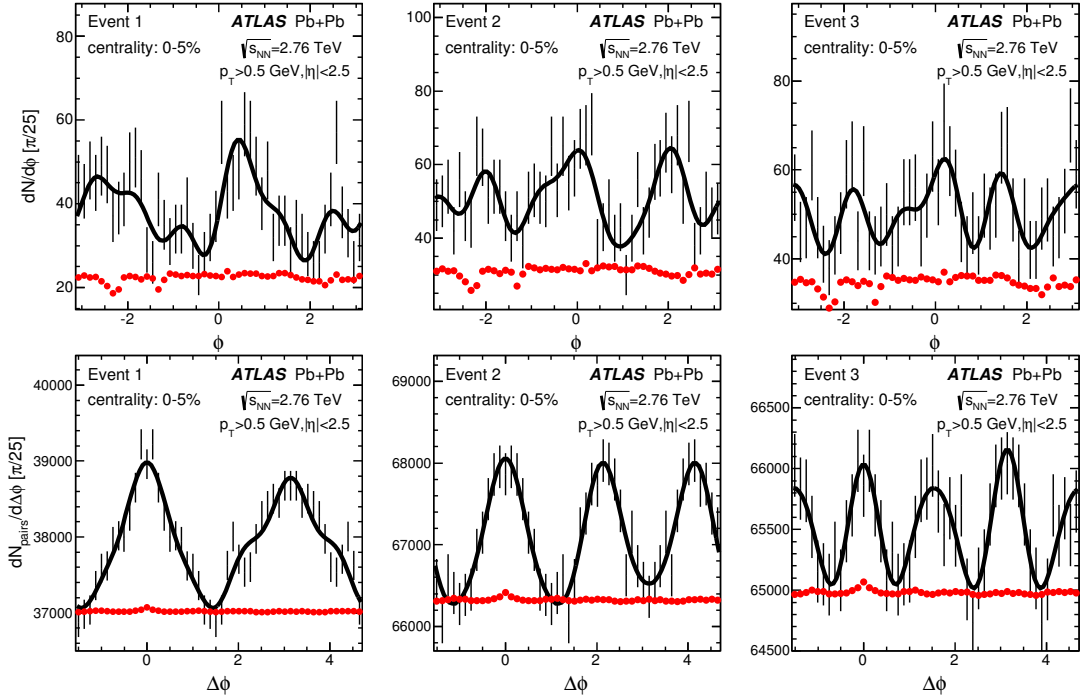
Figure 1. Single-track ϕ (top) and track-pair $\Delta\phi$ (bottom) distributions for three typical events (from left to right) in the 0–5% centrality interval. The pair distributions are folded into the $[-0.5\pi, 1.5\pi]$ interval. The bars indicate the statistical uncertainties of the foreground distributions, the solid curves indicate a Fourier parameterization including the first six harmonics: $\mathrm{d}N/\mathrm{d}\phi = A(1 + 2\sum_{i=1}^{6} c_n \cos n(\phi - \Psi_n))$ for single-track distributions and $\mathrm{d}N/\mathrm{d}\Delta\phi = A(1 + 2\sum_{i=1}^{6} c_n \cos n(\Delta\phi))$ for track-pair distributions, and the solid points indicate the event-averaged distributions (arbitrary normalization).

distributions shown by the solid points (arbitrary normalization), are observed. These EbyE distributions are the inputs to the EbyE v_n analyses.

The azimuthal distribution of charged particles in an event is written as a Fourier series, as in eq. (1.1):

$$\frac{\mathrm{d}N}{\mathrm{d}\phi} \propto 1 + 2\sum_{n=1}^{\infty} v_n^{\mathrm{obs}} \cos n(\phi - \Psi_n^{\mathrm{obs}}) = 1 + 2\sum_{n=1}^{\infty} \left(v_{n,x}^{\mathrm{obs}} \cos n\phi + v_{n,y}^{\mathrm{obs}} \sin n\phi \right) , \qquad (4.1)$$

$$v_n^{\mathrm{obs}} = \sqrt{\left(v_{n,x}^{\mathrm{obs}}\right)^2 + \left(v_{n,y}^{\mathrm{obs}}\right)^2}, v_{n,x}^{\mathrm{obs}} = v_n^{\mathrm{obs}} \cos n\Psi_n^{\mathrm{obs}} = \langle \cos n\phi \rangle, v_{n,y}^{\mathrm{obs}} = v_n^{\mathrm{obs}} \sin n\Psi_n^{\mathrm{obs}} = \langle \sin n\phi \rangle, \qquad (4.2)$$

where the averages are over all particles in the event for the required η range. The v_n^{obs} is the magnitude of the observed EbyE per-particle flow vector: $\vec{v}_n^{\mathrm{obs}} = (v_{n,x}^{\mathrm{obs}}, v_{n,y}^{\mathrm{obs}})$. In the limit of very large multiplicity and in the absence of non-flow effects, it approaches the true flow signal: $v_n^{\mathrm{obs}} \to v_n$. The key issue in measuring the EbyE v_n is to determine the response function $p(v_n^{\mathrm{obs}}|v_n)$, which can be used to unfold the smearing effect due to the finite number of detected particles. Possible non-flow effects from short-range correlations, such as resonance decays, Bose-Einstein correlations and jets, also need to be suppressed.

The rest of this section sets out the steps to obtain the unfolded v_n distribution. Since the data-driven unfolding technique has rarely been used in the study of flow phenomena, details are provided to facilitate the understanding of the methods and systematic uncertainties. Section 4.1 explains how v_n^{obs} and the associated response function can be obtained from the EbyE single-particle distributions, such as those shown in the top panels of figure 1. Section 4.2 describes how v_n^{obs} and the response function can be obtained from EbyE two-particle correlations (2PC), similar to those shown in the lower panels of figure 1. In this paper the 2PC approach is used primarily as a consistency check. The Bayesian unfolding procedure, applicable to either the single-particle or 2PC data, is described in section 4.3. The performance of the unfolding is described in section 4.4, while the systematic uncertainties are discussed in section 4.5.

4.1 Single-particle method

The azimuthal distribution of particles in figure 1 needs to be corrected for non-uniform detector acceptance. This is achieved by dividing the foreground distribution (S) of a given event by the acceptance function (B) obtained as the ϕ distribution of all tracks in all events (see top panels of figure 1):

$$\frac{\mathrm{d}N}{\mathrm{d}\phi} \propto \frac{S(\phi)}{B(\phi)} = \frac{1 + 2\sum_{n=1}^{\infty}\left(v_{n,x}^{\mathrm{raw}}\cos n\phi + v_{n,y}^{\mathrm{raw}}\sin n\phi\right)}{1 + 2\sum_{n=1}^{\infty}\left(v_{n,x}^{\mathrm{det}}\cos n\phi + v_{n,y}^{\mathrm{det}}\sin n\phi\right)} \,, \tag{4.3}$$

$$v_{n,x}^{\mathrm{raw}} = \frac{\sum_i \left(\cos n\phi_i\right)/\epsilon(\eta_i, p_{\mathrm{T},i})}{\sum_i 1/\epsilon(\eta_i, p_{\mathrm{T},i})}, \quad v_{n,y}^{\mathrm{raw}} = \frac{\sum_i \left(\sin n\phi_i\right)/\epsilon(\eta_i, p_{\mathrm{T},i})}{\sum_i 1/\epsilon(\eta_i, p_{\mathrm{T},i})} \,, \tag{4.4}$$

where the index i runs over all tracks in an event, $\epsilon(\eta, p_{\mathrm{T}})$ is the tracking efficiency for a given centrality interval, and $v_{n,x}^{\mathrm{det}}$ and $v_{n,y}^{\mathrm{det}}$ are Fourier coefficients of the acceptance function in azimuth, also weighted by the inverse of the tracking efficiency. The influence of the structures in the acceptance function can be accounted for by taking the leading-order term of the Taylor expansion of $1/B(\phi)$ in terms of $\cos n\phi$ and $\sin n\phi$:

$$v_{n,x}^{\mathrm{obs}} \approx v_{n,x}^{\mathrm{raw}} - v_{n,x}^{\mathrm{det}}, \quad v_{n,y}^{\mathrm{obs}} \approx v_{n,y}^{\mathrm{raw}} - v_{n,y}^{\mathrm{det}} \,, \tag{4.5}$$

where the values of $v_{n,x \text{ or } y}^{\mathrm{det}}$ are less than 0.007 for $n = 2$–4. The higher-order corrections to eq. (4.5) involve products of $v_{n,x \text{ or } y}^{\mathrm{raw}}$ and $v_{n,x \text{ or } y}^{\mathrm{det}}$. They have been estimated and found to have negligible impact on the final v_n distributions for $n = 2$–4.

Figure 2 shows the distribution of the EbyE per-particle flow vector $\vec{v}_2^{\,\mathrm{obs}} = (v_{2,x}^{\mathrm{obs}}, v_{2,y}^{\mathrm{obs}})$ and v_2^{obs} obtained for charged particles with $p_{\mathrm{T}} > 0.5\,\mathrm{GeV}$ in the 20–25% centrality interval. The azimuthal symmetry in the left panel reflects the random orientation of $\vec{v}_2^{\,\mathrm{obs}}$ because of the random orientation of the impact parameter. Due to the finite track multiplicity, the measured flow vector is expected to be smeared randomly around the true flow vector by a 2D response function $p(\vec{v}_n^{\,\mathrm{obs}}|\vec{v}_n)$.

In order to determine $p(\vec{v}_n^{\,\mathrm{obs}}|\vec{v}_n)$, the tracks in the entire inner detector (referred to as full-ID) for a given event are divided into two subevents with symmetric η range, $\eta > 0$ and $\eta < 0$ (labelled by a and b and referred to as half-ID). The two half-IDs have the same average track multiplicity to within 1%. The distribution of flow vector differences between
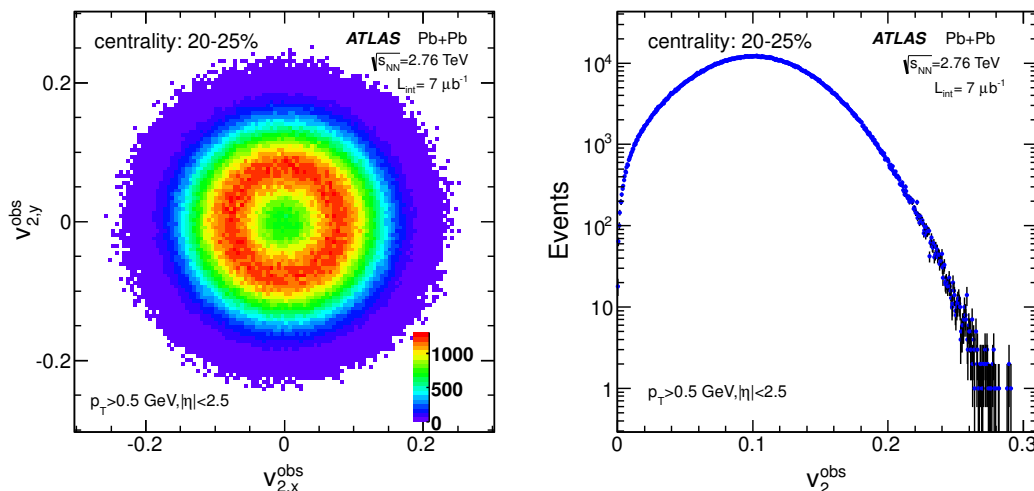
Figure 2. The distribution of EbyE per-particle flow vector $\vec{v}_2^{\,\mathrm{obs}}$ (left panel) and its magnitude v_2^{obs} (right panel) for events in the 20–25% centrality interval.
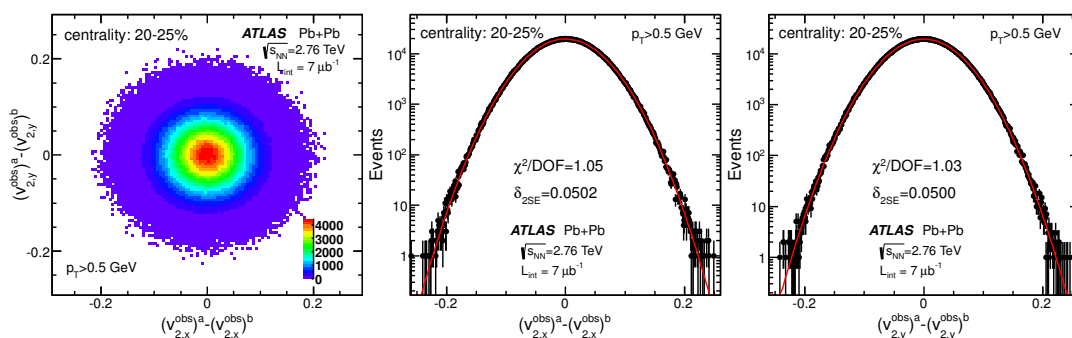

Figure 3. Left: the distribution of the difference between the EbyE per-particle flow vectors of the two half-IDs for events in the 20–25% centrality interval for $n = 2$. Middle: the x-projection overlaid with a fit to a Gaussian. Right: the y-projection overlaid with a fit to a Gaussian. The width from the fit, $\delta_{2\mathrm{SE}}$, and the quality of the fit, χ^2/DOF, are also shown.

the two subevents, $p_{\mathrm{sub}}\left((\vec{v}_n^{\,\mathrm{obs}})^{\mathrm{a}} - (\vec{v}_n^{\,\mathrm{obs}})^{\mathrm{b}}\right)$, is then obtained and is shown in the left panel of figure 3. The physical flow signal cancels in this distribution such that it contains mainly the effects of statistical smearing and non-flow. The middle and right panels of figure 3 show the x- and y- projections of the distribution, together with fits to a Gaussian function. The fits describe the data very well ($\chi^2/\mathrm{DOF} \approx 1$) across five orders of magnitude with the same widths in both directions, implying that the smearing effects and any effects due to non-flow short-range correlations are purely statistical. This would be the case if either the non-flow effects are small and the smearing is mostly driven by finite particle multiplicity, or the number of sources responsible for non-flow is proportional to the multiplicity and they are not correlated between the subevents [31]. The latter could be true for resonance decays, Bose-Einstein correlations, and jets. Similar behaviour is observed for all harmonics up to centrality interval 50–55%. Beyond that the distributions are found to be described better by the Student's t-distribution, which is a general probability density function for the difference between two estimates of the mean from independent samples. The t-distribution approaches a Gaussian distribution when the number of tracks is large.

Denoting the width of these 1D distributions by δ_{2SE}, the widths of the response functions for the half-ID and the full-ID are $\delta_{2SE}/\sqrt{2}$ and $\delta_{2SE}/2$, respectively. The response functions themselves can be obtained by rescaling the left panel of figure 3 in both dimensions by constant factors of 2 and $\sqrt{2}$ for the full-ID and half-ID, respectively [31]:

$$p(\vec{v}_n^{\,\mathrm{obs}}|\vec{v}_n) \propto e^{-\frac{\left(\vec{v}_n^{\,\mathrm{obs}}-\vec{v}_n\right)^2}{2\delta^2}}, \quad \delta = \begin{cases} \delta_{2SE}/\sqrt{2} & \text{for half-ID} \\ \delta_{2SE}/2 & \text{for full-ID} \end{cases}, \tag{4.6}$$

This scaling behaviour was found to be valid in a Monte-Carlo study based on the HIJING event generator [31]. Integrated over azimuth, eq. 4.6 reduces to a Bessel-Gaussian function in 1D:

$$p(v_n^{\mathrm{obs}}|v_n) \propto v_n^{\mathrm{obs}} e^{-\frac{(v_n^{\mathrm{obs}})^2+v_n^2}{2\delta^2}} I_0\left(\frac{v_n^{\mathrm{obs}}v_n}{\delta^2}\right) . \tag{4.7}$$

The difference between the observed and the true signal, denoted by $s = v_n^{\mathrm{obs}} - v_n$, accounts for the statistical smearing. The similarity between eq. (4.7) and eq. (1.4) is a direct consequence of the 2D Gaussian smearing. However, the smearing leading to eq. (4.7) is due to the finite charge-particle multiplicity, while the smearing leading to eq. (1.4) is due to the intrinsic flow fluctuations associated with the initial geometry. Hence the smearing in eq. (4.7) is expected to increase the observed δ_{v_n} value but the value of v_n^{RP} should be relatively stable.

The analytical expression eq. (4.7) can be used to unfold the v_n^{obs} distribution, such as that shown in the right panel of figure 2. Alternatively, the measured distribution $p(v_n^{\mathrm{obs}}|v_n)$, taking into account sample statistics, can be used directly in the unfolding. This measured distribution is obtained by integrating out the azimuthal angle in the 2D response function, and the response function is obtained by rescaling the left panel of figure 3 as described earlier. This approach is more suitable for peripheral collisions where the analytical description using eq. (4.7) is not precise enough.

4.2 Two-particle correlation method

The EbyE two-particle correlation (2PC) method starts from the $\Delta\phi$ information in each event, where $\Delta\phi$ is calculated for each pair of charged tracks as described at the start of section 4. In order to reduce the effect of short-range correlations in η, the tracks in each pair are taken from different half-IDs. This procedure corresponds to convolving the azimuthal distributions of single particles in the two half-IDs:

$$\begin{aligned}
\frac{\mathrm{d}N}{\mathrm{d}\Delta\phi} &\propto \left[1 + 2\sum_n \left(v_{n,x}^{\mathrm{obs_a}}\cos n\phi_{\mathrm{a}} + v_{n,y}^{\mathrm{obs_a}}\sin n\phi_{\mathrm{a}}\right)\right] \\
&\qquad \otimes \left[1 + 2\sum_n \left(v_{n,x}^{\mathrm{obs_b}}\cos n\phi_{\mathrm{b}} + v_{n,y}^{\mathrm{obs_b}}\sin n\phi_{\mathrm{b}}\right)\right] \\
&= 1 + 2\sum_n \left[\left(v_{n,x}^{\mathrm{obs_a}}v_{n,x}^{\mathrm{obs_b}} + v_{n,y}^{\mathrm{obs_a}}v_{n,y}^{\mathrm{obs_b}}\right)\cos n\Delta\phi + \left(v_{n,x}^{\mathrm{obs_a}}v_{n,y}^{\mathrm{obs_b}} - v_{n,y}^{\mathrm{obs_a}}v_{n,x}^{\mathrm{obs_b}}\right)\sin n\Delta\phi\right] \\
&\equiv 1 + 2\sum_n \left(A_n \cos n\Delta\phi + B_n \sin n\Delta\phi\right) ,
\end{aligned} \tag{4.8}$$

where $A_n = \langle \cos n\Delta\phi \rangle$ and $B_n = \langle \sin n\Delta\phi \rangle$. The parameters A_n and B_n are calculated by averaging over the pairs in each event, with each track weighted by the tracking efficiency, as in eq. (4.3). Due to a large rapidity gap on average between the two particles in each pair, the non-flow effects in eq. 4.8 are naturally suppressed compared with the single particle distribution of eq. 4.1.

An EbyE track-pair variable $v_{n,n}^{\mathrm{obs}}$ is subsequently calculated for each event:

$$v_{n,n}^{\mathrm{obs}} \equiv \sqrt{A_n^2 + B_n^2} = \sqrt{\left[\left(v_{n,x}^{\mathrm{obs_a}}\right)^2 + \left(v_{n,y}^{\mathrm{obs_a}}\right)^2\right]\left[\left(v_{n,x}^{\mathrm{obs_b}}\right)^2 + \left(v_{n,y}^{\mathrm{obs_b}}\right)^2\right]} = v_n^{\mathrm{obs_a}} v_n^{\mathrm{obs_b}} \ . \quad (4.9)$$

The observed flow signal from the two-particle correlation analysis is then calculated as:

$$v_n^{\mathrm{obs,2PC}} \equiv \sqrt{v_{n,n}^{\mathrm{obs}}} = \sqrt{v_n^{\mathrm{obs_a}} v_n^{\mathrm{obs_b}}} = \sqrt{(v_n + s_{\mathrm{a}})(v_n + s_{\mathrm{b}})} \ , \quad (4.10)$$

where $s_{\mathrm{a}} = v_n^{\mathrm{obs_a}} - v_n$ and $s_{\mathrm{b}} = v_n^{\mathrm{obs_b}} - v_n$ are independent variables described by the probability distribution in eq. (4.7) with $\delta = \delta_{\mathrm{2SE}}/\sqrt{2}$. The response function for $v_n^{\mathrm{obs,2PC}}$ is very different from that for the single-particle method, but nevertheless can be either calculated analytically via eq. (4.7) or generated from the measured distribution such as that shown in figure 3. For small v_n values, the $s_{\mathrm{a}}s_{\mathrm{b}}$ term dominates eq. (4.10) and the distribution of $v_n^{\mathrm{obs,2PC}}$ is broader than v_n^{obs}. For large v_n values, the distributions of s_{a} and s_{b} are approximately described by Gaussian functions and hence:

$$v_n^{\mathrm{obs,2PC}} \approx \sqrt{v_n^2 + v_n(s_{\mathrm{a}} + s_{\mathrm{b}})} \approx v_n + \frac{s_{\mathrm{a}} + s_{\mathrm{b}}}{2} \equiv v_n + s \ , \quad (4.11)$$

where the fact that the average of two Gaussian random variables is equivalent to a Gaussian with a narrower width has been used, and the smearing of the flow vector for the half-IDs (s_{a} and s_{b}) is taken to be a factor of $\sqrt{2}$ broader than that for the full-ID (s). Hence the distribution of $v_n^{\mathrm{obs,2PC}}$ is expected to approach the v_n^{obs} distribution of the full-ID when $v_n \gg \delta_{\mathrm{2SE}}/\sqrt{2}$.

4.3 Unfolding procedure

In this analysis, the standard Bayesian unfolding procedure [41], as implemented in the RooUnfold framework [42], is used to obtain the v_n distribution. In this procedure, the true v_n distribution ("cause" $\hat{c}$) is obtained from the measured v_n^{obs} or $v_n^{\mathrm{obs,2PC}}$ distribution ("effect" $\hat{e}$) and the response function $A_{ji} \equiv p(e_j|c_i)$ (i,j are bins) as:

$$\hat{c}^{\mathrm{iter}+1} = \hat{M}^{\mathrm{iter}}\hat{e}, \quad M_{ij}^{\mathrm{iter}} = \frac{A_{ji}c_i^{\mathrm{iter}}}{\sum_{m,k} A_{mi}A_{jk}c_k^{\mathrm{iter}}} \ , \quad (4.12)$$

where the unfolding matrix $\hat{M}^0$ is determined from the response function and some initial estimate of the true distribution $\hat{c}^0$ (referred to as the prior). The matrix $\hat{M}^0$ is used to obtain the unfolded distribution $\hat{c}^1$ and $\hat{M}^1$, and the process is then iterated. More iterations reduce the dependence on the prior and give results closer to the true distributions but with increased statistical fluctuations. Therefore the number of iterations N_{iter} is

adjusted according to the sample size and binning. The prior can be chosen to be the v_n^{obs} distribution from the full-ID for the single-particle unfolding, or the $v_n^{\mathrm{obs,2PC}}$ distribution obtained by convolving the two half-IDs (eq. (4.8)) for the 2PC unfolding. However, a more realistic prior can be obtained by rescaling the v_n^{obs} in each event by a constant factor R to obtain a distribution with a mean that is closer to that of the true distribution:

$$v_n^{\mathrm{obs}} \to R v_n^{\mathrm{obs}},$$

$$R = \frac{v_n^{\mathrm{EP}}}{\langle v_n^{\mathrm{obs}} \rangle} \frac{1}{1 + \left(\sqrt{1 + \left(\sigma_{v_n}^{\mathrm{obs}} / \langle v_n^{\mathrm{obs}} \rangle \right)^2} - 1 \right) f}, \quad f = 0, 0.5, 1, 1.5, 2, 2.5, \quad (4.13)$$

where $\langle v_n^{\mathrm{obs}} \rangle$ and $\sigma_{v_n}^{\mathrm{obs}}$ are the mean and the standard deviation of the v_n^{obs} distribution, respectively, and v_n^{EP} is measured using the FCal event plane method from ref. [16] with the same dataset and the same track selection criteria. The EP method is known to measure a value between the mean and the root-mean-square of the true v_n [25, 28] (see figure 13):

$$\langle v_n \rangle \le v_n^{\mathrm{EP}} \le \sqrt{\langle v_n^2 \rangle} = \sqrt{\langle v_n \rangle^2 + \sigma_{v_n}^2} \,. \quad (4.14)$$

The lower limit is reached when the resolution factor [16] used in the EP method approaches one, and the upper limit is reached when the resolution factor is close to zero. Thus $f = 0$ (default choice) gives a prior that is slightly broader than the true distribution, $f = 1$ gives a distribution that has a mean close to the true distribution, and $f > 1$ typically gives a distribution that is narrower than the true distribution.

The unfolding procedure in this analysis has several beneficial features:

1. The response function is obtained entirely from the data using the subevent method described above (eq. (4.6)).

2. Each event provides one entry for the v_n^{obs} distribution and the response function (no efficiency loss), and these distributions can be determined with high precision (from about 2.4 million events for each 5% centrality interval).

4.4 Unfolding performance

This section describes the unfolding based on the single-particle method and summarizes a series of checks used to verify the robustness of the results: a) the number of iterations used, b) comparison with results obtained from a smaller η range, c) variation of the priors, d) comparison with the results obtained using the 2PC method, and e) estimation of possible biases due to short-range correlations by varying the η gap between the two half-IDs. Only a small subset of the available figures is presented here; a complementary selection can be found in appendix A.

The left and middle panels of figure 4 show the convergence behaviour of the unfolding based on the single-particle method for v_2 in the 20–25% centrality interval measured with the full-ID. Around the peak of the distribution, the results converge to within a few percent of the final answer by $N_{\mathrm{iter}} = 4$, but the convergence is slower in the tails and there are small, systematic improvements at the level of a few percent for $N_{\mathrm{iter}} \ge 8$. The
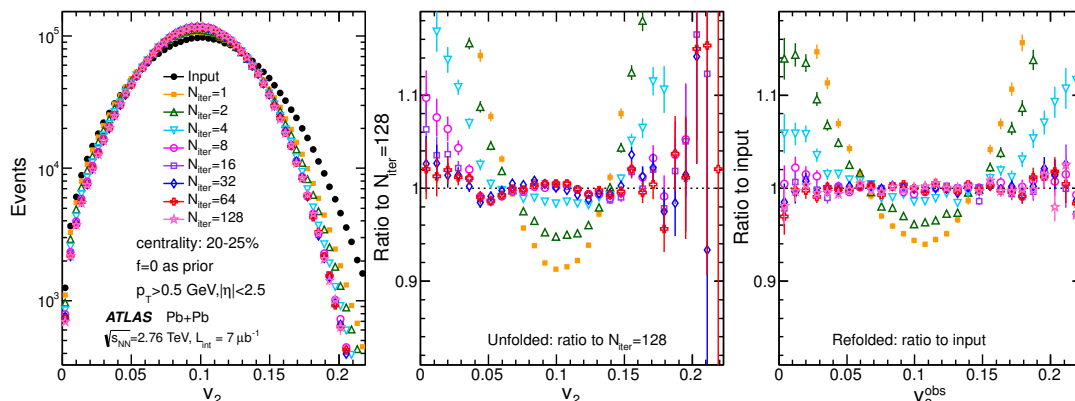
Figure 4. The performance of the unfolding of v_2 for the 20–25% centrality interval (left panel) for various N_{iter}, the ratios of the unfolded distributions to the results after 128 iterations (middle panel), and the ratios of the refolded distributions to the input v_2^{obs} (right panel).
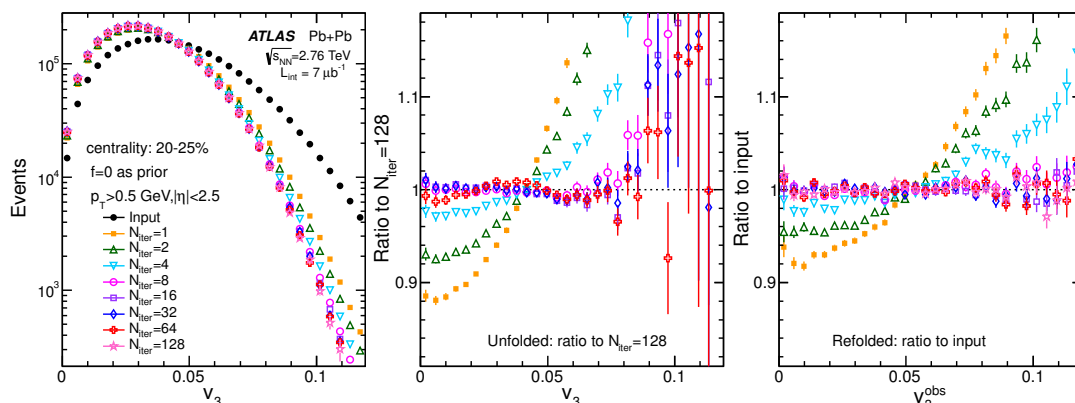

Figure 5. The performance of the unfolding of v_3 for the 20–25% centrality interval (left panel) for various N_{iter}, the ratios of the unfolded distributions to the results after 128 iterations (middle panel), and the ratios of the refolded distributions to the input v_3^{obs} (right panel).

refolded distributions (right panel), obtained by convolving the unfolded distributions with the response function, indicate that convergence is reached for $N_{\mathrm{iter}} \geq 8$. Figures 5 and 6 show similar distributions for v_3 and v_4. The performance of the unfolding is similar to that shown in figure 4, except that the tails of the unfolded distributions require more iterations to converge. For example, figure 6 suggests that the bulk region of the v_4 distributions has converged by $N_{\mathrm{iter}} = 32$, but the tails still exhibit some small changes up to $N_{\mathrm{iter}} = 64$. The slower convergence for higher-order harmonics reflects the fact that the physical v_n signal is smaller for larger n, while the values of δ_{2SE} change only weakly with n. These studies are repeated for all centrality intervals. In general, more iterations are needed for peripheral collisions due to the increase in δ_{2SE}.

The statistical uncertainties in the unfolding procedure are verified via a resampling technique [43]. For small N_{iter}, the statistical uncertainties as given by the diagonal entries of the covariance matrix are much smaller than $\sqrt{N}$, where N is the number of entries in each bin, indicating the presence of statistical bias in the prior. However, these uncertainties
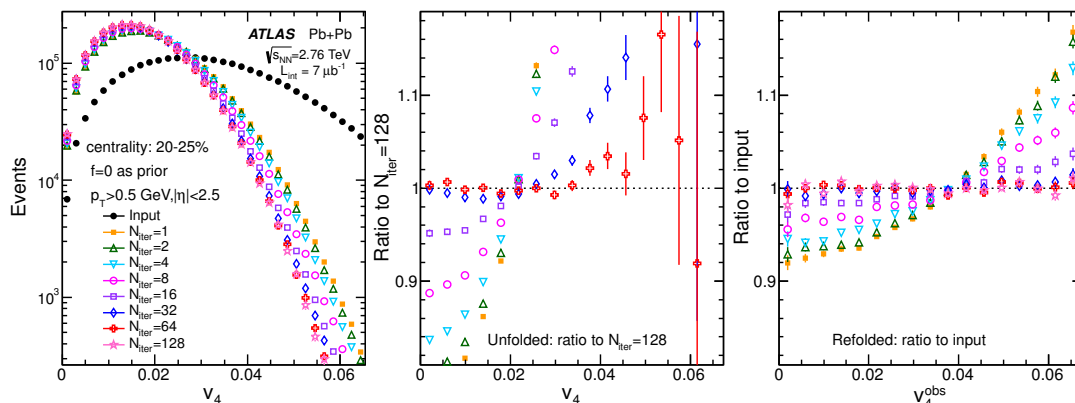
Figure 6. The performance of the unfolding of v_4 for the 20–25% centrality interval (left panel) for various N_{iter}, the ratios of the unfolded distributions to the results after 128 iterations (middle panel), and the ratios of the refolded distributions to the input v_4^{obs} (right panel).

increase with N_{iter}, and generally approach $\sqrt{N}$ for $64 \leq N_{\mathrm{iter}} \leq 128$. In this analysis, the centrality range for each harmonic is chosen such that the difference between $N_{\mathrm{iter}} = 32$ and $N_{\mathrm{iter}} = 128$ is less than 10%. The centrality ranges are 0–70% for v_2, 0–60% for v_3 and 0–45% for v_4.

The robustness of the unfolding procedure is checked by comparing the results measured independently for the half-ID and the full-ID. The results are shown in figure 7. Despite the large differences between their initial distributions, the final unfolded results agree to within a few percent in the bulk region of the unfolded distribution, and they are nearly indistinguishable on a linear scale. This agreement also implies that the influence due to the slight difference (up to 1%) in the average track multiplicity between the two subevents is small. Systematic differences are observed in the tails of the distributions for v_4, especially in peripheral collisions, where the half-ID results are slightly broader. This behaviour reflects mainly the deviation from the expected truth (residual non-convergence) for the half-ID unfolding, since the response function is a factor of $\sqrt{2}$ broader than that for the full-ID.

A wide range of priors has been tried in this analysis, consisting of the measured v_n^{obs} distribution and the six rescaled distributions defined by eq. (4.13). Figure 8 compares the convergence behaviour of these priors for v_3 in the 20–25% centrality interval. Despite the significantly different initial distributions, the unfolded distributions converge to the same answer, to within a few percent, for $N_{\mathrm{iter}} \geq 16$. A prior that is narrower than the unfolded distribution leads to convergence in one direction, and a broader prior leads to convergence from the other direction. Taken together, these checks allow a quantitative evaluation of the residual non-convergence in the unfolded distributions.

Figure 9 compares the convergence behaviour between unfolding of single-particle v_n^{obs} and unfolding of $v_n^{\mathrm{obs,2PC}}$ in the 20–25% centrality interval. Despite very different response functions and initial distributions, the unfolded results agree with each other to within a few percent in the bulk region of the unfolded distribution. The systematic deviations in the tails of the v_4 distribution (bottom-right panel) are due mainly to the remaining
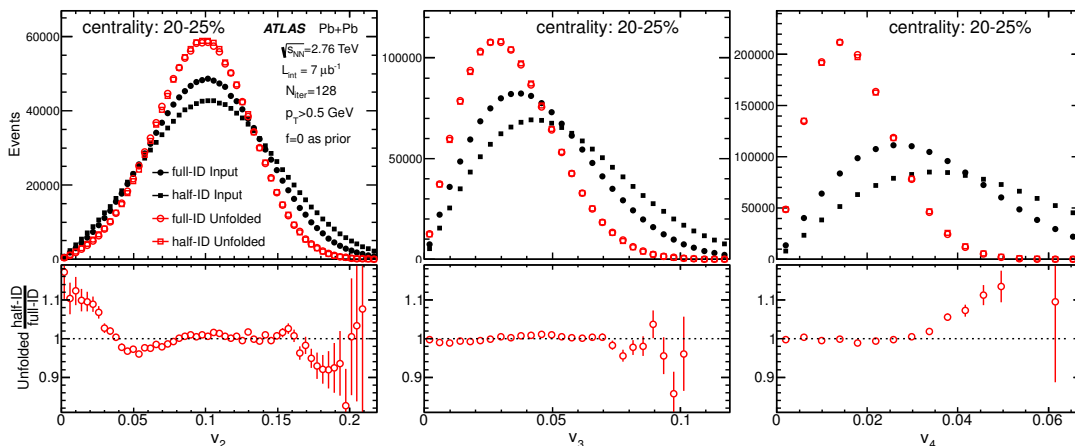
Figure 7. Comparison of the input distributions (solid symbols) and unfolded distributions for $N_{\text{iter}} = 128$ (open symbols) between the half-ID and the full-ID in the 20–25% centrality interval. The ratios of half-ID to full-ID unfolded results are shown in the bottom panels. The results are shown for v_2 (left panels), v_3 (middle panels) and v_4 (right panels).
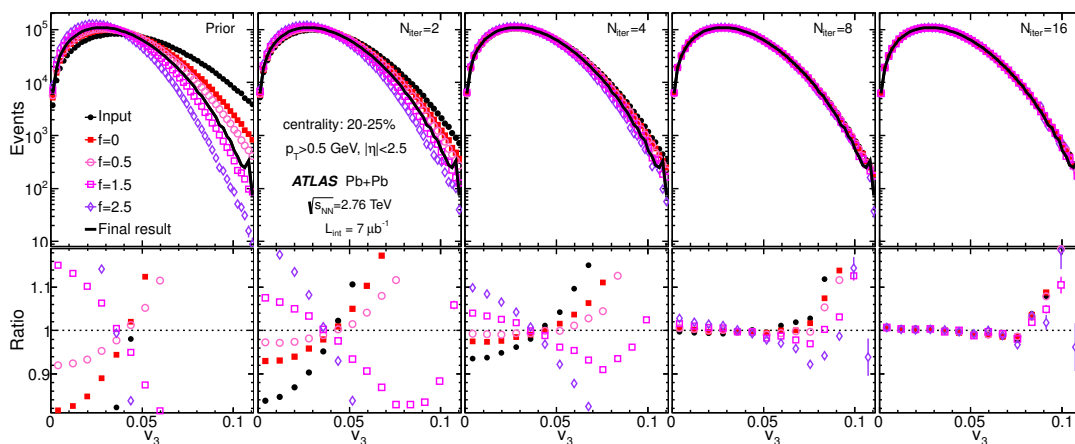

Figure 8. Convergence behaviour of v_3 in the 20–25% centrality interval for five choices of priors for different N_{iter} from left to right. The top panels show the distributions after a certain number of iterations and bottom panels show the ratios to the result for $N_{\text{iter}} = 128$. A common reference, shown by the solid lines in the top panels, is calculated by averaging the results for $f = 0$ and $f = 0.5$ with $N_{\text{iter}} = 128$.

non-convergence in the 2PC method, which has a broader response function than the single-particle method.

One important issue in the EbyE v_n study is the extent to which the unfolded results are biased by non-flow short-range correlations, which may influence both the v_n^{obs} distributions and the response functions. This influence contributes to both the $v_n^{\text{obs}} = |\vec{v}_n^{\text{obs}}|$ distributions and response functions obtained from $(\vec{v}_n^{\text{obs}})^{\text{a}} - (\vec{v}_n^{\text{obs}})^{\text{b}}$ (figure 3), and hence are expected largely to cancel out in the unfolding procedure. This conclusion is supported by a detailed Monte-Carlo model study based on the HIJING event generator with a realistic flow afterburner [31], where the unfolding performance was evaluated. It is also
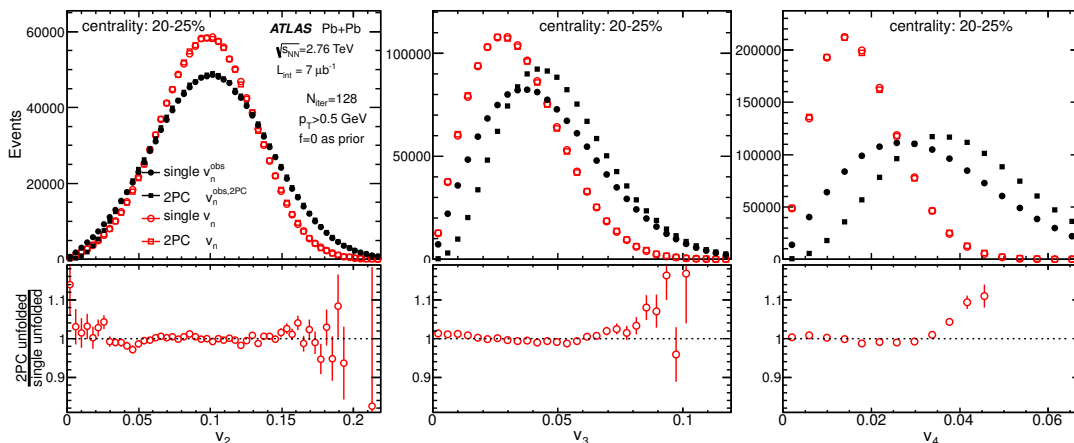
Figure 9. Comparison of the input distributions (solid symbols) and unfolded distributions for $N_{\text{iter}} = 128$ (open symbols) between the single-particle unfolding and 2PC unfolding in the 20–25% centrality interval for v_2 (left panels), v_3 (middle panels) and v_4 (right panels). The ratios of 2PC to single-particle unfolded results are shown in the bottom panels.

supported by the consistency between the single-particle and 2PC methods (figure 9), which have different sensitivities to the non-flow effects. Furthermore, both unfolding methods have been repeated requiring a minimum η gap between the two subevents used to obtain the input distributions and the response functions. Six additional cases, requiring $\eta_{\text{gap}} = 0.2, 0.4, 0.6, 0.8, 1.0, 2.0$, have been studied and the results have been compared (see figure 24). The unfolded v_n distributions are observed to narrow slightly for larger η_{gap}, reflecting the fact that the true v_n decreases slowly at large $|\eta|$ [16] and a larger η_{gap} on average selects particles at large $|\eta|$. However, the results are always consistent between the two methods independent of the η_{gap} value used. This consistency supports further the conclusion that the influence of the short-range non-flow correlations on the final unfolded results is not significant.

The dependence of the EbyE v_n on the p_{T} of the charged particles has also been checked: the particles are divided into those with $0.5 < p_{\text{T}} < 1\,\text{GeV}$ and those with $p_{\text{T}} > 1\,\text{GeV}$, and the EbyE v_n measurements are repeated independently for each group of particles. About 60% of detected particles have $0.5 < p_{\text{T}} < 1\,\text{GeV}$, and this fraction varies weakly with centrality. The unfolding performance is found to be slightly worse for charged particles with $0.5 < p_{\text{T}} < 1\,\text{GeV}$ than for those with $p_{\text{T}} > 1\,\text{GeV}$, due to their much smaller v_n signal. Hence the v_n range of the unfolded distribution for the final results is chosen separately for each p_{T} range.

The final v_n distributions are obtained using the single-particle unfolding with the full-ID and $N_{\text{iter}} = 128$, separately for charged particles in the two aforementioned p_{T} ranges and the combined p_{T} range. The prior is obtained by rescaling the v_n^{obs} distribution according to eq. (4.13) with $f = 0$, and the response function is measured from correlations of the two half-IDs with no η gap in between.

4.5 Systematic uncertainties

The systematic uncertainties associated with the unfolding procedure include contributions from the residual non-convergence, dependence on the prior, uncertainty in the response function, the difference between the single-particle method and the 2PC method, and the tracking efficiency. The residual non-convergence is estimated from the difference between the results for $N_{\text{iter}} = 32$ and $N_{\text{iter}} = 128$ or between the results for the half-ID and full-ID. These two estimates are strongly correlated, so in each bin of the unfolded distribution the larger of the two is used. The dependence on the prior is taken as the difference between the results for $f = 0$ and $f = 2.5$. Note that the prior for $f = 0$ ($f = 2.5$) is broader (narrower) than the final unfolded distributions. The uncertainty of the response function is estimated from the difference between results obtained using the analytical formula eq. (4.7) and results obtained using the measured distribution, as well as the change in the results when the small dependence of $\delta_{2\text{SE}}$ on the observed v_n^{obs} is taken into account. Results for the p_{T}-dependence of the v_n distributions (see section 5 and figure 11) show that the mean values vary with p_{T}, but, after they are rescaled to a common mean, the resulting shapes are almost identical. Motivated by this finding, every source of systematic uncertainty is decomposed into two components: the uncertainty associated with the $\langle v_n \rangle$ or the v_n-scale, and the uncertainty in the shape after adjustment to the same $\langle v_n \rangle$ or the adjusted v_n-shape. The uncertainties are then combined separately for the v_n-scale and the adjusted v_n-shape. Most shape uncertainties can be attributed to σ_{v_n}, such that the remaining uncertainties on the adjusted v_n-shape are generally smaller.

To estimate the uncertainty due to the tracking efficiency, the measurement is repeated without applying the efficiency re-weighting. The final distributions are found to have almost identical shape, while the values of $\langle v_n \rangle$ and σ_{v_n} increase by a few percent. This increase can be ascribed mainly to the smaller fraction of low-p_{T} particles, which have smaller v_n, so this increase should not be considered as a systematic uncertainty on the v_n-scale. Instead, the scale uncertainty is more appropriately estimated from the change in the v_n^{EP} when varying the efficiency correction within its uncertainty range. On the other hand, small changes are observed for $\sigma_{v_n}/\langle v_n \rangle$ and the adjusted v_n-shape. Since these changes are small, they are conservatively included in the total systematic uncertainty in the v_n-shape.

The variation of the efficiency with the detector occupancy may reduce the v_n coefficients in eq. 1.1. This influence has been studied by comparing the v_n values reconstructed via the two-particle correlation method with the generated v_n signal in HJING simulation with flow imposed on the generated particles. The influence is found to be 1% or less, consistent with the findings in [15], and it is included in the uncertainty due to tracking efficiency. It should be pointed out that the influence of detector occupancy is expected to be proportional to the magnitude of the v_n signal, and hence it mainly affects the v_n scale, not the adjusted v_n shape.

Additional systematic uncertainties include those from the track selection, dependence on the running period, and trigger and event selections. These account for the influence of fake tracks, the instability of the detector acceptance and efficiency, variation of the

	Uncertainty in $\langle v_2\rangle$ or σ_{v_2}				Uncertainty in $\sigma_{v_2}/\langle v_2\rangle$			
Centrality	0–10%	10–30%	30–50%	50–70%	0–10%	10–30%	30–50%	50–70%
Non-convergence [%]	<0.1	<0.1	<0.2	3–12	0.9	0.6	0.5–1.4	3–11
Prior [%]	<0.1	<0.1	<0.2	0.2	0.6	<0.3	<0.2	0.2–0.7
Response function [%]	0.3–1	0.3	0.3	0.2–1	1.0	0.7	0.7	0.6–3
Compare to 2PC [%]	<0.2	<0.2	<0.2	0.2–7	0.5–1.5	<0.4	0.4–0.8	1–7
Efficiency [%]	1.3	0.8	0.8	0.7	0.4	0.4	0.4	0.4–0.8
Track selection, trigger, stability [%]	2.2	1.9	1.7	1.7				
Total experimental[%]	2.6	1.9	1.8	3.5–14	1.6–2.2	1.3	1–1.8	3.4–14
Residual non-flow from [31] [%]	1.4–2.3	0.7–1.8	1.5	1.7–3.5	0.1–1.5	1	1	1.5
	Uncertainty in $\langle v_3\rangle$ or σ_{v_3}				Uncertainty in $\sigma_{v_3}/\langle v_3\rangle$			
Centrality	0–10%	10–30%	30–50%	50–60%	0–10%	10–30%	30–50%	50–60%
Non-convergence [%]	0.2	0.3	0.3	1.2–5	0.2–0.8	0.3–0.8	0.4–2	0.5–4
Prior [%]	<0.2	<0.2	<0.2	0.5–1.4	0.6	0.2–0.4	0.2–1.0	3.0
Response function [%]	0.6	0.8	0.8–2.4	2.9–4.6	0.3–0.7	0.2–0.5	0.9–2.5	3–5
Compare to 2PC [%]	0.5	0.2–0.7	0.1	0.2	0.3–1.6	0.4–0.6	0.7–2.5	1–3
Efficiency [%]	1.6	1.2	1	0.9	<0.2	<0.2	<0.3	<0.3
Track selection, trigger, stability [%]	2.1	1.4	1.5–2	2.5–4.5				
Total experimental[%]	2.7	2.2	2–3.3	4.2–8.3	0.8–2	0.6–1.2	1.3–4.2	4.2–7.0
Residual non-flow from [31][%]	0.4	0.6	1.2	2.0–2.5	0.2	0.2	0.5	0.5
	Uncertainty in $\langle v_4\rangle$ or σ_{v_4}				Uncertainty in $\sigma_{v_4}/\langle v_4\rangle$			
Centrality	0–10%	10–30%	30–45%		0–10%	10–30%	30–45%	
Non-convergence [%]	1–2.0	1–1.5	3.0–5.5		1–2	0.5–1	2.0–4.0	
Prior [%]	3.0	3.0	5.0–7.0		2.0	3.0	5.0	
Response function [%]	2.5–4.0	3.0	3.0–5.0		0.5–2	0.6–1.2	2.0–2.3	
Compare to 2PC[%]	0.2-1	0.3	1–4.7		1–2.5	1.2	0.5–1.2	
Efficiency [%]	2.0	1.5	1.2		1	0.4	<0.3	
Track selection, trigger, stability [%]	3.0	2.7	3–6					
Total experimental[%]	5.4	5.4	8–11		3.0	4.0	5–7	
Residual non-flow from [31][%]	0.8–1.4	2.9–3.2	3–5		0.2–0.6	0.4	2.5	

Table 2. Summary of systematic uncertainties as percentages of $\langle v_n\rangle$, σ_{v_n} and $\sigma_{v_n}/\langle v_n\rangle$ ($n = 2$–4) obtained using charged particles with $p_T > 0.5\,\text{GeV}$. The uncertainties for $\langle v_n\rangle$ and σ_{v_n} are similar so the larger of the two is quoted. The uncertainties associated with track selection, the trigger and stability are taken from ref. [16]. For completeness, the model dependent estimates of the residual non-flow effects derived from ref. [31] for unfolding method with the default setup are also listed. Most uncertainties are asymmetric; the quoted numbers refer to the maximum uncertainty range spanned by various centrality intervals in each group.

centrality definition, respectively. All three sources of systematic uncertainty are expected to change only the v_n-scale but not the v_n-shape, and they are taken directly from the published v_n^{EP} measurement [16].

Table 2 summarizes the various systematic uncertainties as percentages of $\langle v_n\rangle$, σ_{v_n} and $\sigma_{v_n}/\langle v_n\rangle$, for charged particles with $p_T > 0.5\,\text{GeV}$. The uncertainties on $\langle v_n\rangle$ and σ_{v_n} are strongly correlated, which in many cases leads to a smaller and asymmetric uncertainty on $\sigma_{v_n}/\langle v_n\rangle$. In most cases, the uncertainties are dominated by tracking efficiency, as well as the track selection, trigger, and run stability assessed in ref. [16]. The uncertainties

associated with the unfolding procedure are usually significant only in peripheral collisions, except for $\langle v_4 \rangle$, where they are important across the full centrality range. The relative uncertainties in table 2 have also been evaluated separately for charged particles with $0.5 < p_T < 1$ GeV and $p_T > 1$ GeV. In general, the systematic uncertainties are larger for the group of particles with $0.5 < p_T < 1$ GeV, due mainly to the increased contributions from residual non-convergence and the choice of priors.

The final v_n distributions are shown over a v_n range that is chosen such that the statistical uncertainties in all bins are less than 15%, and the results obtained with the default setups between $N_{\mathrm{iter}} = 32$ and $N_{\mathrm{iter}} = 128$ are consistent within 10%. The systematic uncertainties on the adjusted shape from the sources discussed above are then combined to give the final uncertainty for the v_n-shape. The total systematic uncertainties are typically a few percent of v_n in the main region of the v_n distributions and increase to 15%-30% in the tails, depending on the value of n and centrality interval (see figure 10). Within the chosen v_n ranges, the statistical uncertainties are found to be always smaller than the systematic uncertainties for the v_n-shape, and the integrals of the v_n distributions outside these ranges are typically $< 0.5\%$ for the 5%-wide centrality intervals and $< 1\%$ for the 1%-wide centrality intervals.

This analysis relies on the data-driven unfolding method to suppress the non-flow effects. In fact, many of the cross-checks presented in section 4.4 are sensitive to the residual non-flow, where "residual non-flow" refers to that component of the non-flow effects that is not removed by the unfolding method. Hence the total experimental systematic uncertainties quoted for the v_n-scale in table 2 and the systematic uncertainties on the v_n-shape discussed above already include an estimate of the residual non-flow effects. An alternative, albeit model-dependent approach, is to rely on simulations. One such study is carried out in ref. [31] based on HIJING with EbyE v_n imposed on the generated particles. This study demonstrates that most non-flow effects are indeed suppressed by the data-driven unfolding method used in this analysis. This study also shows that the residual non-flow effects for the unfolding method with the default setup have no appreciable impact on the v_3 distributions, but broaden slightly the v_2 and v_4 distributions. Furthermore, ref. [31] also shows that most of these changes can be absorbed into simultaneous increases of $\langle v_n \rangle$ and σ_{v_n} values by a few percent. For completeness, these model-dependent estimates of the residual non-flow contribution on the v_n-scale are quoted in table 2: they are found to be smaller than the total systematic uncertainties of the measurement, especially for the higher-order harmonics. Ref. [31] also estimates the influence of residual non-flow on the intrinsic v_n-shape, obtained by comparing the shapes of the unfolded and the input distributions after both distributions are rescaled to have the same $\langle v_n \rangle$. The variations of the intrinsic v_n-shape due to residual non-flow are found to reach a maximum of 5%–15% (of $p(v_n)$) in the tails of the distributions, depending on the choice of n and the centrality interval, but these variations are typically much smaller than the total systematic uncertainties on the v_n-shape in the data (see figure 10). As noted above, a large fraction of the residual non-flow effects estimated by ref. [31] are expected to be already included in various data-driven cross-checks performed in section 4.4. Hence, to avoid double counting, the total systematic uncertainties applied to the data plots do not include the estimates
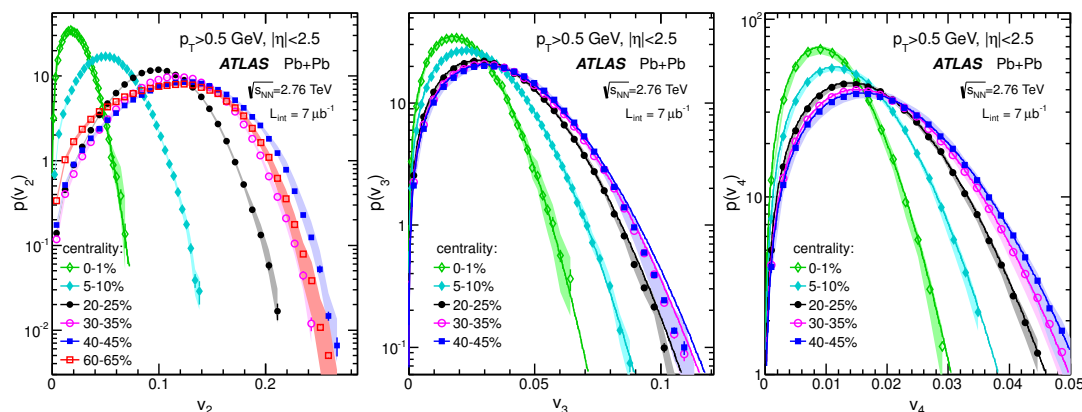
Figure 10. The probability density distributions of the EbyE v_n in several centrality intervals for $n = 2$ (left panel), $n = 3$ (middle panel) and $n = 4$ (right panel). The error bars are statistical uncertainties, and the shaded bands are uncertainties on the v_n-shape. The solid curves are distributions calculated from the measured $\langle v_n \rangle$ according to eq. (1.6). The solid curve is shown only for 0–1% centrality interval for v_2, but for all centrality intervals in case of v_3 and v_4.

from ref. [31]. However, the uncertainties from ref. [31] for the v_n-scale (table 2) and v_n-shape, are well within the total systematic uncertainties derived from the data analysis.

5 Results

Figure 10 shows the probability density distributions of the EbyE v_n in several centrality intervals obtained for charged particles with $p_T > 0.5\,\text{GeV}$. The shaded bands indicate the systematic uncertainties associated with the shape. These uncertainties are strongly correlated in v_n: the data points are allowed to change the shape of the distribution within the band while keeping $\langle v_n \rangle$ unchanged. The v_n distributions are found to broaden from central to peripheral collisions (especially for v_2), reflecting the gradual increase of the magnitude of v_n for more peripheral collisions [15, 16]. The shape of these distributions changes quickly with centrality for v_2, while it changes more slowly for higher-order harmonics. These distributions are compared with the probability density function obtained from eq. (1.6) ($v_n^{\text{RP}} = 0$), which represents a fluctuation-only scenario for v_n. These functions, indicated by the solid curves, are calculated directly from the measured $\langle v_n \rangle$ values via eq. (1.7) for each distribution. The fluctuation-only scenario works reasonably well for v_3 and v_4 over the measured centrality range, but fails for v_2 except for the most central 2% of collisions, i.e. for the centrality interval 0-2%. Hence for v_2 the solid curve representing the fluctuation-only scenario is shown only for the 0-1% centrality interval (the data for the 1-2% interval are not shown). However, there is a small systematic difference between the data and the curve in the tails of the v_3 distributions in mid-central collisions, with a maximum difference of two standard deviations. Using eq. (1.9), this difference is compatible with a non-zero v_3^{RP} similar to the findings reported in ref. [44]. Futhermore, since the measured v_4 distribution covers only a limited range ($v_4 \lesssim 3\delta_{v_4}$), a non-zero v_4^{RP} on the order of δ_{v_4} can not be excluded by this analysis based on eq. (1.9).
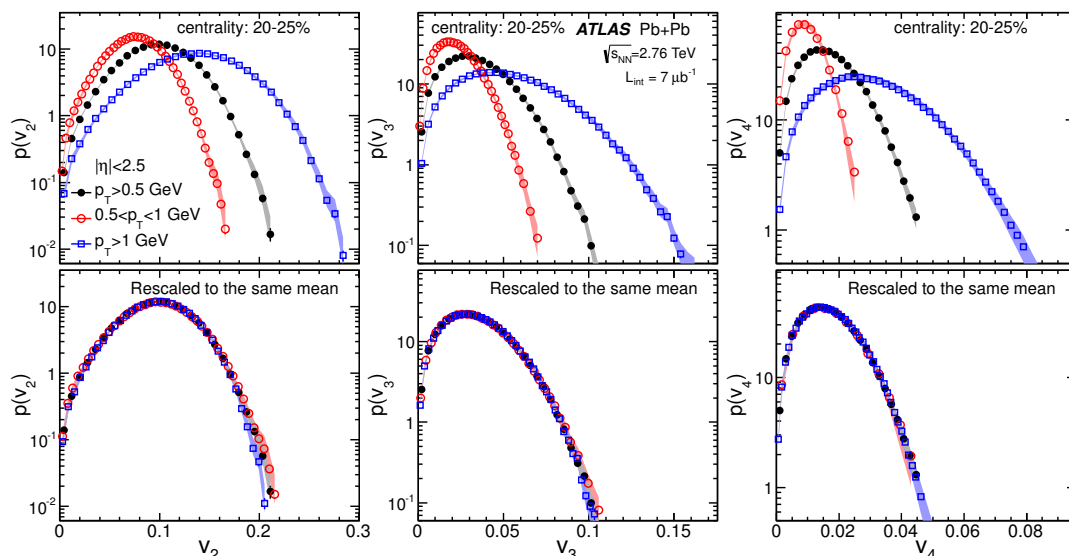
Figure 11. Top panels: the unfolded distributions for v_n in the 20–25% centrality interval for charged particles in the $p_T > 0.5\,\mathrm{GeV}$, $0.5 < p_T < 1\,\mathrm{GeV}$ and $p_T > 1\,\mathrm{GeV}$ ranges. Bottom panels: same distributions but rescaled horizontally so the $\langle v_n \rangle$ values match that for the $p_T > 0.5\,\mathrm{GeV}$ range. The shaded bands represent the systematic uncertainties on the v_n-shape.

Figure 11 compares the unfolded v_n distributions for charged particles in three p_T ranges: $p_T > 0.5\,\mathrm{GeV}$, $0.5 < p_T < 1\,\mathrm{GeV}$ and $p_T > 1\,\mathrm{GeV}$. The v_n distributions for $p_T > 1\,\mathrm{GeV}$ are much wider than for $0.5 < p_T < 1\,\mathrm{GeV}$, reflecting the fact that the v_n values increase strongly with p_T in this region [16]. However, once these distributions are rescaled to the same $\langle v_n \rangle$ as shown in the lower row of figure 11, their shapes are quite similar except in the tails of the distributions for $n = 2$. This behaviour suggests that the hydrodynamic response of the medium to fluctuations in the initial geometry is nearly independent of p_T in the low-p_T region; it also demonstrates the robustness of the unfolding performance against the change in the underlying v_n distributions and response functions.

Figure 12 shows a summary of the quantities derived from the EbyE v_n distributions, i.e. $\langle v_n \rangle$, σ_{v_n} and $\sigma_{v_n}/\langle v_n \rangle$, as a function of $\langle N_{\mathrm{part}} \rangle$. The shaded bands represent the total systematic uncertainties listed in table 2, which generally are asymmetric. Despite the strong p_T dependence of $\langle v_n \rangle$ and σ_{v_n}, the ratio $\sigma_{v_n}/\langle v_n \rangle$ is relatively stable. For v_2, the value of $\sigma_{v_n}/\langle v_n \rangle$ varies strongly with $\langle N_{\mathrm{part}} \rangle$, and reaches a minimum of about 0.34 at $\langle N_{\mathrm{part}} \rangle \sim 200$, corresponding to the 20–30% centrality interval. For v_3 and v_4, the values of $\sigma_{v_n}/\langle v_n \rangle$ are almost independent of $\langle N_{\mathrm{part}} \rangle$, and are consistent with the value expected from the fluctuation-only scenario ($\sqrt{4/\pi - 1}$ via eq. (1.8) as indicated by the dotted lines), except for a small deviation for v_3 in mid-central collisions. This limit is also reached for v_2 in the most central collisions as shown by the top-right panel of figure 12.

Figure 13 compares the $\langle v_n \rangle$ and $\sqrt{\langle v_n^2 \rangle}$ with the v_n^{EP} measured using the FCal event plane method for charged particles with $p_T > 0.5\,\mathrm{GeV}$ [16]. For v_3 and v_4, the values of v_n^{EP} are almost identical to $\sqrt{\langle v_n^2 \rangle}$. However, the values of v_2^{EP} are in between $\langle v_2 \rangle$ and $\sqrt{\langle v_2^2 \rangle}$. As expected [25, 28], and as discussed in section 4.3, they approach $\sqrt{\langle v_2^2 \rangle}$ only in
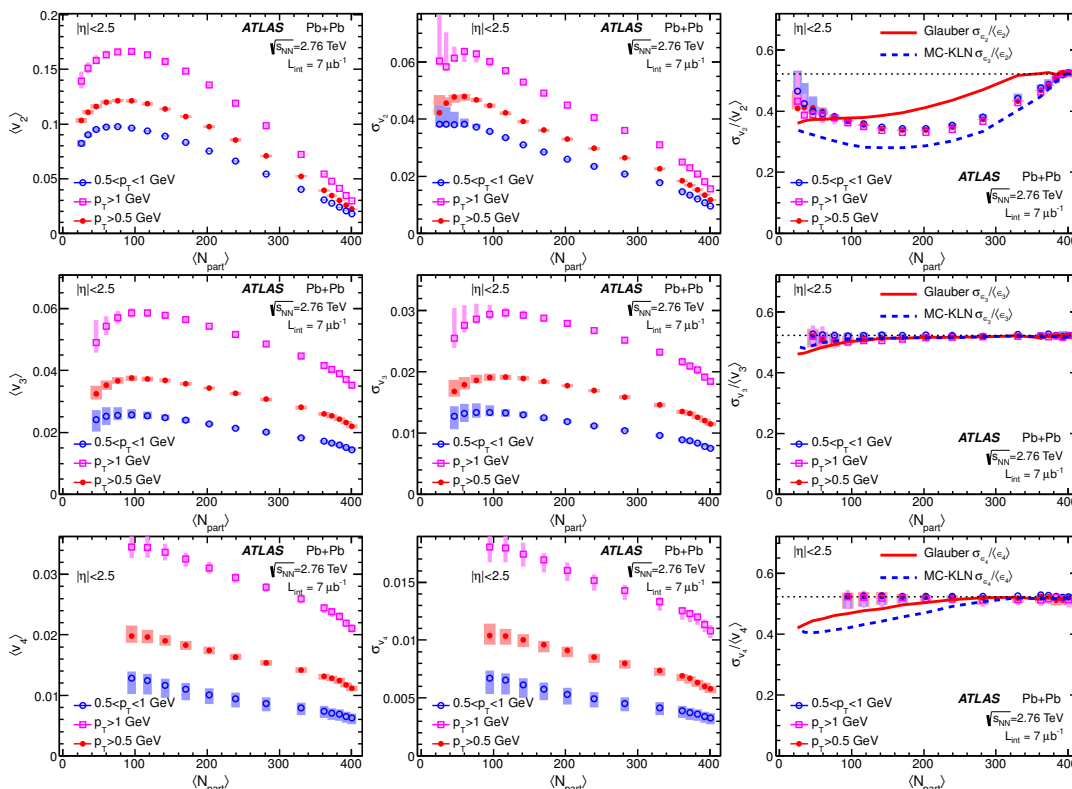
Figure 12. The $\langle N_{\mathrm{part}}\rangle$ dependence of $\langle v_n\rangle$ (left panels), σ_{v_n} (middle panels) and $\sigma_{v_n}/\langle v_n\rangle$ (right panels) for $n = 2$ (top row), $n = 3$ (middle row) and $n = 4$ (bottom row). Each panel shows the results for three p_{T} ranges together with the total systematic uncertainties. The dotted lines in the right column indicate the value $\sqrt{4/\pi - 1}$ expected for the radial projection of a 2D Gaussian distribution centred around origin (see eq. (1.8)). The values of $\sigma_{v_n}/\langle v_n\rangle$ are compared with the $\sigma_{\epsilon_n}/\langle\epsilon_n\rangle$ given by the Glauber model [35] and MC-KLN model [45].

peripheral collisions, where the resolution factor used in the EP method is small.

The results in figures 10 and 12 imply that the distributions of v_2 in central collisions (centrality interval 0-2%), and of v_3 and v_4 in most of the measured centrality range are described by a 2D Gaussian function of $\vec{v}_n$ centred around the origin (eq. 1.6). On the other hand, the deviation of the v_2 distribution from such a description in other centrality intervals suggests that the contribution associated with the average geometry, v_2^{RP}, becomes important. In order to test this hypothesis, the v_2 distributions have been fitted to the Bessel-Gaussian function eq. (1.4), with v_2^{RP} not constrained to be zero. The results of the fit are shown in figure 14 for various centrality intervals. The fit works reasonably well up to the 25–30% centrality interval, although systematic deviations in the tails are apparent already in the 15–20% centrality interval. The deviations increase steadily for more peripheral collisions, which may be due to the fact that the fluctuations of ϵ_2 (eq. 1.2) are no longer Gaussian in peripheral collisions where N_{part} is small [25] (see also figure 18).

The values of v_2^{RP} and δ_{v_2} can be estimated from these fits. Since the value of v_2^{RP} varies rapidly with $\langle N_{\mathrm{part}}\rangle$, especially in central collisions, the extracted v_2^{RP} and δ_{v_2} values can be affected by their spreads if too broad a centrality interval is used. The effect of the
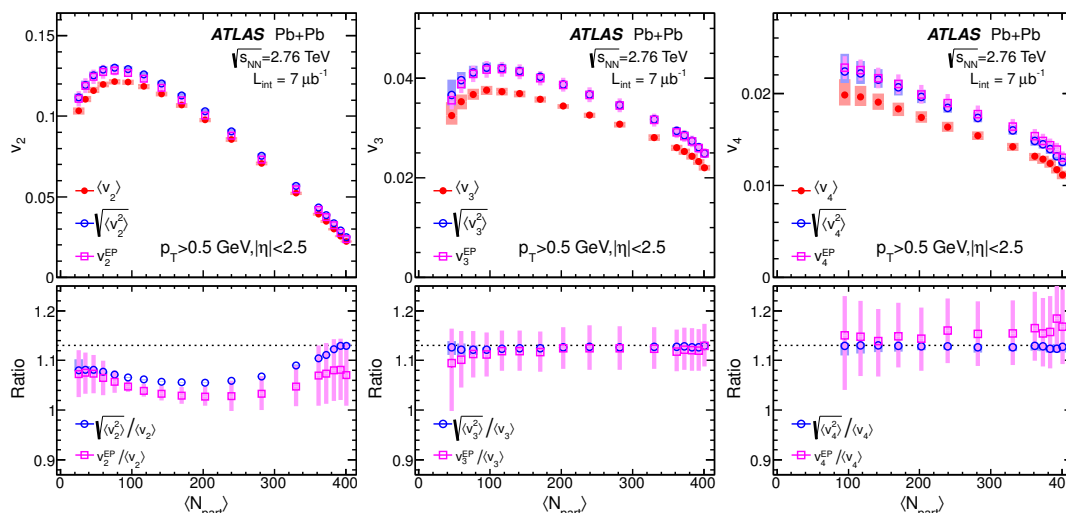
Figure 13. Top panels: comparison of $\langle v_n \rangle$ and $\sqrt{\langle v_n^2 \rangle} \equiv \sqrt{\langle v_n \rangle^2 + \sigma_{v_n}^2}$, derived from the EbyE v_n distributions, with the v_n^{EP} [16]. Bottom panels: the ratios of $\sqrt{\langle v_n^2 \rangle}$ and v_n^{EP} to $\langle v_n \rangle$. The shaded bands represent the systematic uncertainties. The dotted lines in bottom panels indicate $\sqrt{\langle v_n^2 \rangle}/\langle v_n \rangle = 1.13$, expected for the radial projection of a 2D Gaussian distribution centred around origin (eq. (1.8)).

centrality binning has been checked and corrected as follows. Taking the 20–25% interval as an example, the results obtained using the full centrality range within this interval are compared to the results obtained from the average of the five individual 1% intervals: 20–21%,...,24–25%. This procedure has been carried out for each 5% centrality interval, and the difference is found to be significant only for the 0–5% and 5–10% intervals, and negligible for all the others. For the 0–5% interval, results are reported in the individual 1% bins. For the 5–10% bin, results are averaged over the five individual 1% bins.

As a cross-check, the Bessel-Gaussian fits are also performed on the v_2^{obs} distributions before the unfolding. Systematic devations are also observed between the fit and the v_2^{obs} data, but the deviations are smaller than those shown in figure 14. The value of v_2^{RP} from the v_2^{obs} distribution is found to agree to within a few percent with that from the unfolded v_2 distribution, while the value of δ_{v_2} from the v_2^{obs} distribution is significantly larger. This behaviour is expected since the smearing by the response function (eq. 4.7) increases mainly the width, and the value of v_2^{RP} should be stable.

Figure 15 shows the v_2^{RP} and δ_{v_2} values extracted from the v_2 distributions as a function of $\langle N_{\mathrm{part}} \rangle$. They are compared with values of $\langle v_2 \rangle$ and σ_{v_2} obtained directly from the v_2 distributions. The v_2^{RP} value is always smaller than the value for $\langle v_2 \rangle$, and it decreases to zero in the 0–2% centrality interval, consistent with the results shown in figure 10. The value of δ_{v_2} is close to σ_{v_2} except in the most central collisions. This behaviour leads to a value of $\delta_{v_2}/v_2^{\mathrm{RP}}$ larger than $\sigma_{v_2}/\langle v_2 \rangle$ over the full centrality range as shown in the right panel of figure 15. The value of $\delta_{v_2}/v_2^{\mathrm{RP}}$ decreases with $\langle N_{\mathrm{part}} \rangle$ and reaches a minimum of 0.38 ± 0.02 at $\langle N_{\mathrm{part}} \rangle \approx 200$, but then increases for more central collisions. The two points for the 0–1% and 1–2% centrality intervals are omitted as the corresponding v_2^{RP} values
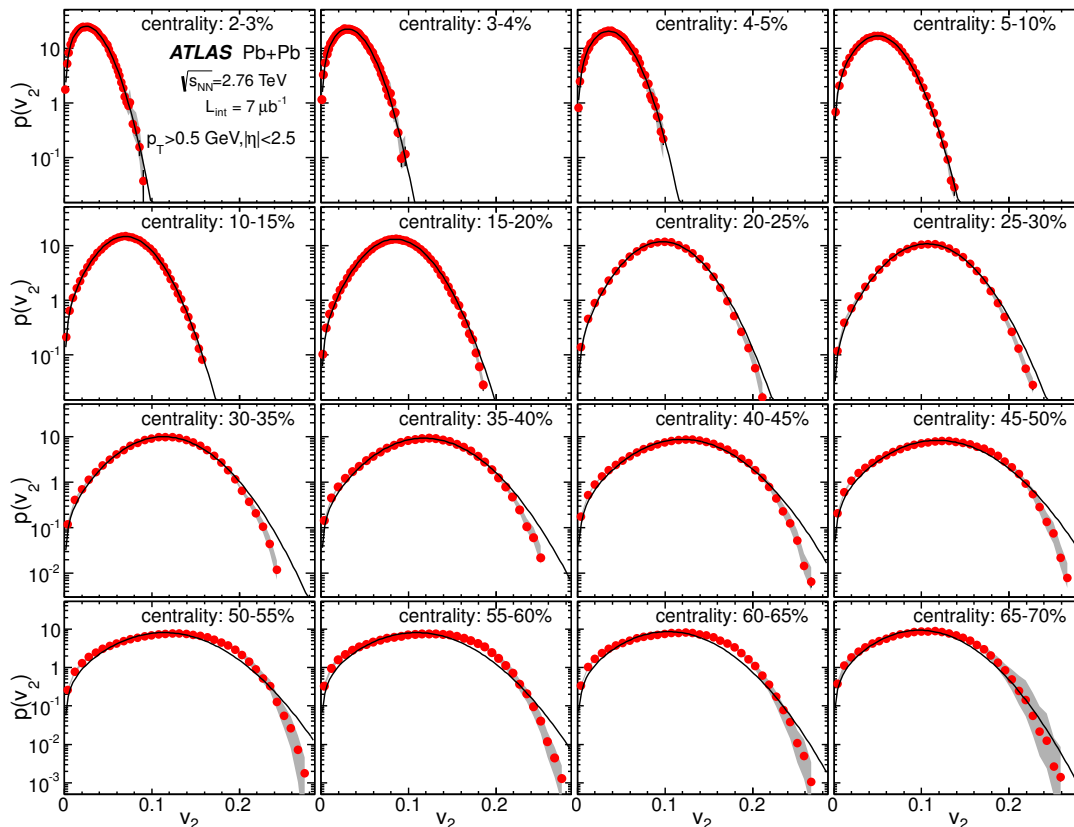
Figure 14. The probability density distributions of v_2 for $p_T > 0.5\,\mathrm{GeV}$ in several centrality intervals, together with fits to the Bessel-Gaussian function eq. (1.4). The fits for the 0–1% and 1–2% centrality intervals are not shown but they can be well described by a Bessel-Gaussian function with $v_2^{\mathrm{RP}} = 0$ (see discussion for figure 10). The $\langle N_{\mathrm{part}} \rangle$ value for each centrality range is given in table 1.

are consistent with zero.

According to eq. (1.5), when the relative fluctuations are small the value of $\langle v_n \rangle$ can be approximated by:

$$\langle v_n \rangle \approx \sqrt{\left(v_n^{\mathrm{RP}}\right)^2 + \delta_{v_n}^2} \; . \tag{5.1}$$

Similarly, the value of v_n^{RP} can be estimated from σ_{v_n} and $\langle v_n \rangle$ without relying on the fit:

$$v_n^{\mathrm{RP}} \approx \sqrt{\langle v_n \rangle^2 - \sigma_{v_n}^2} \; . \tag{5.2}$$

Both relations are shown in the left panel of figure 15 for v_2. Good agreement with the data is observed for $100 < \langle N_{\mathrm{part}} \rangle < 350$, corresponding to 5–45% centrality interval in table 1. However, systematic deviations are observed both in central collisions where fluctuations are dominant, and in peripheral collisions where the Bessel-Gaussian function fails to describe the shape of the v_2 distribution.

Multi-particle cumulant methods have been widely used to estimate the values of v_2^{RP} and δ_{v_2}, as well as to study the deviation of the v_2 distribution from a Bessel-Gaussian
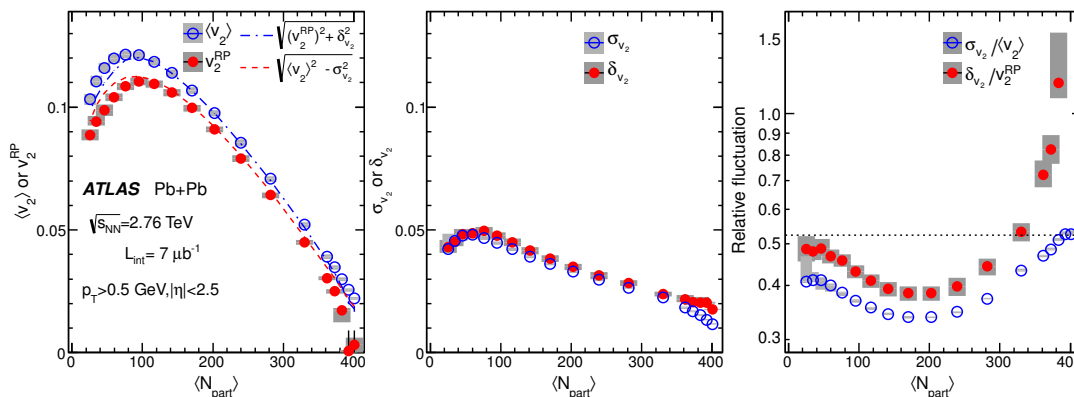
Figure 15. The dependence of v_2^{RP} and $\langle v_2 \rangle$ (left panel), δ_{v_2} and σ_{v_2} (middle panel), δ_{v_2}/v_2^{RP} and $\sigma_{v_2}/\langle v_2 \rangle$ (right panel) on $\langle N_{part} \rangle$. The shaded boxes indicate the systematic uncertainties. The dotted line in the right panel indicates the value $\sqrt{4/\pi - 1}$ expected for the radial projection of a 2D Gaussian distribution centred around origin (see eq. (1.8)).

description [21]. The second-order coefficients for the $2k^{\text{th}}$-order cumulants, $v_2\{2k\}$, are generally calculated via $2k$-particle correlations [20]. These coefficients can also be calculated analytically from the measured v_2 distributions, labelled as $v_2^{\text{calc}}\{2k\}$. The first four terms can be expressed [23] as:

$$v_2^{\text{calc}}\{2\}^2 \equiv \langle v_2^2 \rangle \approx \left(v_2^{\text{RP}}\right)^2 + 2\delta_{v_2}^2 \ ,$$

$$v_2^{\text{calc}}\{4\}^4 \equiv -\langle v_2^4 \rangle + 2\langle v_2^2 \rangle^2 \approx \left(v_2^{\text{RP}}\right)^4 \ ,$$

$$v_2^{\text{calc}}\{6\}^6 \equiv \left(\langle v_2^6 \rangle^2 - 9\langle v_2^4 \rangle\langle v_2^2 \rangle + 12\langle v_2^2 \rangle^3\right)/4 \approx \left(v_2^{\text{RP}}\right)^6 \ , \qquad (5.3)$$

$$v_2^{\text{calc}}\{8\}^8 \equiv -\left(\langle v_2^8 \rangle^2 - 16\langle v_2^6 \rangle\langle v_2^2 \rangle - 18\langle v_2^4 \rangle^2 + 144\langle v_2^4 \rangle\langle v_2^2 \rangle^2 - 144\langle v_2^2 \rangle^4\right)/33 \approx \left(v_2^{\text{RP}}\right)^8 \ .$$

The last part of each equation is exact when the v_2 distribution follows the Bessel-Gaussian function eq. (1.4). In this case only the first two cumulants are independent, and the higher-order cumulants do not provide new information. For the same reason, it has been argued that differences between the higher-order cumulants $v_2\{2k\}$ ($k > 1$) are sensitive to non-Gaussian behaviour in the underlying v_2 distribution [23].

Figure 16 shows results for $v_2^{\text{calc}}\{4\}$, $v_2^{\text{calc}}\{6\}$ and $v_2^{\text{calc}}\{8\}$, calculated directly from the measured v_2 distributions (eq. (5.3)). They are compared with the results for v_2^{RP} obtained from the Bessel-Gaussian fits shown in figure 14. The results calculated from the cumulants agree with the results obtained from the fit, except for $\langle N_{part} \rangle < 100$. However, the calculated coefficients from higher-order cumulants agree with each other over the whole centrality range to within 0.5%-2%, despite the poor description of the v_2 distribution by the Bessel-Gaussian function for the centrality interval 25–70% ($\langle N_{part} \rangle < 200$), shown in figure 14. It therefore follows that similar values of $v_2\{2k\}$ for $k \geq 2$ observed in previous measurements [21, 22] are no guarantee that the distribution is well described by a Bessel-Gaussian over the full range in non-central collisions, since the uncertainties of these measurements are bigger than the differences seen between $v_2^{\text{calc}}\{4\}$, $v_2^{\text{calc}}\{6\}$ and $v_2^{\text{calc}}\{8\}$ in figure 16.
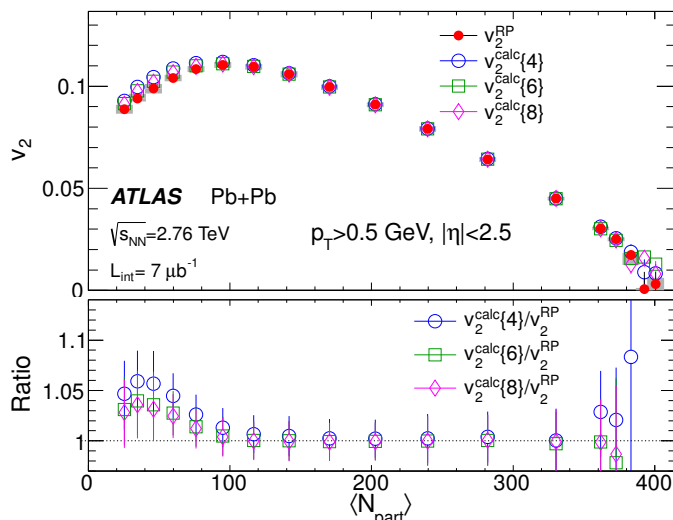
Figure 16. Top panel: comparison of the v_2^{RP} obtained from the Bessel-Gaussian fit of the v_2 distributions with the values for four-particle ($v_2^{\mathrm{calc}}\{4\}$), six-particle ($v_2^{\mathrm{calc}}\{6\}$) and eight-particle ($v_2^{\mathrm{calc}}\{8\}$) cumulants calculated directly from the unfolded v_2 distributions, using eq. (5.3). Bottom panel: the ratios of the cumulants to the fit results, with the error bars representing the total uncertainties.
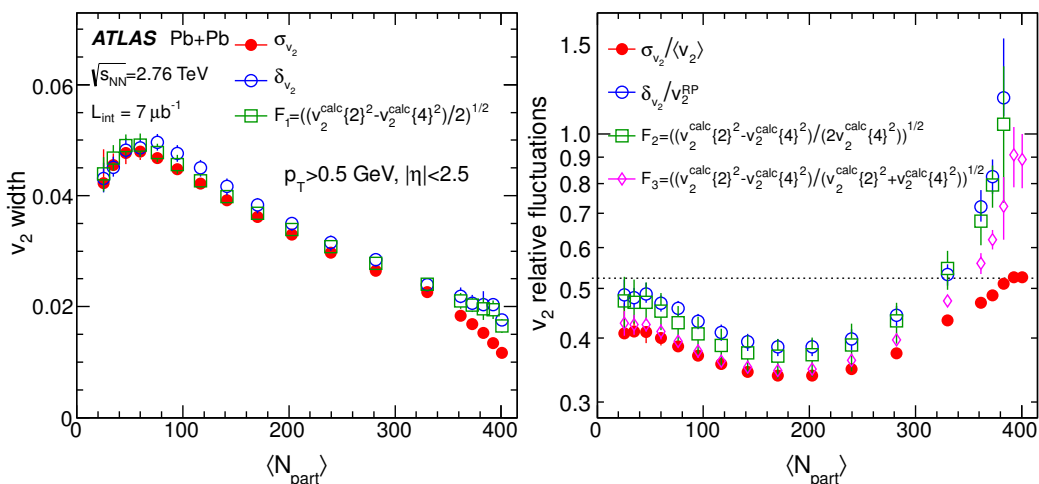

Figure 17. Left panel: the standard deviation (σ_{v_2}), the width obtained from Bessel-Gaussian function (δ_{v_2}), the width estimated from the two-particle cumulant ($v_2^{\mathrm{calc}}\{2\}$) and four-particle cumulant ($v_2^{\mathrm{calc}}\{4\}$). These cumulants are calculated analytically via eq. (5.3) from the v_2 distribution. Right panel: various estimates of the relative fluctuations (see legend).

In previous analyses based on cumulants [7, 22], several other quantities have been used to study the v_2 fluctuations. The definitions of these quantities are given below and their physical meaning can be understood from eq. (5.3):

$$F_1 = ((v_2^{\mathrm{calc}}\{2\}^2 - v_2^{\mathrm{calc}}\{4\}^2)/2)^{1/2} \approx \delta_{v_2}, \tag{5.4}$$

$$F_2 = ((v_2^{\mathrm{calc}}\{2\}^2 - v_2^{\mathrm{calc}}\{4\}^2)/(2v_2^{\mathrm{calc}}\{4\}^2))^{1/2} \approx \delta_{v_2}/v_2^{\mathrm{RP}} \tag{5.5}$$

$$F_3 = ((v_2^{\mathrm{calc}}\{2\}^2 - v_2^{\mathrm{calc}}\{4\}^2)/(v_2^{\mathrm{calc}}\{2\}^2 + v_2^{\mathrm{calc}}\{4\}^2))^{1/2} \approx \delta_{v_2}/\langle v_2 \rangle, \tag{5.6}$$
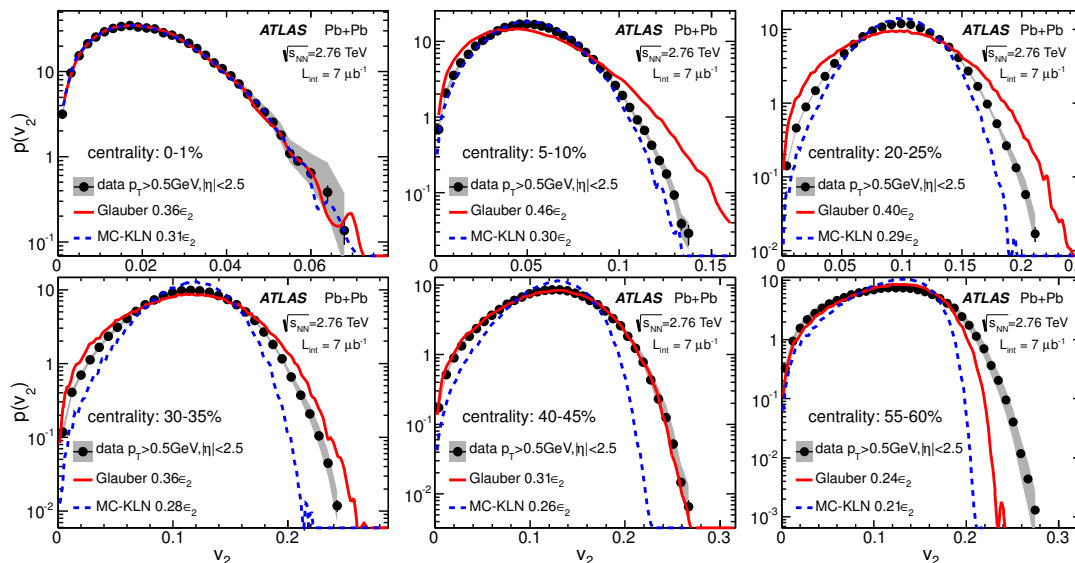
Figure 18. The EbyE v_2 distributions compared with the ϵ_2 distributions from two initial geometry models: a Glauber model (solid lines) and the MC-KLN model (dashed lines). The ϵ_2 distributions have been rescaled to the same mean values. The scale factors are indicated in the legends.

where F_1, F_2, and F_3 are calculated from the unfolded distributions, using eq. (5.3). The approximation for F_3 is valid when $v_2^{\mathrm{RP}} \gg \delta_{v_2}$. In central collisions where $v_2^{\mathrm{RP}} \ll \delta_{v_2}$, the value of F_3 is expected to approach one.

Figure 17 compares the calculated values of F_1, F_2 and F_3 to the rightmost expressions in eqs. (5.4)–(5.6), using δ_{v_2}, v_2^{RP} obtained from fits to the Bessel-Gaussian function, and the mean of the unfolded distribution. The value of F_1 is between σ_{v_2} and δ_{v_2}. The quantities F_2 and F_3 show similar $\langle N_{\mathrm{part}} \rangle$ dependence as $\sigma_{v_2}/\langle v_2 \rangle$ and $\delta_{v_2}/v_2^{\mathrm{RP}}$, however significant discrepancies are observed, especially in the most central collisions where the flow fluctuation is dominant.

Figure 18 compares the EbyE v_2 distributions with the distributions of the eccentricity ϵ_2 of the initial geometry, calculated via eq. (1.2) from the Glauber model [35] and the MC-KLN model [45]. The MC-KLN model is based on the Glauber model but takes into account the corrections to the initial geometry due to gluon saturation effects. Three million events have been generated and grouped into centrality intervals according to the impact parameter. The ϵ_2 distribution for each centrality interval is rescaled to match the $\langle v_2 \rangle$ of the data, and then normalized to form a probability density function. Since v_2 is expected to be proportional to ϵ_2 in most hydrodynamic calculations [6], the deviations between the v_2 distributions and the rescaled ϵ_2 distributions can be used to improve the modeling of the initial geometry. Figure 18 shows that the rescaled ϵ_2 distributions describe the data well for the most central collisions, but not so well for non-central collisions. In peripheral collisions, both the Glauber and MC-KLN models fail to describe the data. A smaller scale factor is generally required for the MC-KLN model, reflecting the fact that the ϵ_2 values from the MC-KLN model are on average larger than those from the Glauber model. Similar comparisons between v_n and ϵ_n for $n = 3$ and $n = 4$ are shown in
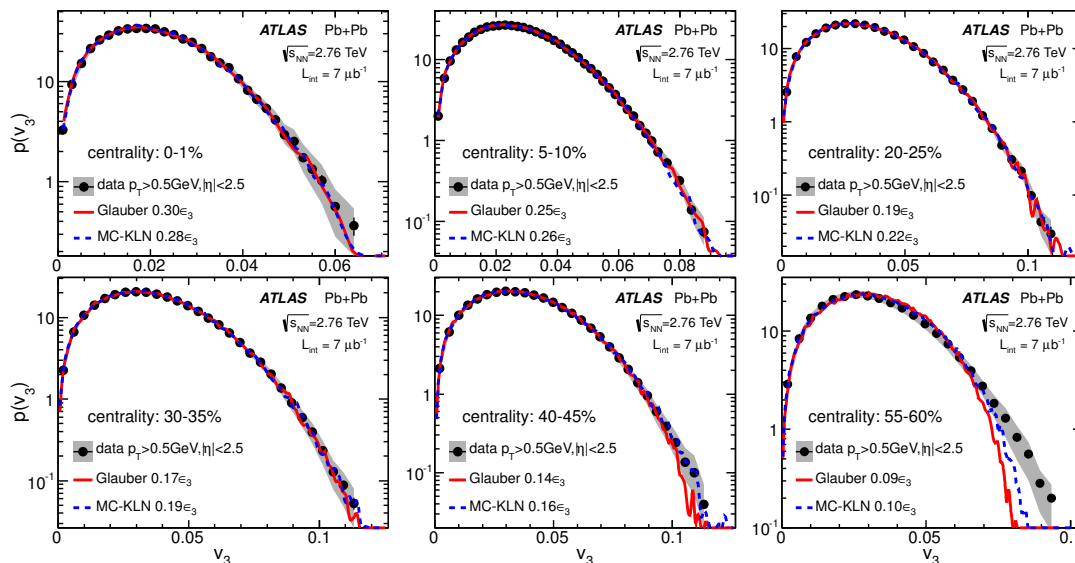
Figure 19. The EbyE v_3 distributions compared with the ϵ_3 distributions from two initial geometry models: a Glauber model (solid lines) and the MC-KLN model (dashed lines). The ϵ_3 distributions have been rescaled to the same mean values. The scale factors are indicated in the legends.

Figure 20. The EbyE v_4 distributions compared with the ϵ_4 distributions from two initial geometry models: a Glauber model (solid lines) and the MC-KLN model (dashed lines). The ϵ_4 distributions have been rescaled to the same mean values. The scale factors are indicated in the legends.
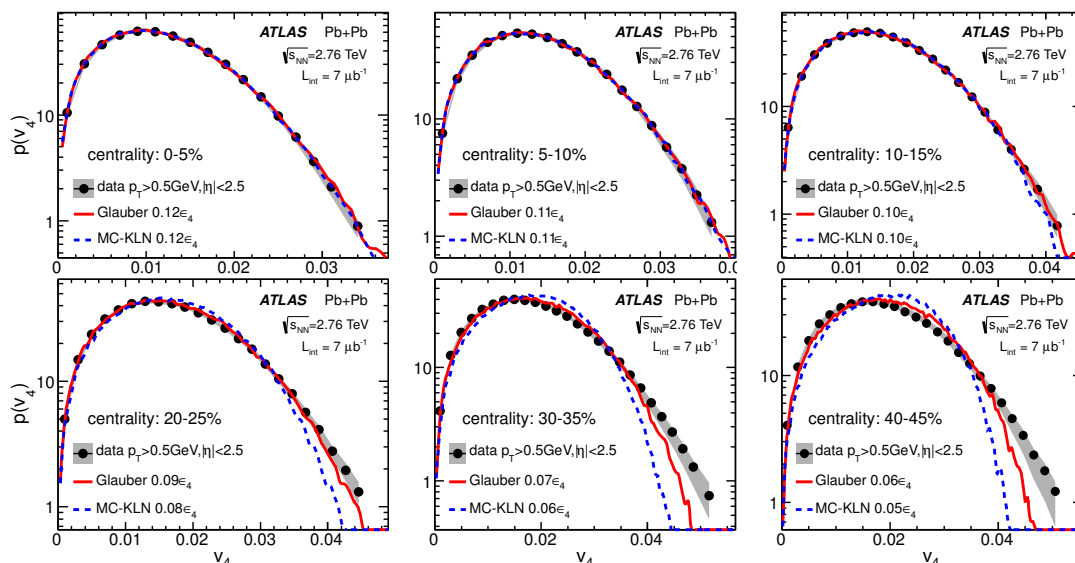
figure 19 and figure 20, respectively. Agreement with the models is better than in the $n = 2$ case. However, this could simply reflect the fact that these distributions are dominated by Gaussian fluctuations, which have a universal shape. The shape differences between the v_n and ϵ_n distributions are also quantified in the right panels of figure 12 by comparing the values of $\sigma_{v_n}/\langle v_n \rangle$ with the values of $\sigma_{\epsilon_n}/\langle \epsilon_n \rangle$. Clearly, both the Glauber and MC-KLN models fail to describe the data consistently, in particular for $n = 2$, across most

of the measured centrality range. It should be noted that in the centrality intervals that correspond to the more peripheral collisions (e.g centrality interval 55–60%), the ϵ_n values have been scaled down by a large factor and the sharp cutoffs of the ϵ_n distributions are a natural consequence of the kinematic constraint $\epsilon_n \leq 1$ (see eq. (1.2)). However, this behaviour also implies that v_n is not proportional to ϵ_n for large ϵ_n values.

6   Summary

Measurements of the event-by-event harmonic flow coefficients v_n for $n = 2, 3$ and 4 have been performed using 7 $\mu\mathrm{b}^{-1}$ of Pb+Pb collision data at $\sqrt{s_{NN}} = 2.76\,\mathrm{TeV}$ collected by the ATLAS experiment at the LHC. The observed v_n distributions are measured using charged particles in the pseudorapidity range $|\eta| < 2.5$ and the transverse momentum range $p_\mathrm{T} > 0.5\,\mathrm{GeV}$, which are then unfolded via a response function to estimate the true v_2 distributions. The response function is constructed via a data-driven method, which maps the true v_n distribution to the observed v_n distribution. The influence of residual non-flow effects are studied by varying the pseudorapidity gap between the two subevents used to obtain the observed v_n distributions and the response functions, as well as by comparing the two different analysis methods based either on the single particle distribution or two-particle correlations. The influence of the residual non-flow is also compared to an estimation based on model simulations [31], and the latter is found to be within the total systematic uncertainty of this measurement.

The v_n distributions are obtained in various centrality intervals: over the 0-70% centrality range for v_2, 0-60% centrality range for v_3 and 0-45% centrality range for v_4. The measured v_2 distributions are found to approach that of a radial projection of a 2D Gaussian distribution centred around zero in the 0–2% centrality range, which is consistent with a scenario where fluctuations are the primary contribution to the overall shape (fluctuation-only scenario) for these most central collisions. Starting with the centrality interval 5-10%, the v_2 distributions differ significantly from this scenario, suggesting that they have a significant component associated with the average collision geometry in the reaction plane, v_2^{RP}. In contrast, the v_3 and v_4 distributions are consistent with a pure 2D Gaussian-fluctuation scenario (i.e., $v_n^{\mathrm{RP}} = 0$) over most of the measured centrality range. However, a systematic deviation from this fluctuation-only scenario is observed for v_3 in mid-central collisions, the presence of a non-zero v_3^{RP} can be allowed. Similarly, due to the limited range of the measured v_4 distribution, a non zero v_4^{RP} on the order of δ_{v_4} can not be excluded by this analysis.

The v_n distributions are also measured separately for charged particles with $0.5 < p_\mathrm{T} < 1\,\mathrm{GeV}$ and $p_\mathrm{T} > 1\,\mathrm{GeV}$. The shape of the unfolded distributions, when rescaled to the same $\langle v_n \rangle$, is found to be nearly the same for the two p_T ranges. This finding suggests that the hydrodynamic response to the eccentricity of the initial geometry has little variation in this p_T region. The ratios of the width to the mean, $\sigma_{v_n}/\langle v_n \rangle$, of these distributions are studied as a function of the average number of participating nucleons ($\langle N_{\mathrm{part}} \rangle$) and p_T. The values of $\sigma_{v_2}/\langle v_2 \rangle$ are observed to reach a minimum of 0.34 for $\langle N_{\mathrm{part}} \rangle \approx 200$, while the values of $\sigma_{v_3}/\langle v_3 \rangle$ and $\sigma_{v_4}/\langle v_4 \rangle$ are nearly independent of $\langle N_{\mathrm{part}} \rangle$ and are close to the value expected for a pure Gaussian-fluctuation scenario.

To understand further the role of average geometry and fluctuations for v_2, the v_2 distributions have been fitted to a Bessel-Gaussian function to estimate the value of v_2^{RP} and the width of the fluctuation δ_{v_2}. In central collisions, where v_2^{RP} values are small and change rapidly with $\langle N_{\mathrm{part}} \rangle$, narrow binning in centrality is necessary in order to obtain reliable estimates for these parameters. The values of $\delta_{v_2}/v_2^{\mathrm{RP}}$ are found to decrease with $\langle N_{\mathrm{part}} \rangle$ and reach a minimum of 0.38 ± 0.02 at $\langle N_{\mathrm{part}} \rangle \approx 200$, but then increase and are greater than one in central collisions. Furthermore, a systematic deviation of the fit from the data is observed for centralities starting in the 15-20% centrality interval, and becoming more pronounced for the more peripheral collisions, suggesting significant non-Gaussian behaviour in the flow fluctuations for collisions with small $\langle N_{\mathrm{part}} \rangle$. Multi-particle cumulant methods have been used to study such non-Gaussian behaviour. However, the v_2 coefficients for the four-, six- and eight-particle cumulants calculated from the v_2 distribution are found to agree with each other over the full centrality range to within 0.5%-2%. Hence the precision of experimental measurements of higher-order cumulants needs to be better than a few percent in order to be sensitive to the non-Gaussian behaviour in the v_n distributions.

To elucidate the relation between the azimuthal anisotropy and underlying collision geometry, the measured v_n distributions are compared with the eccentricity distributions of the initial geometry from the Glauber model and the MC-KLN model. Both models fail to describe the data consistently over most of the measured centrality range.

Acknowledgments

A Comprehensive performance and data plots

For reference, a more complete set of plots detailing the unfolding performance and cross-checks is presented. Figure 21 shows the distribution of the difference of the flow vectors $\vec{v}_2^{\,\mathrm{obs}}$ obtained for two half-IDs in peripheral collisions, calculated either without an η gap or with $\eta_{\mathrm{gap}} = 2$ between the two half-IDs. As mentioned in section 4.1, due to the small number of charged particles in the events, this distribution is expected to be described by the Student's t-distribution instead of the Gaussian distribution. Figures 22 and 23 show the dependence on the priors for v_2 and v_4 in the 20–25% centrality interval. Despite the very different shapes of the underlying flow distributions, the convergence is robust and independent of the prior. Figure 24 compares the unfolding performance for the single-particle and 2PC methods for several choices of η_{gap} and demonstrates the consistency of the two methods for all η_{gap} values considered. Figures 25 and 26 are similar to figure 11 but are obtained for other centrality intervals. They demonstrate that the shapes of the v_n distributions are the same for $0.5 < p_{\mathrm{T}} < 1\,\mathrm{GeV}$ and $p_{\mathrm{T}} > 1\,\mathrm{GeV}$ ranges in all centrality intervals. Figures 27 and 28 show a comparison between $\langle v_n \rangle$, $\sqrt{\langle v_n^2 \rangle}$ and v_n^{EP} in two different p_{T} ranges; the trends are similar to those seen in figure 13.

Figures 29 compares the v_2^{RP} from the Bessel-Gaussian fit of the v_2 distribution with $v_2^{\mathrm{calc}}\{2k\}$ values for $0.5 < p_{\mathrm{T}} < 1\,\mathrm{GeV}$ and $p_{\mathrm{T}} > 1\,\mathrm{GeV}$ ranges. The trends are similar to those seen in figure 16. However a slightly bigger deviation between v_2^{RP} and $v_2^{\mathrm{calc}}\{2k\}$ is observed in peripheral collisions for the $p_{\mathrm{T}} > 1\,\mathrm{GeV}$ range. Figures 30 and 31 show the Bessel-Gaussian fits to the v_2^{obs} and v_2 distributions in several centrality intervals. Deviations from the fits are observed in both types of distributions with a similar trend, but the deviations are smaller for the v_2^{obs} distributions. Figure 32 compares the centrality dependence of v_2^{RP} and δ_{v_2} from the fits to distributions before and after unfolding. The effects of smearing by the response function increase the values for δ_{v_2}, but the values of v_2^{RP} only increase slightly. This is expected since the true v_2 distributions in the bulk region are close to a Bessel-Gaussian shape and the smearing due to the response function is nearly Gaussian (see eqs. 1.4 and 4.7). The slightly larger v_2^{RP} values for the v_2^{obs} distribution may reflect non-flow contributions in v_2^{obs} or deviation of the response function from a Gaussian (figure 21).

Figure 33 shows the probability density distributions of v_2 for the full 0–5% centrality interval and the five individual 1% centrality intervals, together with the fits to the Bessel-Gaussian function. The deviation of the data from the Bessel-Gaussian description for the 0-5% centrality interval is due mainly to the rapid change of v_2^{RP} with centrality within this interval. This supports the need to use small centrality intervals for the most central collisions when calculating quantities such as $\langle v_2 \rangle$, σ_{v_2}, v_2^{RP} and δ_{v_2} (see figure 15).
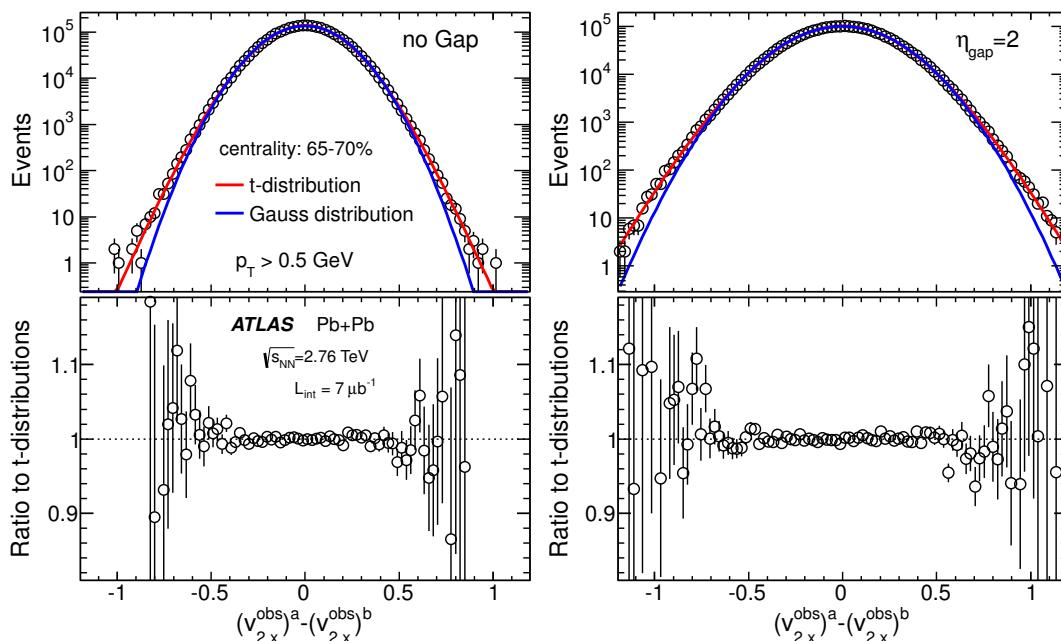
Figure 21. Top panels: the x-projection of the differences of $\vec{v}_2$ vectors calculated for the two half-IDs $p_{\text{sub}}\left((\vec{v}_2^{\text{obs}})^a - (\vec{v}_2^{\text{obs}})^b\right)$ (arbitrary normalization) for the 65–70% centrality interval with $\eta_{\text{gap}} = 0$ (left panel) and $\eta_{\text{gap}} = 2$ (right panel), together with fits to a Gaussian function and a Student's t-distribution. Bottom panels: the ratios of the data to the t-distribution fits. The distributions are wider for $\eta_{\text{gap}} = 2$ since the average number of tracks used is smaller.
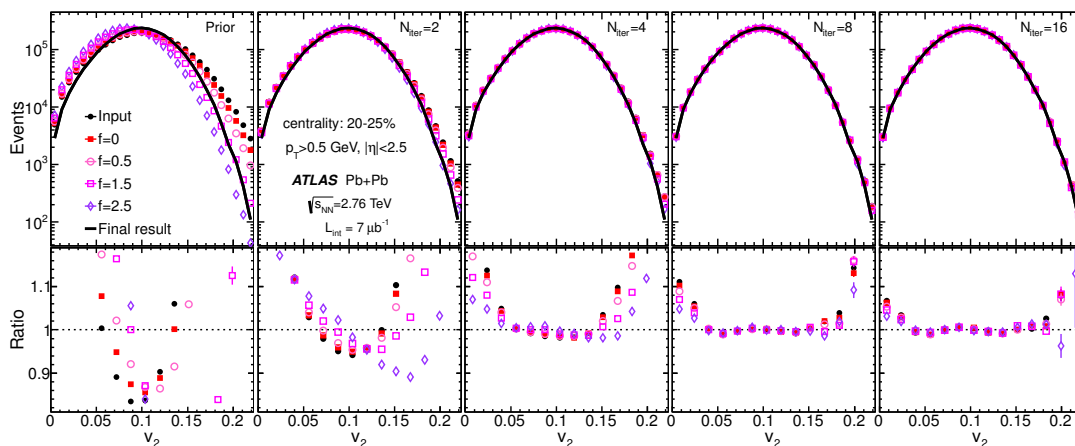
Figure 22. Convergence behaviour of v_2 in the 20–25% centrality interval for five choices of priors for several values of N_{iter}, increasing from left to right. The top panels show the distributions after a certain number of iterations and bottom panels show the ratios to the result for $N_{\text{iter}} = 128$. A common reference, shown by the solid lines in the top panels, is calculated by averaging the result for $f = 0$ and $f = 0.5$ (eq. (4.13)) with $N_{\text{iter}} = 128$.
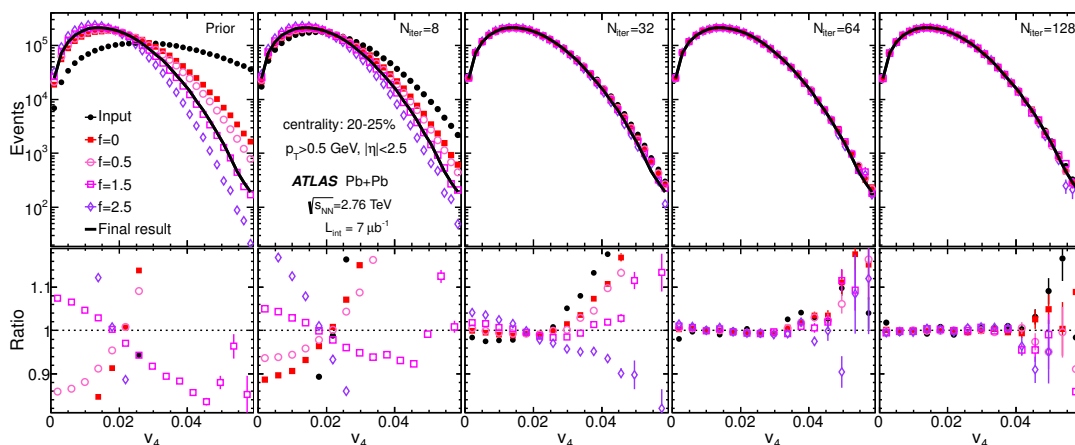
Figure 23. Convergence behaviour of v_4 in the 20–25% centrality interval for five choices of priors for several values of N_{iter}, increasing from left to right. The top panels show the distributions after a certain number of iterations and bottom panels show the ratios to the result for $N_{\mathrm{iter}} = 128$. A common reference, shown by the solid lines in the top panels, is calculated by averaging the result for $f = 0$ and $f = 0.5$ (eq. (4.13)) with $N_{\mathrm{iter}} = 128$.
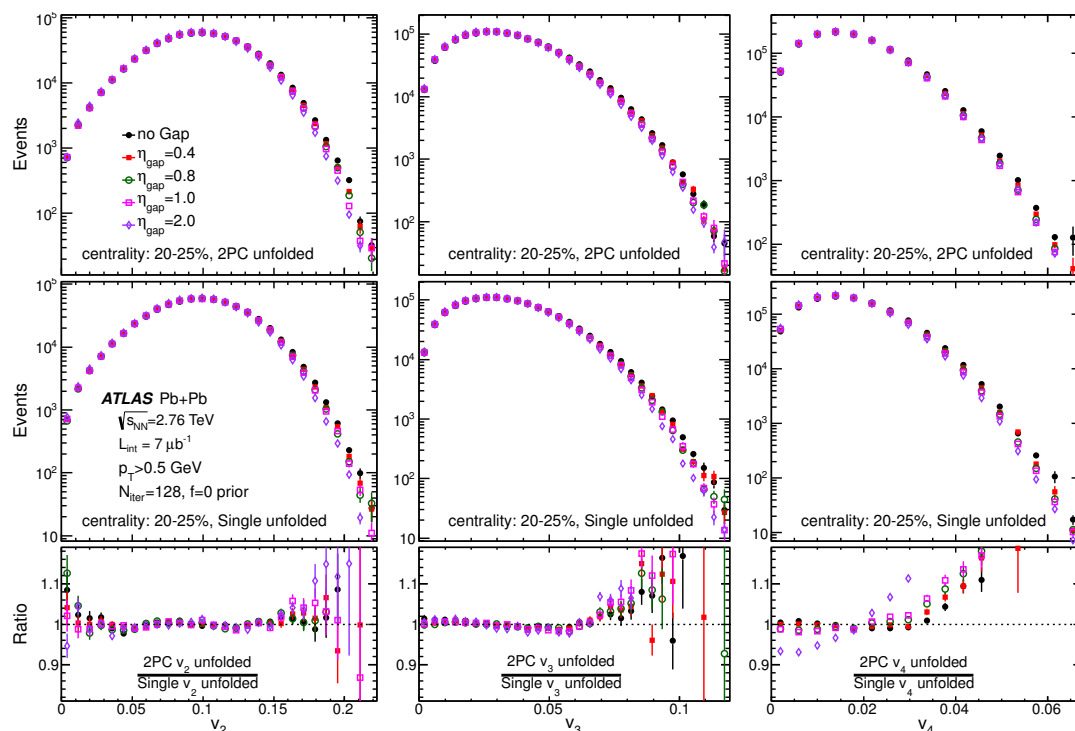
Figure 24. The unfolded distributions from 2PC method (top row), single-particle method (middle row) and the ratios of the two (bottom row) for different values of η_{gap} in the 20–25% centrality interval and for $n = 2$ (left panels), $n = 3$ (middle panels) and $n = 4$ (right panels).
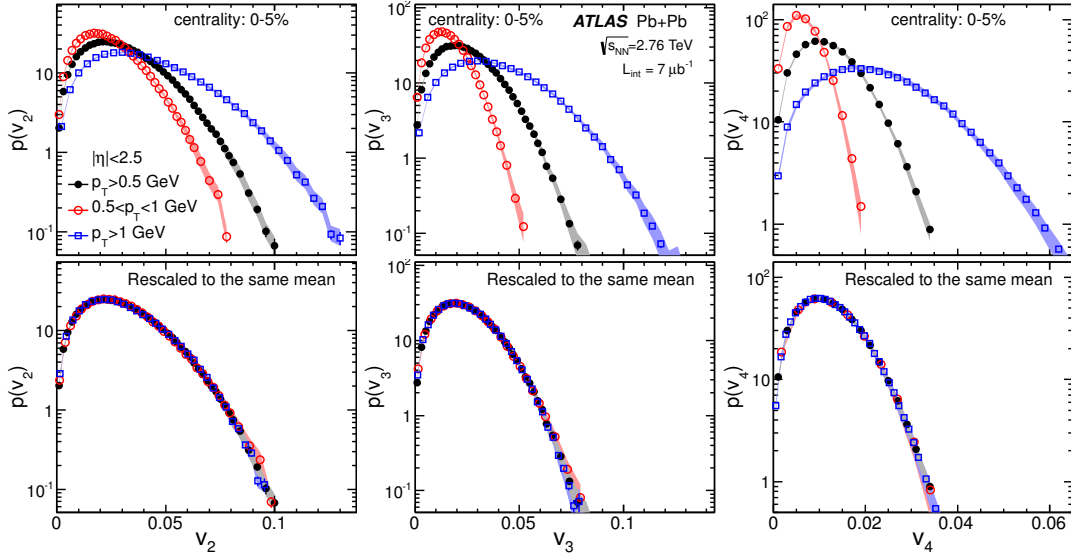
Figure 25. Top panels: the unfolded distributions for v_n in the 0–5% centrality interval for charged particles in the $p_T > 0.5\,\mathrm{GeV}$, $0.5 < p_T < 1\,\mathrm{GeV}$ and $p_T > 1\,\mathrm{GeV}$ ranges. Bottom panels: same distributions but rescaled horizontally so the $\langle v_n \rangle$ values match that for the $p_T > 0.5\,\mathrm{GeV}$ range. The shaded bands represent the systematic uncertainties on the v_n-shape.
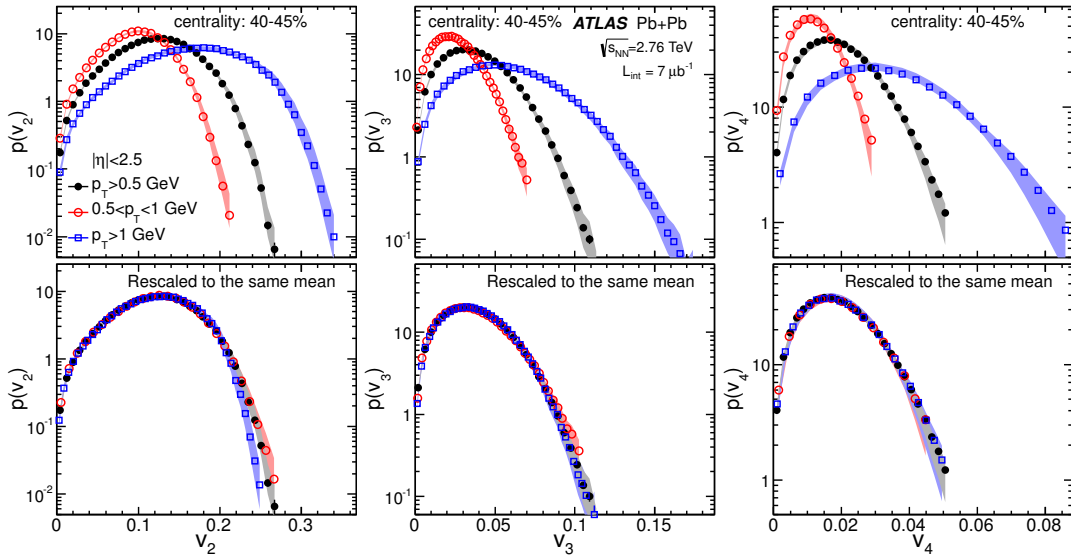
Figure 26. Top panels: the unfolded distributions for v_n in the 40–45% centrality interval for charged particles in the $p_T > 0.5\,\mathrm{GeV}$, $0.5 < p_T < 1\,\mathrm{GeV}$ and $p_T > 1\,\mathrm{GeV}$ ranges. Bottom panels: same distributions but rescaled horizontally so the $\langle v_n \rangle$ values match that for the $p_T > 0.5\,\mathrm{GeV}$ range. The shaded bands represent the systematic uncertainties on the v_n-shape.
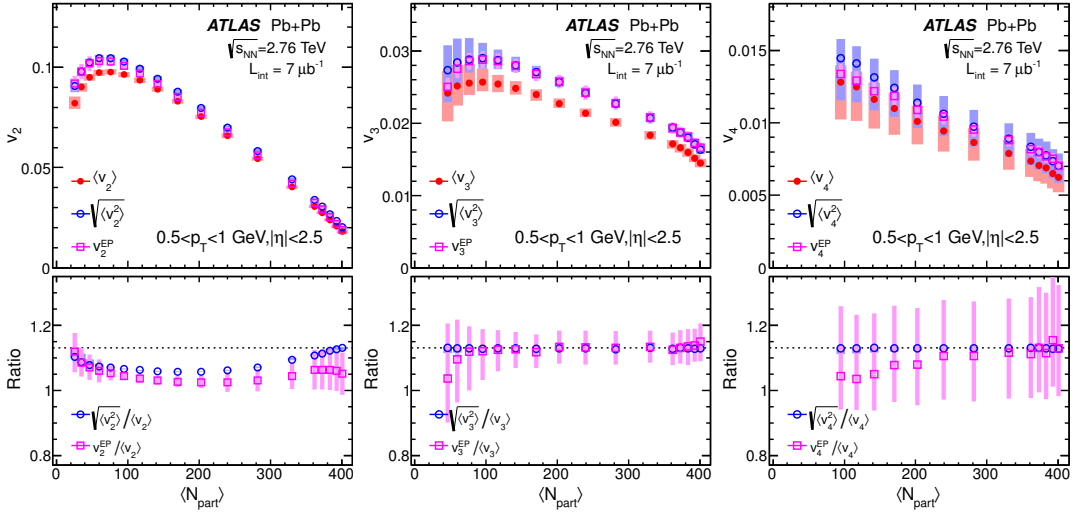
Figure 27. Top panels: comparison of $\langle v_n \rangle$ and $\sqrt{\langle v_n^2 \rangle} \equiv \sqrt{\langle v_n \rangle^2 + \sigma_{v_n}^2}$, derived from the EbyE v_n distributions, with the v_n^{EP} [16], for charged particles in the $0.5 < p_{\mathrm{T}} < 1\,\mathrm{GeV}$ range. Bottom panels: the ratios of $\sqrt{\langle v_n^2 \rangle}$ and v_n^{EP} to $\langle v_n \rangle$. The shaded bands represent the systematic uncertainties. The dotted lines in bottom panels indicate $\sqrt{\langle v_n^2 \rangle}/\langle v_n \rangle = 1.13$, the value expected for the radial projection of a 2D Gaussian distribution (eq. (1.8)).
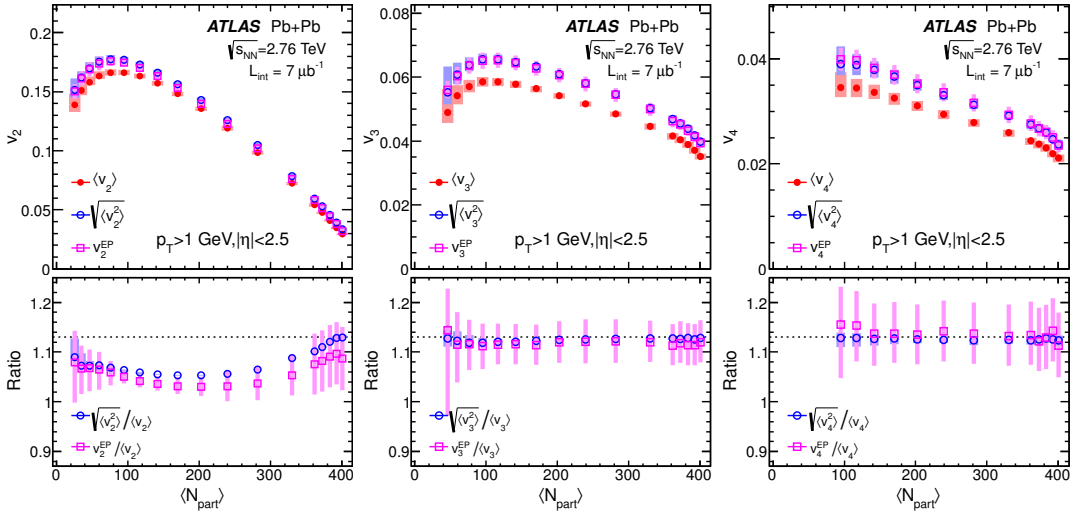
Figure 28. Top panels: comparison of $\langle v_n \rangle$ and $\sqrt{\langle v_n^2 \rangle} \equiv \sqrt{\langle v_n \rangle^2 + \sigma_{v_n}^2}$, derived from the EbyE v_n distributions, with the v_n^{EP} [16], for charged particles in the $p_{\mathrm{T}} > 1\,\mathrm{GeV}$ range. Bottom panels: the ratios of $\sqrt{\langle v_n^2 \rangle}$ and v_n^{EP} to $\langle v_n \rangle$. The shaded bands represent the systematic uncertainties. The dotted lines in bottom panels indicate $\sqrt{\langle v_n^2 \rangle}/\langle v_n \rangle = 1.13$, the value expected for the radial projection of a 2D Gaussian distribution (eq. (1.8)).
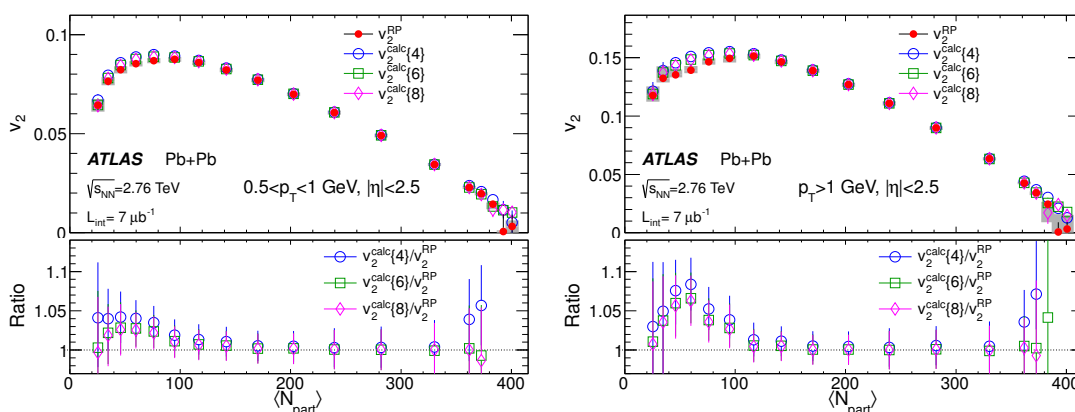
Figure 29. Comparison in $0.5 < p_T < 1\,\mathrm{GeV}$ (left panel) and $p_T > 1\,\mathrm{GeV}$ (right panel) of the v_2^{RP} obtained from the Bessel-Gaussian fit of the v_2 distributions with the values for four-particle ($v_2^{\mathrm{calc}}\{4\}$), six-particle ($v_2^{\mathrm{calc}}\{6\}$) and eight-particle ($v_2^{\mathrm{calc}}\{8\}$) cumulants calculated directly from the v_2 distributions via eq. (5.3). The bottom part of each panel shows the ratios of the cumulants to the fit results, with the error bars representing the total uncertainties.
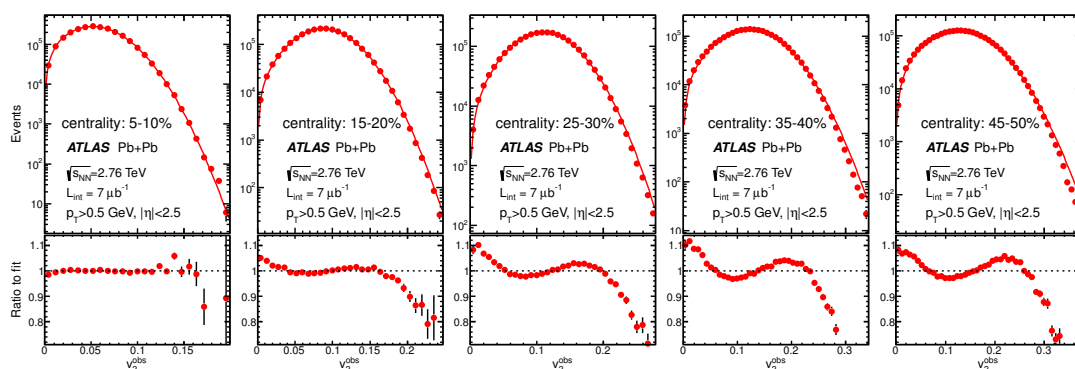
Figure 30. The v_2^{obs} distributions before unfolding (top) and their ratios to the Bessel-Gaussian fits (bottom) in various centrality ranges (see legends).
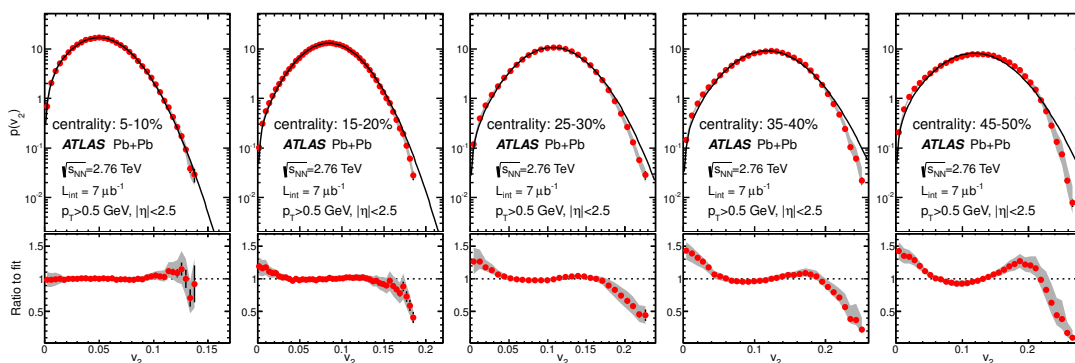
Figure 31. The final v_2 distributions obtained from unfolding (top) and their ratios to the Bessel-Gaussian fits (bottom) in various centrality ranges (see legends).
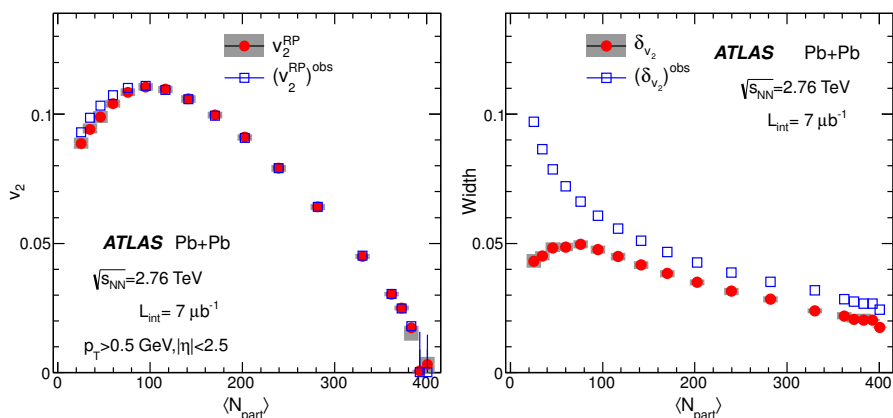
Figure 32. The values of v_2^{RP} and $(v_2^{\mathrm{RP}})^{\mathrm{obs}}$ (left panel) and the values of δ_{v_2} and $(\delta_{v_2})^{\mathrm{obs}}$ (right panel) obtained from the Bessel-Gaussian fits to the v_2 and v_2^{obs} distributions.
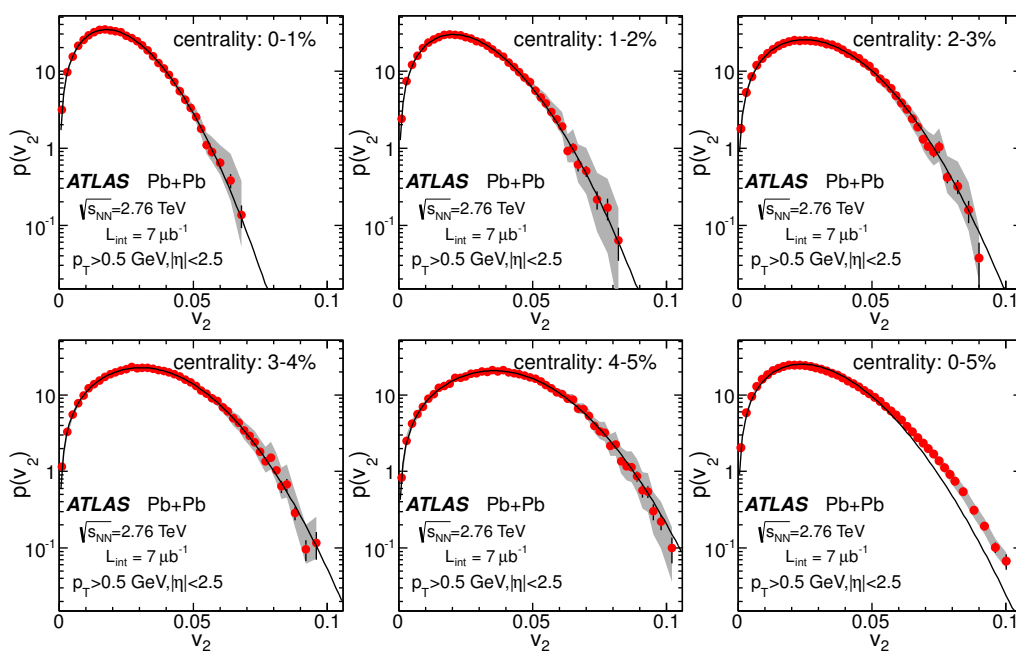
Figure 33. The probability density distributions of v_2 for the 0–5% centrality interval and the five individual 1% centrality ranges, together with the fit to the Bessel-Gaussian function.

References

[1] J.-Y. Ollitrault, *Anisotropy as a signature of transverse collective flow*, *Phys. Rev.* **D 46** (1992) 229 [ɪɴSPIRE].

[2] A.M. Poskanzer and S. Voloshin, *Methods for analyzing anisotropic flow in relativistic nuclear collisions*, *Phys. Rev.* **C 58** (1998) 1671 [nucl-ex/9805001] [ɪɴSPIRE].

[3] B. Alver and G. Roland, *Collision geometry fluctuations and triangular flow in heavy-ion collisions*, *Phys. Rev.* **C 81** (2010) 054905 [*Erratum ibid.* **C 82** (2010) 039903] [arXiv:1003.0194] [ɪɴSPIRE].

[4] G.-Y. Qin, H. Petersen, S.A. Bass and B. Müller, *Translation of collision geometry fluctuations into momentum anisotropies in relativistic heavy-ion collisions*, *Phys. Rev.* **C 82** (2010) 064903 [arXiv:1009.1847] [ɪɴSPIRE].

[5] D. Teaney and L. Yan, *Triangularity and dipole asymmetry in heavy ion collisions*, *Phys. Rev.* **C 83** (2011) 064904 [arXiv:1010.1876] [ɪɴSPIRE].

[6] Z. Qiu and U.W. Heinz, *Event-by-event shape and flow fluctuations of relativistic heavy-ion collision fireballs*, *Phys. Rev.* **C 84** (2011) 024911 [arXiv:1104.0650] [ɪɴSPIRE].

[7] S.A. Voloshin, A.M. Poskanzer and R. Snellings, *Collective phenomena in non-central nuclear collisions*, arXiv:0809.2949 [ɪɴSPIRE].

[8] D.A. Teaney, *Viscous hydrodynamics and the quark gluon plasma*, arXiv:0905.2433 [ɪɴSPIRE].

[9] B.H. Alver, C. Gombeaud, M. Luzum and J.-Y. Ollitrault, *Triangular flow in hydrodynamics and transport theory*, *Phys. Rev.* **C 82** (2010) 034913 [arXiv:1007.5469] [ɪɴSPIRE].

[10] C. Gale, S. Jeon, B. Schenke, P. Tribedy and R. Venugopalan, *Event-by-event anisotropic flow in heavy-ion collisions from combined Yang-Mills and viscous fluid dynamics*, *Phys. Rev. Lett.* **110** (2013) 012302 [arXiv:1209.6330] [ɪɴSPIRE].

[11] H. Niemi, G. Denicol, H. Holopainen and P. Huovinen, *Event-by-event distributions of azimuthal asymmetries in ultrarelativistic heavy-ion collisions*, *Phys. Rev.* **C 87** (2013) 054901 [arXiv:1212.1008] [ɪɴSPIRE].

[12] PHENIX collaboration, A. Adare et al., *Measurements of higher-order flow harmonics in Au+Au collisions at $\sqrt{s_{NN}} = 200$ GeV*, *Phys. Rev. Lett.* **107** (2011) 252301 [arXiv:1105.3928] [ɪɴSPIRE].

[13] STAR collaboration, L. Adamczyk et al., *Third harmonic flow of charged particles in Au+Au collisions at $\sqrt{s_{NN}} = 200$ GeV*, *Phys. Rev.* **C 88** (2013) 014904 [arXiv:1301.2187] [ɪɴSPIRE].

[14] ALICE collaboration, *Harmonic decomposition of two-particle angular correlations in Pb-Pb collisions at $\sqrt{s_{NN}} = 2.76$ TeV*, *Phys. Lett.* **B 708** (2012) 249 [arXiv:1109.2501] [ɪɴSPIRE].

[15] ATLAS collaboration, *Measurement of the pseudorapidity and transverse momentum dependence of the elliptic flow of charged particles in lead-lead collisions at $\sqrt{s_{NN}} = 2.76$ TeV with the ATLAS detector*, *Phys. Lett.* **B 707** (2012) 330 [arXiv:1108.6018] [ɪɴSPIRE].

[16] ATLAS collaboration, *Measurement of the azimuthal anisotropy for charged particle production in $\sqrt{s_{NN}} = 2.76$ TeV lead-lead collisions with the ATLAS detector*, *Phys. Rev.* **C 86** (2012) 014907 [arXiv:1203.3087] [ɪɴSPIRE].

[17] CMS collaboration, *Centrality dependence of dihadron correlations and azimuthal anisotropy harmonics in PbPb collisions at $\sqrt{s_{NN}} = 2.76$ TeV*, *Eur. Phys. J.* **C 72** (2012) 2012 [arXiv:1201.3158] [ɪɴSPIRE].

[18] CMS collaboration, *Measurement of the elliptic anisotropy of charged particles produced in PbPb collisions at nucleon-nucleon center-of-mass energy = 2.76 TeV*, *Phys. Rev.* **C 87** (2013) 014902 [arXiv:1204.1409] [inSPIRE].

[19] PHOBOS collaboration, B. Alver et al., *Event-by-event fluctuations of azimuthal particle anisotropy in Au + Au collisions at $\sqrt{s_{NN}}$ = 200 GeV*, *Phys. Rev. Lett.* **104** (2010) 142301 [nucl-ex/0702036] [inSPIRE].

[20] N. Borghini, P.M. Dinh and J.-Y. Ollitrault, *A new method for measuring azimuthal distributions in nucleus-nucleus collisions*, *Phys. Rev.* **C 63** (2001) 054906 [nucl-th/0007063] [inSPIRE].

[21] STAR collaboration, G. Agakishiev et al., *Energy and system-size dependence of two- and four-particle v_2 measurements in heavy-ion collisions at RHIC and their implications on flow fluctuations and nonflow*, *Phys. Rev.* **C 86** (2012) 014904 [arXiv:1111.5637] [inSPIRE].

[22] ALICE collaboration, *Anisotropic flow of charged hadrons, pions and (anti-)protons measured at high transverse momentum in Pb-Pb collisions at $\sqrt{s_{NN}}$ = 2.76 TeV*, *Phys. Lett.* **B 719** (2013) 18 [arXiv:1205.5761] [inSPIRE].

[23] S.A. Voloshin, A.M. Poskanzer, A. Tang and G. Wang, *Elliptic flow in the Gaussian model of eccentricity fluctuations*, *Phys. Lett.* **B 659** (2008) 537 [arXiv:0708.0800] [inSPIRE].

[24] R.S. Bhalerao and J.-Y. Ollitrault, *Eccentricity fluctuations and elliptic flow at RHIC*, *Phys. Lett.* **B 641** (2006) 260 [nucl-th/0607009] [inSPIRE].

[25] B. Alver et al., *Importance of correlations and fluctuations on the initial source eccentricity in high-energy nucleus-nucleus collisions*, *Phys. Rev.* **C 77** (2008) 014906 [arXiv:0711.3724] [inSPIRE].

[26] S. Voloshin and Y. Zhang, *Flow study in relativistic nuclear collisions by Fourier expansion of azimuthal particle distributions*, *Z. Phys.* **C 70** (1996) 665 [hep-ph/9407282] [inSPIRE].

[27] W. Broniowski, P. Bozek and M. Rybczynski, *Fluctuating initial conditions in heavy-ion collisions from the Glauber approach*, *Phys. Rev.* **C 76** (2007) 054905 [arXiv:0706.4266] [inSPIRE].

[28] J.-Y. Ollitrault, A.M. Poskanzer and S.A. Voloshin, *Effect of flow fluctuations and nonflow on elliptic flow methods*, *Phys. Rev.* **C 80** (2009) 014904 [arXiv:0904.2315] [inSPIRE].

[29] STAR collaboration, J. Adams et al., *Azimuthal anisotropy in Au+Au collisions at $\sqrt{s_{NN}}$ = 200 GeV*, *Phys. Rev.* **C 72** (2005) 014904 [nucl-ex/0409033] [inSPIRE].

[30] ALICE collaboration, *Anisotropic flow of charged particles at $\sqrt{s_{NN}}$ = 2.76 TeV measured with the ALICE detector*, *J. Phys.* **G 38** (2011) 124052 [arXiv:1106.6209] [inSPIRE].

[31] J. Jia and S. Mohapatra, *Disentangling flow and nonflow correlations via Bayesian unfolding of the event-by-event distributions of harmonic coefficients in ultrarelativistic heavy-ion collisions*, *Phys. Rev.* **C 88** (2013) 014907 [arXiv:1304.1471] [inSPIRE].

[32] ATLAS collaboration, *The ATLAS experiment at the CERN Large Hadron Collider*, 2008 *JINST* **3** S08003 [inSPIRE].

[33] ATLAS collaboration, *Jet energy measurement with the ATLAS detector in proton-proton collisions at $\sqrt{s}$ = 7 TeV*, *Eur. Phys. J.* **C 73** (2013) 2304 [arXiv:1112.6426] [inSPIRE].

[34] ATLAS collaboration, *Measurement of the centrality dependence of the charged particle pseudorapidity distribution in lead-lead collisions at $\sqrt{s_{NN}}$ = 2.76 TeV with the ATLAS detector*, *Phys. Lett.* **B 710** (2012) 363 [arXiv:1108.6027] [inSPIRE].

[35] M.L. Miller, K. Reygers, S.J. Sanders and P. Steinberg, *Glauber modeling in high energy nuclear collisions*, *Ann. Rev. Nucl. Part. Sci.* **57** (2007) 205 [nucl-ex/0701025] [inSPIRE].

[36] ATLAS collaboration, *Charged-particle multiplicities in pp interactions measured with the ATLAS detector at the LHC*, *New J. Phys.* **13** (2011) 053033 [arXiv:1012.5104] [INSPIRE].

[37] M. Gyulassy and X.-N. Wang, *HIJING 1.0: a Monte Carlo program for parton and particle production in high-energy hadronic and nuclear collisions*, *Comput. Phys. Commun.* **83** (1994) 307 [nucl-th/9502021] [INSPIRE].

[38] M. Masera, G. Ortona, M. Poghosyan and F. Prino, *Anisotropic transverse flow introduction in Monte Carlo generators for heavy ion collisions*, *Phys. Rev.* **C 79** (2009) 064909 [INSPIRE].

[39] GEANT4 collaboration, S. Agostinelli et al., *GEANT4: a simulation toolkit*, *Nucl. Instrum. Meth.* **A 506** (2003) 250 [INSPIRE].

[40] ATLAS collaboration, *Measurement of the centrality dependence of charged particle spectra and RCP in lead-lead collisions at $\sqrt{s_{NN}} = 2.76$ TeV with the ATLAS detector at the LHC*, ATLAS-CONF-2011-079 (2011).

[41] G. D'Agostini, *A multidimensional unfolding method based on Bayes' theorem*, *Nucl. Instrum. Meth.* **A 362** (1995) 487 [INSPIRE].

[42] T. Adye, *Unfolding algorithms and tests using RooUnfold*, arXiv:1105.1160 [INSPIRE].

[43] G. Bohm and G. Zech, *Introduction to statistics and measurement analysis for physicists*, DESY, Hamburg Germany (2010).

[44] ALICE collaboration, *Higher harmonic anisotropic flow measurements of charged particles in Pb-Pb collisions at $\sqrt{s_{NN}} = 2.76$ TeV*, *Phys. Rev. Lett.* **107** (2011) 032301 [arXiv:1105.3865] [INSPIRE].

[45] H.-J. Drescher, A. Dumitru, A. Hayashigaki and Y. Nara, *The eccentricity in heavy-ion collisions from color glass condensate initial conditions*, *Phys. Rev.* **C 74** (2006) 044905 [nucl-th/0605012] [INSPIRE].

The ATLAS collaboration

G. Aad[48], T. Abajyan[21], B. Abbott[112], J. Abdallah[12], S. Abdel Khalek[116], A.A. Abdelalim[49],
O. Abdinov[11], R. Aben[106], B. Abi[113], M. Abolins[89], O.S. AbouZeid[159], H. Abramowicz[154],
H. Abreu[137], Y. Abulaiti[147a,147b], B.S. Acharya[165a,165b,a], L. Adamczyk[38a], D.L. Adams[25],
T.N. Addy[56], J. Adelman[177], S. Adomeit[99], T. Adye[130], S. Aefsky[23], J.A. Aguilar-Saavedra[125b,b],
M. Agustoni[17], S.P. Ahlen[22], F. Ahles[48], A. Ahmad[149], M. Ahsan[41], G. Aielli[134a,134b],
T.P.A. Åkesson[80], G. Akimoto[156], A.V. Akimov[95], M.A. Alam[76], J. Albert[170], S. Albrand[55],
M.J. Alconada Verzini[70], M. Aleksa[30], I.N. Aleksandrov[64], F. Alessandria[90a], C. Alexa[26a],
G. Alexander[154], G. Alexandre[49], T. Alexopoulos[10], M. Alhroob[165a,165c], M. Aliev[16],
G. Alimonti[90a], J. Alison[31], B.M.M. Allbrooke[18], L.J. Allison[71], P.P. Allport[73],
S.E. Allwood-Spiers[53], J. Almond[83], A. Aloisio[103a,103b], R. Alon[173], A. Alonso[36], F. Alonso[70],
A. Altheimer[35], B. Alvarez Gonzalez[89], M.G. Alviggi[103a,103b], K. Amako[65],
Y. Amaral Coutinho[24a], C. Amelung[23], V.V. Ammosov[129,*], S.P. Amor Dos Santos[125a],
A. Amorim[125a,c], S. Amoroso[48], N. Amram[154], C. Anastopoulos[30], L.S. Ancu[17], N. Andari[30],
T. Andeen[35], C.F. Anders[58b], G. Anders[58a], K.J. Anderson[31], A. Andreazza[90a,90b], V. Andrei[58a],
X.S. Anduaga[70], S. Angelidakis[9], P. Anger[44], A. Angerami[35], F. Anghinolfi[30], A. Anisenkov[108],
N. Anjos[125a], A. Annovi[47], A. Antonaki[9], M. Antonelli[47], A. Antonov[97], J. Antos[145b],
F. Anulli[133a], M. Aoki[102], L. Aperio Bella[18], R. Apolle[119,d], G. Arabidze[89], I. Aracena[144],
Y. Arai[65], A.T.H. Arce[45], S. Arfaoui[149], J-F. Arguin[94], S. Argyropoulos[42], E. Arik[19a,*],
M. Arik[19a], A.J. Armbruster[88], O. Arnaez[82], V. Arnal[81], A. Artamonov[96], G. Artoni[133a,133b],
D. Arutinov[21], S. Asai[156], N. Asbah[94], S. Ask[28], B. Åsman[147a,147b], L. Asquith[6], K. Assamagan[25],
R. Astalos[145a], A. Astbury[170], M. Atkinson[166], B. Auerbach[6], E. Auge[116], K. Augsten[127],
M. Aurousseau[146b], G. Avolio[30], D. Axen[169], G. Azuelos[94,e], Y. Azuma[156], M.A. Baak[30],
C. Bacci[135a,135b], A.M. Bach[15], H. Bachacou[137], K. Bachas[155], M. Backes[49], M. Backhaus[21],
J. Backus Mayes[144], E. Badescu[26a], P. Bagiacchi[133a,133b], P. Bagnaia[133a,133b], Y. Bai[33a],
D.C. Bailey[159], T. Bain[35], J.T. Baines[130], O.K. Baker[177], S. Baker[77], P. Balek[128], F. Balli[137],
E. Banas[39], P. Banerjee[94], Sw. Banerjee[174], D. Banfi[30], A. Bangert[151], V. Bansal[170], H.S. Bansil[18],
L. Barak[173], S.P. Baranov[95], T. Barber[48], E.L. Barberio[87], D. Barberis[50a,50b], M. Barbero[84],
D.Y. Bardin[64], T. Barillari[100], M. Barisonzi[176], T. Barklow[144], N. Barlow[28], B.M. Barnett[130],
R.M. Barnett[15], A. Baroncelli[135a], G. Barone[49], A.J. Barr[119], F. Barreiro[81], J. Barreiro
Guimarães da Costa[57], R. Bartoldus[144], A.E. Barton[71], V. Bartsch[150], A. Basye[166], R.L. Bates[53],
L. Batkova[145a], J.R. Batley[28], A. Battaglia[17], M. Battistin[30], F. Bauer[137], H.S. Bawa[144,f],
S. Beale[99], T. Beau[79], P.H. Beauchemin[162], R. Beccherle[50a], P. Bechtle[21], H.P. Beck[17],
K. Becker[176], S. Becker[99], M. Beckingham[139], K.H. Becks[176], A.J. Beddall[19c], A. Beddall[19c],
S. Bedikian[177], V.A. Bednyakov[64], C.P. Bee[84], L.J. Beemster[106], T.A. Beermann[176], M. Begel[25],
C. Belanger-Champagne[86], P.J. Bell[49], W.H. Bell[49], G. Bella[154], L. Bellagamba[20a], A. Bellerive[29],
M. Bellomo[30], A. Belloni[57], O. Beloborodova[108,g], K. Belotskiy[97], O. Beltramello[30], O. Benary[154],
D. Benchekroun[136a], K. Bendtz[147a,147b], N. Benekos[166], Y. Benhammou[154], E. Benhar Noccioli[49],
J.A. Benitez Garcia[160b], D.P. Benjamin[45], J.R. Bensinger[23], K. Benslama[131], S. Bentvelsen[106],
D. Berge[30], E. Bergeaas Kuutmann[16], N. Berger[5], F. Berghaus[170], E. Berglund[106], J. Beringer[15],
P. Bernat[77], R. Bernhard[48], C. Bernius[78], F.U. Bernlochner[170], T. Berry[76], C. Bertella[84],
F. Bertolucci[123a,123b], M.I. Besana[90a,90b], G.J. Besjes[105], N. Besson[137], S. Bethke[100], W. Bhimji[46],
R.M. Bianchi[30], L. Bianchini[23], M. Bianco[72a,72b], O. Biebel[99], S.P. Bieniek[77], K. Bierwagen[54],
J. Biesiada[15], M. Biglietti[135a], H. Bilokon[47], M. Bindi[20a,20b], S. Binet[116], A. Bingul[19c],
C. Bini[133a,133b], B. Bittner[100], C.W. Black[151], J.E. Black[144], K.M. Black[22], D. Blackburn[139],
R.E. Blair[6], J.-B. Blanchard[137], T. Blazek[145a], I. Bloch[42], C. Blocker[23], J. Blocki[39], W. Blum[82],
U. Blumenschein[54], G.J. Bobbink[106], V.S. Bobrovnikov[108], S.S. Bocchetta[80], A. Bocci[45],
C.R. Boddy[119], M. Boehler[48], J. Boek[176], T.T. Boek[176], N. Boelaert[36], J.A. Bogaerts[30],
A. Bogdanchikov[108], A. Bogouch[91,*], C. Bohm[147a], J. Bohm[126], V. Boisvert[76], T. Bold[38a],
V. Boldea[26a], N.M. Bolnet[137], M. Bomben[79], M. Bona[75], M. Boonekamp[137], S. Bordoni[79],
C. Borer[17], A. Borisov[129], G. Borissov[71], M. Borri[83], S. Borroni[42], J. Bortfeldt[99],
V. Bortolotto[135a,135b], K. Bos[106], D. Boscherini[20a], M. Bosman[12], H. Boterenbrood[106],

J. Bouchami[94], J. Boudreau[124], E.V. Bouhova-Thacker[71], D. Boumediene[34], C. Bourdarios[116],
N. Bousson[84], S. Boutouil[136d], A. Boveia[31], J. Boyd[30], I.R. Boyko[64], I. Bozovic-Jelisavcic[13b],
J. Bracinik[18], P. Branchini[135a], A. Brandt[8], G. Brandt[15], O. Brandt[54], U. Bratzler[157], B. Brau[85],
J.E. Brau[115], H.M. Braun[176,*], S.F. Brazzale[165a,165c], B. Brelier[159], J. Bremer[30],
K. Brendlinger[121], R. Brenner[167], S. Bressler[173], T.M. Bristow[146c], D. Britton[53], F.M. Brochu[28],
I. Brock[21], R. Brock[89], F. Broggi[90a], C. Bromberg[89], J. Bronner[100], G. Brooijmans[35],
T. Brooks[76], W.K. Brooks[32b], E. Brost[115], G. Brown[83], P.A. Bruckman de Renstrom[39],
D. Bruncko[145b], R. Bruneliere[48], S. Brunet[60], A. Bruni[20a], G. Bruni[20a], M. Bruschi[20a],
L. Bryngemark[80], T. Buanes[14], Q. Buat[55], F. Bucci[49], J. Buchanan[119], P. Buchholz[142],
R.M. Buckingham[119], A.G. Buckley[46], S.I. Buda[26a], I.A. Budagov[64], B. Budick[109], L. Bugge[118],
O. Bulekov[97], A.C. Bundock[73], M. Bunse[43], T. Buran[118,*], H. Burckhart[30], S. Burdin[73],
T. Burgess[14], S. Burke[130], E. Busato[34], V. Büscher[82], P. Bussey[53], C.P. Buszello[167], B. Butler[57],
J.M. Butler[22], C.M. Buttar[53], J.M. Butterworth[77], W. Buttinger[28], M. Byszewski[10], S. Cabrera
Urbán[168], D. Caforio[20a,20b], O. Cakir[4a], P. Calafiura[15], G. Calderini[79], P. Calfayan[99],
R. Calkins[107], L.P. Caloba[24a], R. Caloi[133a,133b], D. Calvet[34], S. Calvet[34], R. Camacho Toro[49],
P. Camarri[134a,134b], D. Cameron[118], L.M. Caminada[15], R. Caminal Armadans[12], S. Campana[30],
M. Campanelli[77], V. Canale[103a,103b], F. Canelli[31], A. Canepa[160a], J. Cantero[81], R. Cantrill[76],
T. Cao[40], M.D.M. Capeans Garrido[30], I. Caprini[26a], M. Caprini[26a], D. Capriotti[100],
M. Capua[37a,37b], R. Caputo[82], R. Cardarelli[134a], T. Carli[30], G. Carlino[103a], L. Carminati[90a,90b],
S. Caron[105], E. Carquin[32b], G.D. Carrillo-Montoya[146c], A.A. Carter[75], J.R. Carter[28],
J. Carvalho[125a,h], D. Casadei[109], M.P. Casado[12], M. Cascella[123a,123b], C. Caso[50a,50b,*],
E. Castaneda-Miranda[174], A. Castelli[106], V. Castillo Gimenez[168], N.F. Castro[125a], G. Cataldi[72a],
P. Catastini[57], A. Catinaccio[30], J.R. Catmore[30], A. Cattai[30], G. Cattani[134a,134b], S. Caughron[89],
V. Cavaliere[166], D. Cavalli[90a], M. Cavalli-Sforza[12], V. Cavasinni[123a,123b], F. Ceradini[135a,135b],
B. Cerio[45], A.S. Cerqueira[24b], A. Cerri[15], L. Cerrito[75], F. Cerutti[15], A. Cervelli[17], S.A. Cetin[19b],
A. Chafaq[136a], D. Chakraborty[107], I. Chalupkova[128], K. Chan[3], P. Chang[166], B. Chapleau[86],
J.D. Chapman[28], J.W. Chapman[88], D.G. Charlton[18], V. Chavda[83], C.A. Chavez Barajas[30],
S. Cheatham[86], S. Chekanov[6], S.V. Chekulaev[160a], G.A. Chelkov[64], M.A. Chelstowska[105],
C. Chen[63], H. Chen[25], S. Chen[33c], X. Chen[174], Y. Chen[35], Y. Cheng[31], A. Cheplakov[64],
R. Cherkaoui El Moursli[136e], V. Chernyatin[25], E. Cheu[7], S.L. Cheung[159], L. Chevalier[137],
V. Chiarella[47], G. Chiefari[103a,103b], J.T. Childers[30], A. Chilingarov[71], G. Chiodini[72a],
A.S. Chisholm[18], R.T. Chislett[77], A. Chitan[26a], M.V. Chizhov[64], G. Choudalakis[31],
S. Chouridou[9], B.K.B. Chow[99], I.A. Christidi[77], A. Christov[48], D. Chromek-Burckhart[30],
M.L. Chu[152], J. Chudoba[126], G. Ciapetti[133a,133b], A.K. Ciftci[4a], R. Ciftci[4a], D. Cinca[62],
V. Cindro[74], A. Ciocio[15], M. Cirilli[88], P. Cirkovic[13b], Z.H. Citron[173], M. Citterio[90a],
M. Ciubancan[26a], A. Clark[49], P.J. Clark[46], R.N. Clarke[15], J.C. Clemens[84], B. Clement[55],
C. Clement[147a,147b], Y. Coadou[84], M. Cobal[165a,165c], A. Coccaro[139], J. Cochran[63], S. Coelli[90a],
L. Coffey[23], J.G. Cogan[144], J. Coggeshall[166], J. Colas[5], S. Cole[107], A.P. Colijn[106], N.J. Collins[18],
C. Collins-Tooth[53], J. Collot[55], T. Colombo[120a,120b], G. Colon[85], G. Compostella[100], P. Conde
Muiño[125a], E. Coniavitis[167], M.C. Conidi[12], S.M. Consonni[90a,90b], V. Consorti[48],
S. Constantinescu[26a], C. Conta[120a,120b], G. Conti[57], F. Conventi[103a,i], M. Cooke[15],
B.D. Cooper[77], A.M. Cooper-Sarkar[119], N.J. Cooper-Smith[76], K. Copic[15], T. Cornelissen[176],
M. Corradi[20a], F. Corriveau[86,j], A. Corso-Radu[164], A. Cortes-Gonzalez[166], G. Cortiana[100],
G. Costa[90a], M.J. Costa[168], D. Costanzo[140], D. Côté[30], G. Cottin[32a], L. Courneyea[170],
G. Cowan[76], B.E. Cox[83], K. Cranmer[109], S. Crépé-Renaudin[55], F. Crescioli[79], M. Cristinziani[21],
G. Crosetti[37a,37b], C.-M. Cuciuc[26a], C. Cuenca Almenar[177], T. Cuhadar Donszelmann[140],
J. Cummings[177], M. Curatolo[47], C.J. Curtis[18], C. Cuthbert[151], H. Czirr[142], P. Czodrowski[44],
Z. Czyczula[177], S. D'Auria[53], M. D'Onofrio[73], A. D'Orazio[133a,133b],
M.J. Da Cunha Sargedas De Sousa[125a], C. Da Via[83], W. Dabrowski[38a], A. Dafinca[119], T. Dai[88],
F. Dallaire[94], C. Dallapiccola[85], M. Dam[36], D.S. Damiani[138], A.C. Daniells[18], H.O. Danielsson[30],
V. Dao[105], G. Darbo[50a], G.L. Darlea[26c], S. Darmora[8], J.A. Dassoulas[42], W. Davey[21],
T. Davidek[128], N. Davidson[87], E. Davies[119,d], M. Davies[94], O. Davignon[79], A.R. Davison[77],

Y. Davygora[58a], E. Dawe[143], I. Dawson[140], R.K. Daya-Ishmukhametova[23], K. De[8],
R. de Asmundis[103a], S. De Castro[20a,20b], S. De Cecco[79], J. de Graat[99], N. De Groot[105],
P. de Jong[106], C. De La Taille[116], H. De la Torre[81], F. De Lorenzi[63], L. De Nooij[106],
D. De Pedis[133a], A. De Salvo[133a], U. De Sanctis[165a,165c], A. De Santo[150],
J.B. De Vivie De Regie[116], G. De Zorzi[133a,133b], W.J. Dearnaley[71], R. Debbe[25], C. Debenedetti[46],
B. Dechenaux[55], D.V. Dedovich[64], J. Degenhardt[121], J. Del Peso[81], T. Del Prete[123a,123b],
T. Delemontex[55], M. Deliyergiyev[74], A. Dell'Acqua[30], L. Dell'Asta[22], M. Della Pietra[103a,i],
D. della Volpe[103a,103b], M. Delmastro[5], P.A. Delsart[55], C. Deluca[106], S. Demers[177],
M. Demichev[64], A. Demilly[79], B. Demirkoz[12,k], S.P. Denisov[129], D. Derendarz[39],
J.E. Derkaoui[136d], F. Derue[79], P. Dervan[73], K. Desch[21], P.O. Deviveiros[106], A. Dewhurst[130],
B. DeWilde[149], S. Dhaliwal[106], R. Dhullipudi[78,l], A. Di Ciaccio[134a,134b], L. Di Ciaccio[5],
C. Di Donato[103a,103b], A. Di Girolamo[30], B. Di Girolamo[30], S. Di Luise[135a,135b], A. Di Mattia[153],
B. Di Micco[135a,135b], R. Di Nardo[47], A. Di Simone[134a,134b], R. Di Sipio[20a,20b], M.A. Diaz[32a],
E.B. Diehl[88], J. Dietrich[42], T.A. Dietzsch[58a], S. Diglio[87], K. Dindar Yagci[40], J. Dingfelder[21],
F. Dinut[26a], C. Dionisi[133a,133b], P. Dita[26a], S. Dita[26a], F. Dittus[30], F. Djama[84], T. Djobava[51b],
M.A.B. do Vale[24c], A. Do Valle Wemans[125a,m], T.K.O. Doan[5], D. Dobos[30], E. Dobson[77],
J. Dodd[35], C. Doglioni[49], T. Doherty[53], T. Dohmae[156], Y. Doi[65,*], J. Dolejsi[128], Z. Dolezal[128],
B.A. Dolgoshein[97,*], M. Donadelli[24d], J. Donini[34], J. Dopke[30], A. Doria[103a], A. Dos Anjos[174],
A. Dotti[123a,123b], M.T. Dova[70], A.T. Doyle[53], M. Dris[10], J. Dubbert[88], S. Dube[15], E. Dubreuil[34],
E. Duchovni[173], G. Duckeck[99], D. Duda[176], A. Dudarev[30], F. Dudziak[63], L. Duflot[116],
M-A. Dufour[86], L. Duguid[76], M. Dührssen[30], M. Dunford[58a], H. Duran Yildiz[4a], M. Düren[52],
M. Dwuznik[38a], J. Ebke[99], S. Eckweiler[82], W. Edson[2], C.A. Edwards[76], N.C. Edwards[53],
W. Ehrenfeld[21], T. Eifert[144], G. Eigen[14], K. Einsweiler[15], E. Eisenhandler[75], T. Ekelof[167],
M. El Kacimi[136c], M. Ellert[167], S. Elles[5], F. Ellinghaus[82], K. Ellis[75], N. Ellis[30], J. Elmsheuser[99],
M. Elsing[30], D. Emeliyanov[130], Y. Enari[156], O.C. Endner[82], R. Engelmann[149], A. Engl[99],
J. Erdmann[177], A. Ereditato[17], D. Eriksson[147a], J. Ernst[2], M. Ernst[25], J. Ernwein[137],
D. Errede[166], S. Errede[166], E. Ertel[82], M. Escalier[116], H. Esch[43], C. Escobar[124],
X. Espinal Curull[12], B. Esposito[47], F. Etienne[84], A.I. Etienvre[137], E. Etzion[154],
D. Evangelakou[54], H. Evans[60], L. Fabbri[20a,20b], C. Fabre[30], G. Facini[30], R.M. Fakhrutdinov[129],
S. Falciano[133a], Y. Fang[33a], M. Fanti[90a,90b], A. Farbin[8], A. Farilla[135a], T. Farooque[159],
S. Farrell[164], S.M. Farrington[171], P. Farthouat[30], F. Fassi[168], P. Fassnacht[30], D. Fassouliotis[9],
B. Fatholahzadeh[159], A. Favareto[90a,90b], L. Fayard[116], P. Federic[145a], O.L. Fedin[122],
W. Fedorko[169], M. Fehling-Kaschek[48], L. Feligioni[84], C. Feng[33d], E.J. Feng[6], H. Feng[88],
A.B. Fenyuk[129], J. Ferencei[145b], W. Fernando[6], S. Ferrag[53], J. Ferrando[53], V. Ferrara[42],
A. Ferrari[167], P. Ferrari[106], R. Ferrari[120a], D.E. Ferreira de Lima[53], A. Ferrer[168], D. Ferrere[49],
C. Ferretti[88], A. Ferretto Parodi[50a,50b], M. Fiascaris[31], F. Fiedler[82], A. Filipčič[74], F. Filthaut[105],
M. Fincke-Keeler[170], K.D. Finelli[45], M.C.N. Fiolhais[125a,h], L. Fiorini[168], A. Firan[40], J. Fischer[176],
M.J. Fisher[110], E.A. Fitzgerald[23], M. Flechl[48], I. Fleck[142], P. Fleischmann[175], S. Fleischmann[176],
G.T. Fletcher[140], G. Fletcher[75], T. Flick[176], A. Floderus[80], L.R. Flores Castillo[174],
A.C. Florez Bustos[160b], M.J. Flowerdew[100], T. Fonseca Martin[17], A. Formica[137], A. Forti[83],
D. Fortin[160a], D. Fournier[116], H. Fox[71], P. Francavilla[12], M. Franchini[20a,20b], S. Franchino[30],
D. Francis[30], M. Franklin[57], S. Franz[30], M. Fraternali[120a,120b], S. Fratina[121], S.T. French[28],
C. Friedrich[42], F. Friedrich[44], D. Froidevaux[30], J.A. Frost[28], C. Fukunaga[157],
E. Fullana Torregrosa[128], B.G. Fulsom[144], J. Fuster[168], C. Gabaldon[30], O. Gabizon[173],
A. Gabrielli[20a,20b], A. Gabrielli[133a,133b], S. Gadatsch[106], T. Gadfort[25], S. Gadomski[49],
G. Gagliardi[50a,50b], P. Gagnon[60], C. Galea[99], B. Galhardo[125a], E.J. Gallas[119], V. Gallo[17],
B.J. Gallop[130], P. Gallus[127], K.K. Gan[110], R.P. Gandrajula[62], Y.S. Gao[144,f], A. Gaponenko[15],
F.M. Garay Walls[46], F. Garberson[177], C. García[168], J.E. García Navarro[168], M. Garcia-Sciveres[15],
R.W. Gardner[31], N. Garelli[144], V. Garonne[30], C. Gatti[47], G. Gaudio[120a], B. Gaur[142],
L. Gauthier[94], P. Gauzzi[133a,133b], I.L. Gavrilenko[95], C. Gay[169], G. Gaycken[21], E.N. Gazis[10],
P. Ge[33d,n], Z. Gecse[169], C.N.P. Gee[130], D.A.A. Geerts[106], Ch. Geich-Gimbel[21],
K. Gellerstedt[147a,147b], C. Gemme[50a], A. Gemmell[53], M.H. Genest[55], S. Gentile[133a,133b],

M. George[54], S. George[76], D. Gerbaudo[164], A. Gershon[154], H. Ghazlane[136b], N. Ghodbane[34],
B. Giacobbe[20a], S. Giagu[133a,133b], V. Giangiobbe[12], P. Giannetti[123a,123b], F. Gianotti[30],
B. Gibbard[25], A. Gibson[159], S.M. Gibson[30], M. Gilchriese[15], T.P.S. Gillam[28], D. Gillberg[30],
A.R. Gillman[130], D.M. Gingrich[3,e], N. Giokaris[9], M.P. Giordani[165a,165c], R. Giordano[103a,103b],
F.M. Giorgi[16], P. Giovannini[100], P.F. Giraud[137], D. Giugni[90a], C. Giuliani[48], M. Giunta[94],
B.K. Gjelsten[118], I. Gkialas[155,o], L.K. Gladilin[98], C. Glasman[81], J. Glatzer[21], A. Glazov[42],
G.L. Glonti[64], J.R. Goddard[75], J. Godfrey[143], J. Godlewski[30], M. Goebel[42], C. Goeringer[82],
S. Goldfarb[88], T. Golling[177], D. Golubkov[129], A. Gomes[125a,c], L.S. Gomez Fajardo[42],
R. Gonçalo[76], J. Goncalves Pinto Firmino Da Costa[42], L. Gonella[21], S. González de la Hoz[168],
G. Gonzalez Parra[12], M.L. Gonzalez Silva[27], S. Gonzalez-Sevilla[49], J.J. Goodson[149],
L. Goossens[30], P.A. Gorbounov[96], H.A. Gordon[25], I. Gorelov[104], G. Gorfine[176], B. Gorini[30],
E. Gorini[72a,72b], A. Gorišek[74], E. Gornicki[39], A.T. Goshaw[6], C. Gössling[43], M.I. Gostkin[64],
I. Gough Eschrich[164], M. Gouighri[136a], D. Goujdami[136c], M.P. Goulette[49], A.G. Goussiou[139],
C. Goy[5], S. Gozpinar[23], L. Graber[54], I. Grabowska-Bold[38a], P. Grafström[20a,20b], K-J. Grahn[42],
E. Gramstad[118], F. Grancagnolo[72a], S. Grancagnolo[16], V. Grassi[149], V. Gratchev[122],
H.M. Gray[30], J.A. Gray[149], E. Graziani[135a], O.G. Grebenyuk[122], T. Greenshaw[73],
Z.D. Greenwood[78,l], K. Gregersen[36], I.M. Gregor[42], P. Grenier[144], J. Griffiths[8], N. Grigalashvili[64],
A.A. Grillo[138], K. Grimm[71], S. Grinstein[12], Ph. Gris[34], Y.V. Grishkevich[98], J.-F. Grivaz[116],
J.P. Grohs[44], A. Grohsjean[42], E. Gross[173], J. Grosse-Knetter[54], J. Groth-Jensen[173], K. Grybel[142],
F. Guescini[49], D. Guest[177], O. Gueta[154], C. Guicheney[34], E. Guido[50a,50b], T. Guillemin[116],
S. Guindon[2], U. Gul[53], J. Gunther[127], J. Guo[35], P. Gutierrez[112], N. Guttman[154], O. Gutzwiller[174],
C. Guyot[137], C. Gwenlan[119], C.B. Gwilliam[73], A. Haas[109], S. Haas[30], C. Haber[15],
H.K. Hadavand[8], P. Haefner[21], Z. Hajduk[39], H. Hakobyan[178], D. Hall[119], G. Halladjian[62],
K. Hamacher[176], P. Hamal[114], K. Hamano[87], M. Hamer[54], A. Hamilton[146a,p], S. Hamilton[162],
L. Han[33b], K. Hanagaki[117], K. Hanawa[161], M. Hance[15], C. Handel[82], P. Hanke[58a], J.R. Hansen[36],
J.B. Hansen[36], J.D. Hansen[36], P.H. Hansen[36], P. Hansson[144], K. Hara[161], A.S. Hard[174],
T. Harenberg[176], S. Harkusha[91], D. Harper[88], R.D. Harrington[46], O.M. Harris[139], J. Hartert[48],
F. Hartjes[106], T. Haruyama[65], A. Harvey[56], S. Hasegawa[102], Y. Hasegawa[141], S. Hassani[137],
S. Haug[17], M. Hauschild[30], R. Hauser[89], M. Havranek[21], C.M. Hawkes[18], R.J. Hawkings[30],
A.D. Hawkins[80], T. Hayakawa[66], T. Hayashi[161], D. Hayden[76], C.P. Hays[119], H.S. Hayward[73],
S.J. Haywood[130], S.J. Head[18], T. Heck[82], V. Hedberg[80], L. Heelan[8], S. Heim[121], B. Heinemann[15],
S. Heisterkamp[36], J. Hejbal[126], L. Helary[22], C. Heller[99], M. Heller[30], S. Hellman[147a,147b],
D. Hellmich[21], C. Helsens[30], J. Henderson[119], R.C.W. Henderson[71], M. Henke[58a], A. Henrichs[177],
A.M. Henriques Correia[30], S. Henrot-Versille[116], C. Hensel[54], G.H. Herbert[16], C.M. Hernandez[8],
Y. Hernández Jiménez[168], R. Herrberg-Schubert[16], G. Herten[48], R. Hertenberger[99], L. Hervas[30],
G.G. Hesketh[77], N.P. Hessey[106], R. Hickling[75], E. Higón-Rodriguez[168], J.C. Hill[28], K.H. Hiller[42],
S. Hillert[21], S.J. Hillier[18], I. Hinchliffe[15], E. Hines[121], M. Hirose[117], D. Hirschbuehl[176],
J. Hobbs[149], N. Hod[106], M.C. Hodgkinson[140], P. Hodgson[140], A. Hoecker[30], M.R. Hoeferkamp[104],
J. Hoffman[40], D. Hoffmann[84], J.I. Hofmann[58a], M. Hohlfeld[82], S.O. Holmgren[147a],
J.L. Holzbauer[89], T.M. Hong[121], L. Hooft van Huysduynen[109], J-Y. Hostachy[55], S. Hou[152],
A. Hoummada[136a], J. Howard[119], J. Howarth[83], M. Hrabovsky[114], I. Hristova[16], J. Hrivnac[116],
T. Hryn'ova[5], P.J. Hsu[82], S.-C. Hsu[139], D. Hu[35], X. Hu[25], Z. Hubacek[30], F. Hubaut[84],
F. Huegging[21], A. Huettmann[42], T.B. Huffman[119], E.W. Hughes[35], G. Hughes[71], M. Huhtinen[30],
T.A. Hülsing[82], M. Hurwitz[15], N. Huseynov[64,q], J. Huston[89], J. Huth[57], G. Iacobucci[49],
G. Iakovidis[10], I. Ibragimov[142], L. Iconomidou-Fayard[116], J. Idarraga[116], P. Iengo[103a],
O. Igonkina[106], Y. Ikegami[65], K. Ikematsu[142], M. Ikeno[65], D. Iliadis[155], N. Ilic[159], T. Ince[100],
P. Ioannou[9], M. Iodice[135a], K. Iordanidou[9], V. Ippolito[133a,133b], A. Irles Quiles[168], C. Isaksson[167],
M. Ishino[67], M. Ishitsuka[158], R. Ishmukhametov[110], C. Issever[119], S. Istin[19a], A.V. Ivashin[129],
W. Iwanski[39], H. Iwasaki[65], J.M. Izen[41], V. Izzo[103a], B. Jackson[121], J.N. Jackson[73], P. Jackson[1],
M.R. Jaekel[30], V. Jain[2], K. Jakobs[48], S. Jakobsen[36], T. Jakoubek[126], J. Jakubek[127],
D.O. Jamin[152], D.K. Jana[112], E. Jansen[77], H. Jansen[30], J. Janssen[21], A. Jantsch[100], M. Janus[48],
R.C. Jared[174], G. Jarlskog[80], L. Jeanty[57], G.-Y. Jeng[151], I. Jen-La Plante[31], D. Jennens[87],

P. Jenni[30], J. Jentzsch[43], C. Jeske[171], P. Jež[36], S. Jézéquel[5], M.K. Jha[20a], H. Ji[174], W. Ji[82],
J. Jia[149], Y. Jiang[33b], M. Jimenez Belenguer[42], S. Jin[33a], O. Jinnouchi[158], M.D. Joergensen[36],
D. Joffe[40], M. Johansen[147a,147b], K.E. Johansson[147a], P. Johansson[140], S. Johnert[42], K.A. Johns[7],
K. Jon-And[147a,147b], G. Jones[171], R.W.L. Jones[71], T.J. Jones[73], P.M. Jorge[125a], K.D. Joshi[83],
J. Jovicevic[148], T. Jovin[13b], X. Ju[174], C.A. Jung[43], R.M. Jungst[30], P. Jussel[61], A. Juste Rozas[12],
S. Kabana[17], M. Kaci[168], A. Kaczmarska[39], P. Kadlecik[36], M. Kado[116], H. Kagan[110], M. Kagan[57],
E. Kajomovitz[153], S. Kalinin[176], S. Kama[40], N. Kanaya[156], M. Kaneda[30], S. Kaneti[28],
T. Kanno[158], V.A. Kantserov[97], J. Kanzaki[65], B. Kaplan[109], A. Kapliy[31], D. Kar[53],
K. Karakostas[10], M. Karnevskiy[82], V. Kartvelishvili[71], A.N. Karyukhin[129], L. Kashif[174],
G. Kasieczka[58b], R.D. Kass[110], A. Kastanas[14], Y. Kataoka[156], J. Katzy[42], V. Kaushik[7],
K. Kawagoe[69], T. Kawamoto[156], G. Kawamura[54], S. Kazama[156], V.F. Kazanin[108],
M.Y. Kazarinov[64], R. Keeler[170], P.T. Keener[121], R. Kehoe[40], M. Keil[54], J.S. Keller[139],
H. Keoshkerian[5], O. Kepka[126], B.P. Keršhevan[74], S. Kersten[176], K. Kessoku[156], J. Keung[159],
F. Khalil-zada[11], H. Khandanyan[147a,147b], A. Khanov[113], D. Kharchenko[64], A. Khodinov[97],
A. Khomich[58a], T.J. Khoo[28], G. Khoriauli[21], A. Khoroshilov[176], V. Khovanskiy[96], E. Khramov[64],
J. Khubua[51b], H. Kim[147a,147b], S.H. Kim[161], N. Kimura[172], O. Kind[16], B.T. King[73], M. King[66],
R.S.B. King[119], S.B. King[169], J. Kirk[130], A.E. Kiryunin[100], T. Kishimoto[66], D. Kisielewska[38a],
T. Kitamura[66], T. Kittelmann[124], K. Kiuchi[161], E. Kladiva[145b], M. Klein[73], U. Klein[73],
K. Kleinknecht[82], M. Klemetti[86], A. Klier[173], P. Klimek[147a,147b], A. Klimentov[25],
R. Klingenberg[43], J.A. Klinger[83], E.B. Klinkby[36], T. Klioutchnikova[30], P.F. Klok[105],
E.-E. Kluge[58a], P. Kluit[106], S. Kluth[100], E. Kneringer[61], E.B.F.G. Knoops[84], A. Knue[54],
B.R. Ko[45], T. Kobayashi[156], M. Kobel[44], M. Kocian[144], P. Kodys[128], S. Koenig[82],
F. Koetsveld[105], P. Koevesarki[21], T. Koffas[29], E. Koffeman[106], L.A. Kogan[119], S. Kohlmann[176],
F. Kohn[54], Z. Kohout[127], T. Kohriki[65], T. Koi[144], H. Kolanoski[16], I. Koletsou[90a], J. Koll[89],
A.A. Komar[95], Y. Komori[156], T. Kondo[65], K. Köneke[30], A.C. König[105], T. Kono[42,r],
A.I. Kononov[48], R. Konoplich[109,s], N. Konstantinidis[77], R. Kopeliansky[153], S. Koperny[38a],
L. Köpke[82], A.K. Kopp[48], K. Korcyl[39], K. Kordas[155], A. Korn[46], A. Korol[108], I. Korolkov[12],
E.V. Korolkova[140], V.A. Korotkov[129], O. Kortner[100], S. Kortner[100], V.V. Kostyukhin[21],
S. Kotov[100], V.M. Kotov[64], A. Kotwal[45], C. Kourkoumelis[9], V. Kouskoura[155], A. Koutsman[160a],
R. Kowalewski[170], T.Z. Kowalski[38a], W. Kozanecki[137], A.S. Kozhin[129], V. Kral[127],
V.A. Kramarenko[98], G. Kramberger[74], M.W. Krasny[79], A. Krasznahorkay[109], J.K. Kraus[21],
A. Kravchenko[25], S. Kreiss[109], J. Kretzschmar[73], K. Kreutzfeldt[52], N. Krieger[54], P. Krieger[159],
K. Kroeninger[54], H. Kroha[100], J. Kroll[121], J. Kroseberg[21], J. Krstic[13a], U. Kruchonak[64],
H. Krüger[21], T. Kruker[17], N. Krumnack[63], Z.V. Krumshteyn[64], A. Kruse[174], M.K. Kruse[45],
M. Kruskal[22], T. Kubota[87], S. Kuday[4a], S. Kuehn[48], A. Kugel[58c], T. Kuhl[42], V. Kukhtin[64],
Y. Kulchitsky[91], S. Kuleshov[32b], M. Kuna[79], J. Kunkle[121], A. Kupco[126], H. Kurashige[66],
M. Kurata[161], Y.A. Kurochkin[91], V. Kus[126], E.S. Kuwertz[148], M. Kuze[158], J. Kvita[143],
R. Kwee[16], A. La Rosa[49], L. La Rotonda[37a,37b], L. Labarga[81], S. Lablak[136a], C. Lacasta[168],
F. Lacava[133a,133b], J. Lacey[29], H. Lacker[16], D. Lacour[79], V.R. Lacuesta[168], E. Ladygin[64],
R. Lafaye[5], B. Laforge[79], T. Lagouri[177], S. Lai[48], H. Laier[58a], E. Laisne[55], L. Lambourne[77],
C.L. Lampen[7], W. Lampl[7], E. Lançon[137], U. Landgraf[48], M.P.J. Landon[75], V.S. Lang[58a],
C. Lange[42], A.J. Lankford[164], F. Lanni[25], K. Lantzsch[30], A. Lanza[120a], S. Laplace[79],
C. Lapoire[21], J.F. Laporte[137], T. Lari[90a], A. Larner[119], M. Lassnig[30], P. Laurelli[47],
V. Lavorini[37a,37b], W. Lavrijsen[15], P. Laycock[73], O. Le Dortz[79], E. Le Guirriec[84],
E. Le Menedeu[12], T. LeCompte[6], F. Ledroit-Guillon[55], H. Lee[106], J.S.H. Lee[117], S.C. Lee[152],
L. Lee[177], G. Lefebvre[79], M. Lefebvre[170], M. Legendre[137], F. Legger[99], C. Leggett[15],
M. Lehmacher[21], G. Lehmann Miotto[30], A.G. Leister[177], M.A.L. Leite[24d], R. Leitner[128],
D. Lellouch[173], B. Lemmer[54], V. Lendermann[58a], K.J.C. Leney[146c], T. Lenz[106], G. Lenzen[176],
B. Lenzi[30], K. Leonhardt[44], S. Leontsinis[10], F. Lepold[58a], C. Leroy[94], J-R. Lessard[170],
C.G. Lester[28], C.M. Lester[121], J. Levêque[5], D. Levin[88], L.J. Levinson[173], A. Lewis[119],
G.H. Lewis[109], A.M. Leyko[21], M. Leyton[16], B. Li[33b], B. Li[84], H. Li[149], H.L. Li[31], S. Li[33b,t],
X. Li[88], Z. Liang[119,u], H. Liao[34], B. Liberti[134a], P. Lichard[30], K. Lie[166], J. Liebal[21], W. Liebig[14],

C. Limbach[21], A. Limosani[87], M. Limper[62], S.C. Lin[152,v], F. Linde[106], B.E. Lindquist[149],
J.T. Linnemann[89], E. Lipeles[121], A. Lipniacka[14], M. Lisovyi[42], T.M. Liss[166], D. Lissauer[25],
A. Lister[169], A.M. Litke[138], D. Liu[152], J.B. Liu[33b], K. Liu[33b,w], L. Liu[88], M. Liu[45], M. Liu[33b],
Y. Liu[33b], M. Livan[120a,120b], S.S.A. Livermore[119], A. Lleres[55], J. Llorente Merino[81], S.L. Lloyd[75],
F. Lo Sterzo[133a,133b], E. Lobodzinska[42], P. Loch[7], W.S. Lockman[138], T. Loddenkoetter[21],
F.K. Loebinger[83], A.E. Loevschall-Jensen[36], A. Loginov[177], C.W. Loh[169], T. Lohse[16],
K. Lohwasser[48], M. Lokajicek[126], V.P. Lombardo[5], R.E. Long[71], L. Lopes[125a], D. Lopez Mateos[57],
J. Lorenz[99], N. Lorenzo Martinez[116], M. Losada[163], P. Loscutoff[15], M.J. Losty[160a,*], X. Lou[41],
A. Lounis[116], K.F. Loureiro[163], J. Love[6], P.A. Love[71], A.J. Lowe[144,f], F. Lu[33a], H.J. Lubatti[139],
C. Luci[133a,133b], A. Lucotte[55], D. Ludwig[42], I. Ludwig[48], J. Ludwig[48], F. Luehring[60], W. Lukas[61],
L. Luminari[133a], E. Lund[118], J. Lundberg[147a,147b], O. Lundberg[147a,147b], B. Lund-Jensen[148],
J. Lundquist[36], M. Lungwitz[82], D. Lynn[25], R. Lysak[126], E. Lytken[80], H. Ma[25], L.L. Ma[174],
G. Maccarrone[47], A. Macchiolo[100], B. Maček[74], J. Machado Miguens[125a], D. Macina[30],
R. Mackeprang[36], R. Madar[48], R.J. Madaras[15], H.J. Maddocks[71], W.F. Mader[44], A. Madsen[167],
M. Maeno[5], T. Maeno[25], L. Magnoni[164], E. Magradze[54], K. Mahboubi[48], J. Mahlstedt[106],
S. Mahmoud[73], G. Mahout[18], C. Maiani[137], C. Maidantchik[24a], A. Maio[125a,c], S. Majewski[115],
Y. Makida[65], N. Makovec[116], P. Mal[137,x], B. Malaescu[79], Pa. Malecki[39], P. Malecki[39],
V.P. Maleev[122], F. Malek[55], U. Mallik[62], D. Malon[6], C. Malone[144], S. Maltezos[10], V. Malyshev[108],
S. Malyukov[30], J. Mamuzic[13b], L. Mandelli[90a], I. Mandić[74], R. Mandrysch[62], J. Maneira[125a],
A. Manfredini[100], L. Manhaes de Andrade Filho[24b], J.A. Manjarres Ramos[137], A. Mann[99],
P.M. Manning[138], A. Manousakis-Katsikakis[9], B. Mansoulie[137], R. Mantifel[86], L. Mapelli[30],
L. March[168], J.F. Marchand[29], F. Marchese[134a,134b], G. Marchiori[79], M. Marcisovsky[126],
C.P. Marino[170], C.N. Marques[125a], F. Marroquim[24a], Z. Marshall[121], L.F. Marti[17],
S. Marti-Garcia[168], B. Martin[30], B. Martin[89], J.P. Martin[94], T.A. Martin[171], V.J. Martin[46],
B. Martin dit Latour[49], H. Martinez[137], M. Martinez[12], S. Martin-Haugh[150], A.C. Martyniuk[170],
M. Marx[83], F. Marzano[133a], A. Marzin[112], L. Masetti[82], T. Mashimo[156], R. Mashinistov[95],
J. Masik[83], A.L. Maslennikov[108], I. Massa[20a,20b], N. Massol[5], P. Mastrandrea[149],
A. Mastroberardino[37a,37b], T. Masubuchi[156], H. Matsunaga[156], T. Matsushita[66], P. Mättig[176],
S. Mättig[42], C. Mattravers[119,d], J. Maurer[84], S.J. Maxfield[73], D.A. Maximov[108,g], R. Mazini[152],
M. Mazur[21], L. Mazzaferro[134a,134b], M. Mazzanti[90a], S.P. Mc Kee[88], A. McCarn[166],
R.L. McCarthy[149], T.G. McCarthy[29], N.A. McCubbin[130], K.W. McFarlane[56,*], J.A. Mcfayden[140],
G. Mchedlidze[51b], T. Mclaughlan[18], S.J. McMahon[130], R.A. McPherson[170,j], A. Meade[85],
J. Mechnich[106], M. Mechtel[176], M. Medinnis[42], S. Meehan[31], R. Meera-Lebbai[112], T. Meguro[117],
S. Mehlhase[36], A. Mehta[73], K. Meier[58a], C. Meineck[99], B. Meirose[80], C. Melachrinos[31],
B.R. Mellado Garcia[146c], F. Meloni[90a,90b], L. Mendoza Navas[163], A. Mengarelli[20a,20b],
S. Menke[100], E. Meoni[162], K.M. Mercurio[57], N. Meric[137], P. Mermod[49], L. Merola[103a,103b],
C. Meroni[90a], F.S. Merritt[31], H. Merritt[110], A. Messina[30,y], J. Metcalfe[25], A.S. Mete[164],
C. Meyer[82], C. Meyer[31], J-P. Meyer[137], J. Meyer[30], J. Meyer[54], S. Michal[30], R.P. Middleton[130],
S. Migas[73], L. Mijović[137], G. Mikenberg[173], M. Mikestikova[126], M. Mikuž[74], D.W. Miller[31],
W.J. Mills[169], C. Mills[57], A. Milov[173], D.A. Milstead[147a,147b], D. Milstein[173], A.A. Minaenko[129],
M. Miñano Moya[168], I.A. Minashvili[64], A.I. Mincer[109], B. Mindur[38a], M. Mineev[64], Y. Ming[174],
L.M. Mir[12], G. Mirabelli[133a], J. Mitrevski[138], V.A. Mitsou[168], S. Mitsui[65], P.S. Miyagawa[140],
J.U. Mjörnmark[80], T. Moa[147a,147b], V. Moeller[28], S. Mohapatra[149], W. Mohr[48], R. Moles-Valls[168],
A. Molfetas[30], K. Mönig[42], C. Monini[55], J. Monk[36], E. Monnier[84], J. Montejo Berlingen[12],
F. Monticelli[70], S. Monzani[20a,20b], R.W. Moore[3], C. Mora Herrera[49], A. Moraes[53], N. Morange[62],
J. Morel[54], D. Moreno[82], M. Moreno Llácer[168], P. Morettini[50a], M. Morgenstern[44], M. Morii[57],
S. Moritz[82], A.K. Morley[30], G. Mornacchi[30], J.D. Morris[75], L. Morvaj[102], N. Möser[21],
H.G. Moser[100], M. Mosidze[51b], J. Moss[110], R. Mount[144], E. Mountricha[10,z], S.V. Mouraviev[95,*],
E.J.W. Moyse[85], R.D. Mudd[18], F. Mueller[58a], J. Mueller[124], K. Mueller[21], T. Mueller[28],
T. Mueller[82], D. Muenstermann[30], Y. Munwes[154], J.A. Murillo Quijada[18], W.J. Murray[130],
I. Mussche[106], E. Musto[153], A.G. Myagkov[129,aa], M. Myska[126], O. Nackenhorst[54], J. Nadal[12],
K. Nagai[161], R. Nagai[158], Y. Nagai[84], K. Nagano[65], A. Nagarkar[110], Y. Nagasaka[59], M. Nagel[100],

A.M. Nairz[30], Y. Nakahama[30], K. Nakamura[65], T. Nakamura[156], I. Nakano[111],
H. Namasivayam[41], G. Nanava[21], A. Napier[162], R. Narayan[58b], M. Nash[77,d], T. Nattermann[21],
T. Naumann[42], G. Navarro[163], H.A. Neal[88], P.Yu. Nechaeva[95], T.J. Neep[83], A. Negri[120a,120b],
G. Negri[30], M. Negrini[20a], S. Nektarijevic[49], A. Nelson[164], T.K. Nelson[144], S. Nemecek[126],
P. Nemethy[109], A.A. Nepomuceno[24a], M. Nessi[30,ab], M.S. Neubauer[166], M. Neumann[176],
A. Neusiedl[82], R.M. Neves[109], P. Nevski[25], F.M. Newcomer[121], P.R. Newman[18], D.H. Nguyen[6],
V. Nguyen Thi Hong[137], R.B. Nickerson[119], R. Nicolaidou[137], B. Nicquevert[30], F. Niedercorn[116],
J. Nielsen[138], N. Nikiforou[35], A. Nikiforov[16], V. Nikolaenko[129,aa], I. Nikolic-Audit[79],
K. Nikolics[49], K. Nikolopoulos[18], P. Nilsson[8], Y. Ninomiya[156], A. Nisati[133a], R. Nisius[100],
T. Nobe[158], L. Nodulman[6], M. Nomachi[117], I. Nomidis[155], S. Norberg[112], M. Nordberg[30],
J. Novakova[128], M. Nozaki[65], L. Nozka[114], A.-E. Nuncio-Quiroz[21], G. Nunes Hanninger[87],
T. Nunnemann[99], E. Nurse[77], B.J. O'Brien[46], D.C. O'Neil[143], V. O'Shea[53], L.B. Oakes[99],
F.G. Oakham[29,e], H. Oberlack[100], J. Ocariz[79], A. Ochi[66], M.I. Ochoa[77], S. Oda[69], S. Odaka[65],
J. Odier[84], H. Ogren[60], A. Oh[83], S.H. Oh[45], C.C. Ohm[30], T. Ohshima[102], W. Okamura[117],
H. Okawa[25], Y. Okumura[31], T. Okuyama[156], A. Olariu[26a], A.G. Olchevski[64],
S.A. Olivares Pino[46], M. Oliveira[125a,h], D. Oliveira Damazio[25], E. Oliver Garcia[168], D. Olivito[121],
A. Olszewski[39], J. Olszowska[39], A. Onofre[125a,ac], P.U.E. Onyisi[31,ad], C.J. Oram[160a],
M.J. Oreglia[31], Y. Oren[154], D. Orestano[135a,135b], N. Orlando[72a,72b], C. Oropeza Barrera[53],
R.S. Orr[159], B. Osculati[50a,50b], R. Ospanov[121], G. Otero y Garzon[27], J.P. Ottersbach[106],
M. Ouchrif[136d], E.A. Ouellette[170], F. Ould-Saada[118], A. Ouraou[137], Q. Ouyang[33a],
A. Ovcharova[15], M. Owen[83], S. Owen[140], V.E. Ozcan[19a], N. Ozturk[8], K. Pachal[119],
A. Pacheco Pages[12], C. Padilla Aranda[12], S. Pagan Griso[15], E. Paganis[140], C. Pahl[100], F. Paige[25],
P. Pais[85], K. Pajchel[118], G. Palacino[160b], C.P. Paleari[7], S. Palestini[30], D. Pallin[34], A. Palma[125a],
J.D. Palmer[18], Y.B. Pan[174], E. Panagiotopoulou[10], J.G. Panduro Vazquez[76], P. Pani[106],
N. Panikashvili[88], S. Panitkin[25], D. Pantea[26a], A. Papadelis[147a], Th.D. Papadopoulou[10],
K. Papageorgiou[155,o], A. Paramonov[6], D. Paredes Hernandez[34], W. Park[25,ae], M.A. Parker[28],
F. Parodi[50a,50b], J.A. Parsons[35], U. Parzefall[48], S. Pashapour[54], E. Pasqualucci[133a],
S. Passaggio[50a], A. Passeri[135a], F. Pastore[135a,135b,*], Fr. Pastore[76], G. Pásztor[49,af],
S. Pataraia[176], N.D. Patel[151], J.R. Pater[83], S. Patricelli[103a,103b], T. Pauly[30], J. Pearce[170],
M. Pedersen[118], S. Pedraza Lopez[168], M.I. Pedraza Morales[174], S.V. Peleganchuk[108],
D. Pelikan[167], H. Peng[33b], B. Penning[31], A. Penson[35], J. Penwell[60], T. Perez Cavalcanti[42],
E. Perez Codina[160a], M.T. Pérez García-Estañ[168], V. Perez Reale[35], L. Perini[90a,90b],
H. Pernegger[30], R. Perrino[72a], P. Perrodo[5], V.D. Peshekhonov[64], K. Peters[30], R.F.Y. Peters[54,ag],
B.A. Petersen[30], J. Petersen[30], T.C. Petersen[36], E. Petit[5], A. Petridis[147a,147b], C. Petridou[155],
E. Petrolo[133a], F. Petrucci[135a,135b], D. Petschull[42], M. Petteni[143], R. Pezoa[32b], A. Phan[87],
P.W. Phillips[130], G. Piacquadio[144], E. Pianori[171], A. Picazio[49], E. Piccaro[75], M. Piccinini[20a,20b],
S.M. Piec[42], R. Piegaia[27], D.T. Pignotti[110], J.E. Pilcher[31], A.D. Pilkington[83], J. Pina[125a,c],
M. Pinamonti[165a,165c,ah], A. Pinder[119], J.L. Pinfold[3], A. Pingel[36], B. Pinto[125a], C. Pizio[90a,90b],
M.-A. Pleier[25], V. Pleskot[128], E. Plotnikova[64], P. Plucinski[147a,147b], S. Poddar[58a], F. Podlyski[34],
R. Poettgen[82], L. Poggioli[116], D. Pohl[21], M. Pohl[49], G. Polesello[120a], A. Policicchio[37a,37b],
R. Polifka[159], A. Polini[20a], V. Polychronakos[25], D. Pomeroy[23], K. Pommès[30], L. Pontecorvo[133a],
B.G. Pope[89], G.A. Popeneciu[26b], D.S. Popovic[13a], A. Poppleton[30], X. Portell Bueso[12],
G.E. Pospelov[100], S. Pospisil[127], I.N. Potrap[64], C.J. Potter[150], C.T. Potter[115], G. Poulard[30],
J. Poveda[60], V. Pozdnyakov[64], R. Prabhu[77], P. Pralavorio[84], A. Pranko[15], S. Prasad[30],
R. Pravahan[25], S. Prell[63], K. Pretzl[17], D. Price[60], J. Price[73], L.E. Price[6], D. Prieur[124],
M. Primavera[72a], M. Proissl[46], K. Prokofiev[109], F. Prokoshin[32b], E. Protopapadaki[137],
S. Protopopescu[25], J. Proudfoot[6], X. Prudent[44], M. Przybycien[38a], H. Przysieczniak[5],
S. Psoroulas[21], E. Ptacek[115], E. Pueschel[85], D. Puldon[149], M. Purohit[25,ae], P. Puzo[116],
Y. Pylypchenko[62], J. Qian[88], A. Quadt[54], D.R. Quarrie[15], W.B. Quayle[174], D. Quilty[53],
M. Raas[105], V. Radeka[25], V. Radescu[42], P. Radloff[115], F. Ragusa[90a,90b], G. Rahal[179],
S. Rajagopalan[25], M. Rammensee[48], M. Rammes[142], A.S. Randle-Conde[40], K. Randrianarivony[29],
C. Rangel-Smith[79], K. Rao[164], F. Rauscher[99], T.C. Rave[48], T. Ravenscroft[53], M. Raymond[30],

A.L. Read[118], D.M. Rebuzzi[120a,120b], A. Redelbach[175], G. Redlinger[25], R. Reece[121], K. Reeves[41],
A. Reinsch[115], I. Reisinger[43], M. Relich[164], C. Rembser[30], Z.L. Ren[152], A. Renaud[116],
M. Rescigno[133a], S. Resconi[90a], B. Resende[137], P. Reznicek[99], R. Rezvani[94], R. Richter[100],
E. Richter-Was[38b], M. Ridel[79], P. Rieck[16], M. Rijssenbeek[149], A. Rimoldi[120a,120b], L. Rinaldi[20a],
R.R. Rios[40], E. Ritsch[61], I. Riu[12], G. Rivoltella[90a,90b], F. Rizatdinova[113], E. Rizvi[75],
S.H. Robertson[86,j], A. Robichaud-Veronneau[119], D. Robinson[28], J.E.M. Robinson[83], A. Robson[53],
J.G. Rocha de Lima[107], C. Roda[123a,123b], D. Roda Dos Santos[30], A. Roe[54], S. Roe[30],
O. Røhne[118], S. Rolli[162], A. Romaniouk[97], M. Romano[20a,20b], G. Romeo[27], E. Romero Adam[168],
N. Rompotis[139], L. Roos[79], E. Ros[168], S. Rosati[133a], K. Rosbach[49], A. Rose[150], M. Rose[76],
G.A. Rosenbaum[159], P.L. Rosendahl[14], O. Rosenthal[142], V. Rossetti[12], E. Rossi[133a,133b],
L.P. Rossi[50a], M. Rotaru[26a], I. Roth[173], J. Rothberg[139], D. Rousseau[116], C.R. Royon[137],
A. Rozanov[84], Y. Rozen[153], X. Ruan[146c], F. Rubbo[12], I. Rubinskiy[42], N. Ruckstuhl[106],
V.I. Rud[98], C. Rudolph[44], M.S. Rudolph[159], F. Rühr[7], A. Ruiz-Martinez[63], L. Rumyantsev[64],
Z. Rurikova[48], N.A. Rusakovich[64], A. Ruschke[99], J.P. Rutherfoord[7], N. Ruthmann[48],
P. Ruzicka[126], Y.F. Ryabov[122], M. Rybar[128], G. Rybkin[116], N.C. Ryder[119], A.F. Saavedra[151],
A. Saddique[3], I. Sadeh[154], H.F-W. Sadrozinski[138], R. Sadykov[64], F. Safai Tehrani[133a],
H. Sakamoto[156], G. Salamanna[75], A. Salamon[134a], M. Saleem[112], D. Salek[30], D. Salihagic[100],
A. Salnikov[144], J. Salt[168], B.M. Salvachua Ferrando[6], D. Salvatore[37a,37b], F. Salvatore[150],
A. Salvucci[105], A. Salzburger[30], D. Sampsonidis[155], A. Sanchez[103a,103b], J. Sánchez[168],
V. Sanchez Martinez[168], H. Sandaker[14], H.G. Sander[82], M.P. Sanders[99], M. Sandhoff[176],
T. Sandoval[28], C. Sandoval[163], R. Sandstroem[100], D.P.C. Sankey[130], A. Sansoni[47], C. Santoni[34],
R. Santonico[134a,134b], H. Santos[125a], I. Santoyo Castillo[150], K. Sapp[124], J.G. Saraiva[125a],
T. Sarangi[174], E. Sarkisyan-Grinbaum[8], B. Sarrazin[21], F. Sarri[123a,123b], G. Sartisohn[176],
O. Sasaki[65], Y. Sasaki[156], N. Sasao[67], I. Satsounkevitch[91], G. Sauvage[5,*], E. Sauvan[5],
J.B. Sauvan[116], P. Savard[159,e], V. Savinov[124], D.O. Savu[30], C. Sawyer[119], L. Sawyer[78,l],
D.H. Saxon[53], J. Saxon[121], C. Sbarra[20a], A. Sbrizzi[3], D.A. Scannicchio[164], M. Scarcella[151],
J. Schaarschmidt[116], P. Schacht[100], D. Schaefer[121], A. Schaelicke[46], S. Schaepe[21], S. Schaetzel[58b],
U. Schäfer[82], A.C. Schaffer[116], D. Schaile[99], R.D. Schamberger[149], V. Scharf[58a],
V.A. Schegelsky[122], D. Scheirich[88], M. Schernau[164], M.I. Scherzer[35], C. Schiavi[50a,50b],
J. Schieck[99], C. Schillo[48], M. Schioppa[37a,37b], S. Schlenker[30], E. Schmidt[48], K. Schmieden[21],
C. Schmitt[82], C. Schmitt[99], S. Schmitt[58b], B. Schneider[17], Y.J. Schnellbach[73], U. Schnoor[44],
L. Schoeffel[137], A. Schoening[58b], A.L.S. Schorlemmer[54], M. Schott[82], D. Schouten[160a],
J. Schovancova[126], M. Schram[86], C. Schroeder[82], N. Schroer[58c], M.J. Schultens[21],
H.-C. Schultz-Coulon[58a], H. Schulz[16], M. Schumacher[48], B.A. Schumm[138], Ph. Schune[137],
A. Schwartzman[144], Ph. Schwegler[100], Ph. Schwemling[137], R. Schwienhorst[89], J. Schwindling[137],
T. Schwindt[21], M. Schwoerer[5], F.G. Sciacca[17], E. Scifo[116], G. Sciolla[23], W.G. Scott[130],
F. Scutti[21], J. Searcy[88], G. Sedov[42], E. Sedykh[122], S.C. Seidel[104], A. Seiden[138], F. Seifert[44],
J.M. Seixas[24a], G. Sekhniaidze[103a], S.J. Sekula[40], K.E. Selbach[46], D.M. Seliverstov[122],
G. Sellers[73], M. Seman[145b], N. Semprini-Cesari[20a,20b], C. Serfon[30], L. Serin[116], L. Serkin[54],
T. Serre[84], R. Seuster[160a], H. Severini[112], A. Sfyrla[30], E. Shabalina[54], M. Shamim[115],
L.Y. Shan[33a], J.T. Shank[22], Q.T. Shao[87], M. Shapiro[15], P.B. Shatalov[96], K. Shaw[165a,165c],
P. Sherwood[77], S. Shimizu[102], M. Shimojima[101], T. Shin[56], M. Shiyakova[64], A. Shmeleva[95],
M.J. Shochet[31], D. Short[119], S. Shrestha[63], E. Shulga[97], M.A. Shupe[7], P. Sicho[126], A. Sidoti[133a],
F. Siegert[48], Dj. Sijacki[13a], O. Silbert[173], J. Silva[125a], Y. Silver[154], D. Silverstein[144],
S.B. Silverstein[147a], V. Simak[127], O. Simard[5], Lj. Simic[13a], S. Simion[116], E. Simioni[82],
B. Simmons[77], R. Simoniello[90a,90b], M. Simonyan[36], P. Sinervo[159], N.B. Sinev[115], V. Sipica[142],
G. Siragusa[175], A. Sircar[78], A.N. Sisakyan[64,*], S.Yu. Sivoklokov[98], J. Sjölin[147a,147b],
T.B. Sjursen[14], L.A. Skinnari[15], H.P. Skottowe[57], K. Skovpen[108], P. Skubic[112], M. Slater[18],
T. Slavicek[127], K. Sliwa[162], V. Smakhtin[173], B.H. Smart[46], L. Smestad[118], S.Yu. Smirnov[97],
Y. Smirnov[97], L.N. Smirnova[98,ai], O. Smirnova[80], K.M. Smith[53], M. Smizanska[71], K. Smolek[127],
A.A. Snesarev[95], G. Snidero[75], J. Snow[112], S. Snyder[25], R. Sobie[170,j], J. Sodomka[127], A. Soffer[154],
D.A. Soh[152,u], C.A. Solans[30], M. Solar[127], J. Solc[127], E.Yu. Soldatov[97], U. Soldevila[168],

E. Solfaroli Camillocci[133a,133b], A.A. Solodkov[129], O.V. Solovyanov[129], V. Solovyev[122], N. Soni[1],
A. Sood[15], V. Sopko[127], B. Sopko[127], M. Sosebee[8], R. Soualah[165a,165c], P. Soueid[94],
A. Soukharev[108], D. South[42], S. Spagnolo[72a,72b], F. Spanò[76], R. Spighi[20a], G. Spigo[30],
R. Spiwoks[30], M. Spousta[128,aj], T. Spreitzer[159], B. Spurlock[8], R.D. St. Denis[53], J. Stahlman[121],
R. Stamen[58a], E. Stanecka[39], R.W. Stanek[6], C. Stanescu[135a], M. Stanescu-Bellu[42],
M.M. Stanitzki[42], S. Stapnes[118], E.A. Starchenko[129], J. Stark[55], P. Staroba[126], P. Starovoitov[42],
R. Staszewski[39], A. Staude[99], P. Stavina[145a,*], G. Steele[53], P. Steinbach[44], P. Steinberg[25],
I. Stekl[127], B. Stelzer[143], H.J. Stelzer[89], O. Stelzer-Chilton[160a], H. Stenzel[52], S. Stern[100],
G.A. Stewart[30], J.A. Stillings[21], M.C. Stockton[86], M. Stoebe[86], K. Stoerig[48], G. Stoicea[26a],
S. Stonjek[100], A.R. Stradling[8], A. Straessner[44], J. Strandberg[148], S. Strandberg[147a,147b],
A. Strandlie[118], M. Strang[110], E. Strauss[144], M. Strauss[112], P. Strizenec[145b], R. Ströhmer[175],
D.M. Strom[115], J.A. Strong[76,*], R. Stroynowski[40], B. Stugu[14], I. Stumer[25,*], J. Stupak[149],
P. Sturm[176], N.A. Styles[42], D. Su[144], HS. Subramania[3], R. Subramaniam[78], A. Succurro[12],
Y. Sugaya[117], C. Suhr[107], M. Suk[127], V.V. Sulin[95], S. Sultansoy[4c], T. Sumida[67], X. Sun[55],
J.E. Sundermann[48], K. Suruliz[140], G. Susinno[37a,37b], M.R. Sutton[150], Y. Suzuki[65], Y. Suzuki[66],
M. Svatos[126], S. Swedish[169], M. Swiatlowski[144], I. Sykora[145a], T. Sykora[128], D. Ta[106],
K. Tackmann[42], A. Taffard[164], R. Tafirout[160a], N. Taiblum[154], Y. Takahashi[102], H. Takai[25],
R. Takashima[68], H. Takeda[66], T. Takeshita[141], Y. Takubo[65], M. Talby[84], A. Talyshev[108,g],
J.Y.C. Tam[175], M.C. Tamsett[78,ak], K.G. Tan[87], J. Tanaka[156], R. Tanaka[116], S. Tanaka[132],
S. Tanaka[65], A.J. Tanasijczuk[143], K. Tani[66], N. Tannoury[84], S. Tapprogge[82], S. Tarem[153],
F. Tarrade[29], G.F. Tartarelli[90a], P. Tas[128], M. Tasevsky[126], T. Tashiro[67], E. Tassi[37a,37b],
Y. Tayalati[136d], C. Taylor[77], F.E. Taylor[93], G.N. Taylor[87], W. Taylor[160b], M. Teinturier[116],
F.A. Teischinger[30], M. Teixeira Dias Castanheira[75], P. Teixeira-Dias[76], K.K. Temming[48],
H. Ten Kate[30], P.K. Teng[152], S. Terada[65], K. Terashi[156], J. Terron[81], M. Testa[47],
R.J. Teuscher[159,j], J. Therhaag[21], T. Theveneaux-Pelzer[34], S. Thoma[48], J.P. Thomas[18],
E.N. Thompson[35], P.D. Thompson[18], P.D. Thompson[159], A.S. Thompson[53], L.A. Thomsen[36],
E. Thomson[121], M. Thomson[28], W.M. Thong[87], R.P. Thun[88,*], F. Tian[35], M.J. Tibbetts[15],
T. Tic[126], V.O. Tikhomirov[95], Y.A. Tikhonov[108,g], S. Timoshenko[97], E. Tiouchichine[84],
P. Tipton[177], S. Tisserant[84], T. Todorov[5], S. Todorova-Nova[162], B. Toggerson[164], J. Tojo[69],
S. Tokár[145a], K. Tokushuku[65], K. Tollefson[89], L. Tomlinson[83], M. Tomoto[102], L. Tompkins[31],
K. Toms[104], A. Tonoyan[14], C. Topfel[17], N.D. Topilin[64], E. Torrence[115], H. Torres[79], E. Torró
Pastor[168], J. Toth[84,af], F. Touchard[84], D.R. Tovey[140], H.L. Tran[116], T. Trefzger[175],
L. Tremblet[30], A. Tricoli[30], I.M. Trigger[160a], S. Trincaz-Duvoid[79], M.F. Tripiana[70], N. Triplett[25],
W. Trischuk[159], B. Trocmé[55], C. Troncon[90a], M. Trottier-McDonald[143], M. Trovatelli[135a,135b],
P. True[89], M. Trzebinski[39], A. Trzupek[39], C. Tsarouchas[30], J.C-L. Tseng[119], M. Tsiakiris[106],
P.V. Tsiareshka[91], D. Tsionou[137], G. Tsipolitis[10], S. Tsiskaridze[12], V. Tsiskaridze[48],
E.G. Tskhadadze[51a], I.I. Tsukerman[96], V. Tsulaia[15], J.-W. Tsung[21], S. Tsuno[65], D. Tsybychev[149],
A. Tua[140], A. Tudorache[26a], V. Tudorache[26a], J.M. Tuggle[31], A.N. Tuna[121], M. Turala[39],
D. Turecek[127], I. Turk Cakir[4d], R. Turra[90a,90b], P.M. Tuts[35], A. Tykhonov[74], M. Tylmad[147a,147b],
M. Tyndel[130], K. Uchida[21], I. Ueda[156], R. Ueno[29], M. Ughetto[84], M. Ugland[14], M. Uhlenbrock[21],
F. Ukegawa[161], G. Unal[30], A. Undrus[25], G. Unel[164], F.C. Ungaro[48], Y. Unno[65], D. Urbaniec[35],
P. Urquijo[21], G. Usai[8], L. Vacavant[84], V. Vacek[127], B. Vachon[86], S. Vahsen[15], N. Valencic[106],
S. Valentinetti[20a,20b], A. Valero[168], L. Valery[34], S. Valkar[128], E. Valladolid Gallego[168],
S. Vallecorsa[153], J.A. Valls Ferrer[168], R. Van Berg[121], P.C. Van Der Deijl[106], R. van der Geer[106],
H. van der Graaf[106], R. Van Der Leeuw[106], D. van der Ster[30], N. van Eldik[30], P. van Gemmeren[6],
J. Van Nieuwkoop[143], I. van Vulpen[106], M. Vanadia[100], W. Vandelli[30], A. Vaniachine[6],
P. Vankov[42], F. Vannucci[79], R. Vari[133a], E.W. Varnes[7], T. Varol[85], D. Varouchas[15],
A. Vartapetian[8], K.E. Varvell[151], V.I. Vassilakopoulos[56], F. Vazeille[34], T. Vazquez Schroeder[54],
F. Veloso[125a], S. Veneziano[133a], A. Ventura[72a,72b], D. Ventura[85], M. Venturi[48], N. Venturi[159],
V. Vercesi[120a], M. Verducci[139], W. Verkerke[106], J.C. Vermeulen[106], A. Vest[44], M.C. Vetterli[143,e],
I. Vichou[166], T. Vickey[146c,al], O.E. Vickey Boeriu[146c], G.H.A. Viehhauser[119], S. Viel[169],
M. Villa[20a,20b], M. Villaplana Perez[168], E. Vilucchi[47], M.G. Vincter[29], V.B. Vinogradov[64],

J. Virzi[15], O. Vitells[173], M. Viti[42], I. Vivarelli[48], F. Vives Vaque[3], S. Vlachos[10], D. Vladoiu[99],
M. Vlasak[127], A. Vogel[21], P. Vokac[127], G. Volpi[47], M. Volpi[87], G. Volpini[90a],
H. von der Schmitt[100], H. von Radziewski[48], E. von Toerne[21], V. Vorobel[128], M. Vos[168], R. Voss[30],
J.H. Vossebeld[73], N. Vranjes[137], M. Vranjes Milosavljevic[106], V. Vrba[126], M. Vreeswijk[106],
T. Vu Anh[48], R. Vuillermet[30], I. Vukotic[31], Z. Vykydal[127], W. Wagner[176], P. Wagner[21],
S. Wahrmund[44], J. Wakabayashi[102], S. Walch[88], J. Walder[71], R. Walker[99], W. Walkowiak[142],
R. Wall[177], P. Waller[73], B. Walsh[177], C. Wang[45], H. Wang[174], H. Wang[40], J. Wang[152],
J. Wang[33a], K. Wang[86], R. Wang[104], S.M. Wang[152], T. Wang[21], X. Wang[177], A. Warburton[86],
C.P. Ward[28], D.R. Wardrope[77], M. Warsinsky[48], A. Washbrook[46], C. Wasicki[42], I. Watanabe[66],
P.M. Watkins[18], A.T. Watson[18], I.J. Watson[151], M.F. Watson[18], G. Watts[139], S. Watts[83],
A.T. Waugh[151], B.M. Waugh[77], M.S. Weber[17], J.S. Webster[31], A.R. Weidberg[119], P. Weigell[100],
J. Weingarten[54], C. Weiser[48], P.S. Wells[30], T. Wenaus[25], D. Wendland[16], Z. Weng[152,u],
T. Wengler[30], S. Wenig[30], N. Wermes[21], M. Werner[48], P. Werner[30], M. Werth[164], M. Wessels[58a],
J. Wetter[162], K. Whalen[29], A. White[8], M.J. White[87], R. White[32b], S. White[123a,123b],
S.R. Whitehead[119], D. Whiteson[164], D. Whittington[60], D. Wicke[176], F.J. Wickens[130],
W. Wiedenmann[174], M. Wielers[80,d], P. Wienemann[21], C. Wiglesworth[36], L.A.M. Wiik-Fuchs[21],
P.A. Wijeratne[77], A. Wildauer[100], M.A. Wildt[42,r], I. Wilhelm[128], H.G. Wilkens[30], J.Z. Will[99],
E. Williams[35], H.H. Williams[121], S. Williams[28], W. Willis[35,*], S. Willocq[85], J.A. Wilson[18],
A. Wilson[88], I. Wingerter-Seez[5], S. Winkelmann[48], F. Winklmeier[30], M. Wittgen[144], T. Wittig[43],
J. Wittkowski[99], S.J. Wollstadt[82], M.W. Wolter[39], H. Wolters[125a,h], W.C. Wong[41], G. Wooden[88],
B.K. Wosiek[39], J. Wotschack[30], M.J. Woudstra[83], K.W. Wozniak[39], K. Wraight[53], M. Wright[53],
B. Wrona[73], S.L. Wu[174], X. Wu[49], Y. Wu[88], E. Wulf[35], B.M. Wynne[46], S. Xella[36], M. Xiao[137],
S. Xie[48], C. Xu[33b,z], D. Xu[33a], L. Xu[33b], B. Yabsley[151], S. Yacoob[146b,am], M. Yamada[65],
H. Yamaguchi[156], Y. Yamaguchi[156], A. Yamamoto[65], K. Yamamoto[63], S. Yamamoto[156],
T. Yamamura[156], T. Yamanaka[156], K. Yamauchi[102], T. Yamazaki[156], Y. Yamazaki[66], Z. Yan[22],
H. Yang[33e], H. Yang[174], U.K. Yang[83], Y. Yang[110], Z. Yang[147a,147b], S. Yanush[92], L. Yao[33a],
Y. Yasu[65], E. Yatsenko[42], K.H. Yau Wong[21], J. Ye[40], S. Ye[25], A.L. Yen[57], E. Yildirim[42],
M. Yilmaz[4b], R. Yoosoofmiya[124], K. Yorita[172], R. Yoshida[6], K. Yoshihara[156], C. Young[144],
C.J.S. Young[119], S. Youssef[22], D. Yu[25], D.R. Yu[15], J. Yu[8], J. Yu[113], L. Yuan[66], A. Yurkewicz[107],
B. Zabinski[39], R. Zaidan[62], A.M. Zaitsev[129,aa], S. Zambito[23], L. Zanello[133a,133b], D. Zanzi[100],
A. Zaytsev[25], C. Zeitnitz[176], M. Zeman[127], A. Zemla[39], O. Zenin[129], T. Ženiš[145a], D. Zerwas[116],
G. Zevi della Porta[57], D. Zhang[88], H. Zhang[89], J. Zhang[6], L. Zhang[152], X. Zhang[33d], Z. Zhang[116],
Z. Zhao[33b], A. Zhemchugov[64], J. Zhong[119], B. Zhou[88], N. Zhou[164], Y. Zhou[152], C.G. Zhu[33d],
H. Zhu[42], J. Zhu[88], Y. Zhu[33b], X. Zhuang[33a], A. Zibell[99], D. Zieminska[60], N.I. Zimin[64],
C. Zimmermann[82], R. Zimmermann[21], S. Zimmermann[21], S. Zimmermann[48], Z. Zinonos[123a,123b],
M. Ziolkowski[142], R. Zitoun[5], L. Živković[35], V.V. Zmouchko[129,*], G. Zobernig[174],
A. Zoccoli[20a,20b], M. zur Nedden[16], V. Zutshi[107], L. Zwalinski[30]

1 School of Chemistry and Physics, University of Adelaide, Adelaide, Australia
2 Physics Department, SUNY Albany, Albany NY, United States of America
3 Department of Physics, University of Alberta, Edmonton AB, Canada
4 (a)Department of Physics, Ankara University, Ankara; (b)Department of Physics, Gazi University, Ankara; (c)Division of Physics, TOBB University of Economics and Technology, Ankara; (d)Turkish Atomic Energy Authority, Ankara, Turkey
5 LAPP, CNRS/IN2P3 and Université de Savoie, Annecy-le-Vieux, France
6 High Energy Physics Division, Argonne National Laboratory, Argonne IL, United States of America
7 Department of Physics, University of Arizona, Tucson AZ, United States of America
8 Department of Physics, The University of Texas at Arlington, Arlington TX, United States of America
9 Physics Department, University of Athens, Athens, Greece
10 Physics Department, National Technical University of Athens, Zografou, Greece
11 Institute of Physics, Azerbaijan Academy of Sciences, Baku, Azerbaijan

12 Institut de Física d'Altes Energies and Departament de Física de la Universitat Autònoma de Barcelona and ICREA, Barcelona, Spain

13 [a]Institute of Physics, University of Belgrade, Belgrade; [b]Vinca Institute of Nuclear Sciences, University of Belgrade, Belgrade, Serbia

14 Department for Physics and Technology, University of Bergen, Bergen, Norway

15 Physics Division, Lawrence Berkeley National Laboratory and University of California, Berkeley CA, United States of America

16 Department of Physics, Humboldt University, Berlin, Germany

17 Albert Einstein Center for Fundamental Physics and Laboratory for High Energy Physics, University of Bern, Bern, Switzerland

18 School of Physics and Astronomy, University of Birmingham, Birmingham, United Kingdom

19 [a]Department of Physics, Bogazici University, Istanbul; [b]Department of Physics, Dogus University, Istanbul; [c]Department of Physics Engineering, Gaziantep University, Gaziantep, Turkey

20 [a]INFN Sezione di Bologna; [b]Dipartimento di Fisica, Università di Bologna, Bologna, Italy

21 Physikalisches Institut, University of Bonn, Bonn, Germany

22 Department of Physics, Boston University, Boston MA, United States of America

23 Department of Physics, Brandeis University, Waltham MA, United States of America

24 [a]Universidade Federal do Rio De Janeiro COPPE/EE/IF, Rio de Janeiro; [b]Federal University of Juiz de Fora (UFJF), Juiz de Fora; [c]Federal University of Sao Joao del Rei (UFSJ), Sao Joao del Rei; [d]Instituto de Fisica, Universidade de Sao Paulo, Sao Paulo, Brazil

25 Physics Department, Brookhaven National Laboratory, Upton NY, United States of America

26 [a]National Institute of Physics and Nuclear Engineering, Bucharest; [b]National Institute for Research and Development of Isotopic and Molecular Technologies, Physics Department, Cluj Napoca; [c]University Politehnica Bucharest, Bucharest; [d]West University in Timisoara, Timisoara, Romania

27 Departamento de Física, Universidad de Buenos Aires, Buenos Aires, Argentina

28 Cavendish Laboratory, University of Cambridge, Cambridge, United Kingdom

29 Department of Physics, Carleton University, Ottawa ON, Canada

30 CERN, Geneva, Switzerland

31 Enrico Fermi Institute, University of Chicago, Chicago IL, United States of America

32 [a]Departamento de Física, Pontificia Universidad Católica de Chile, Santiago; [b]Departamento de Física, Universidad Técnica Federico Santa María, Valparaíso, Chile

33 [a]Institute of High Energy Physics, Chinese Academy of Sciences, Beijing; [b]Department of Modern Physics, University of Science and Technology of China, Anhui; [c]Department of Physics, Nanjing University, Jiangsu; [d]School of Physics, Shandong University, Shandong; [e]Physics Department, Shanghai Jiao Tong University, Shanghai, China

34 Laboratoire de Physique Corpusculaire, Clermont Université and Université Blaise Pascal and CNRS/IN2P3, Clermont-Ferrand, France

35 Nevis Laboratory, Columbia University, Irvington NY, United States of America

36 Niels Bohr Institute, University of Copenhagen, Kobenhavn, Denmark

37 [a]INFN Gruppo Collegato di Cosenza; [b]Dipartimento di Fisica, Università della Calabria, Rende, Italy

38 [a]AGH University of Science and Technology, Faculty of Physics and Applied Computer Science, Krakow; [b]Marian Smoluchowski Institute of Physics, Jagiellonian University, Krakow, Poland

39 The Henryk Niewodniczanski Institute of Nuclear Physics, Polish Academy of Sciences, Krakow, Poland

40 Physics Department, Southern Methodist University, Dallas TX, United States of America

41 Physics Department, University of Texas at Dallas, Richardson TX, United States of America

42 DESY, Hamburg and Zeuthen, Germany

43 Institut für Experimentelle Physik IV, Technische Universität Dortmund, Dortmund, Germany

44 Institut für Kern- und Teilchenphysik, Technical University Dresden, Dresden, Germany

[45] Department of Physics, Duke University, Durham NC, United States of America

[46] SUPA - School of Physics and Astronomy, University of Edinburgh, Edinburgh, United Kingdom

[47] INFN Laboratori Nazionali di Frascati, Frascati, Italy

[48] Fakultät für Mathematik und Physik, Albert-Ludwigs-Universität, Freiburg, Germany

[49] Section de Physique, Université de Genève, Geneva, Switzerland

[50] [a]INFN Sezione di Genova; [b]Dipartimento di Fisica, Università di Genova, Genova, Italy

[51] [a]E. Andronikashvili Institute of Physics, Iv. Javakhishvili Tbilisi State University, Tbilisi; [b]High Energy Physics Institute, Tbilisi State University, Tbilisi, Georgia

[52] II Physikalisches Institut, Justus-Liebig-Universität Giessen, Giessen, Germany

[53] SUPA - School of Physics and Astronomy, University of Glasgow, Glasgow, United Kingdom

[54] II Physikalisches Institut, Georg-August-Universität, Göttingen, Germany

[55] Laboratoire de Physique Subatomique et de Cosmologie, Université Joseph Fourier and CNRS/IN2P3 and Institut National Polytechnique de Grenoble, Grenoble, France

[56] Department of Physics, Hampton University, Hampton VA, United States of America

[57] Laboratory for Particle Physics and Cosmology, Harvard University, Cambridge MA, United States of America

[58] [a]Kirchhoff-Institut für Physik, Ruprecht-Karls-Universität Heidelberg, Heidelberg; [b]Physikalisches Institut, Ruprecht-Karls-Universität Heidelberg, Heidelberg; [c]ZITI Institut für technische Informatik, Ruprecht-Karls-Universität Heidelberg, Mannheim, Germany

[59] Faculty of Applied Information Science, Hiroshima Institute of Technology, Hiroshima, Japan

[60] Department of Physics, Indiana University, Bloomington IN, United States of America

[61] Institut für Astro- und Teilchenphysik, Leopold-Franzens-Universität, Innsbruck, Austria

[62] University of Iowa, Iowa City IA, United States of America

[63] Department of Physics and Astronomy, Iowa State University, Ames IA, United States of America

[64] Joint Institute for Nuclear Research, JINR Dubna, Dubna, Russia

[65] KEK, High Energy Accelerator Research Organization, Tsukuba, Japan

[66] Graduate School of Science, Kobe University, Kobe, Japan

[67] Faculty of Science, Kyoto University, Kyoto, Japan

[68] Kyoto University of Education, Kyoto, Japan

[69] Department of Physics, Kyushu University, Fukuoka, Japan

[70] Instituto de Física La Plata, Universidad Nacional de La Plata and CONICET, La Plata, Argentina

[71] Physics Department, Lancaster University, Lancaster, United Kingdom

[72] [a]INFN Sezione di Lecce; [b]Dipartimento di Matematica e Fisica, Università del Salento, Lecce, Italy

[73] Oliver Lodge Laboratory, University of Liverpool, Liverpool, United Kingdom

[74] Department of Physics, Jožef Stefan Institute and University of Ljubljana, Ljubljana, Slovenia

[75] School of Physics and Astronomy, Queen Mary University of London, London, United Kingdom

[76] Department of Physics, Royal Holloway University of London, Surrey, United Kingdom

[77] Department of Physics and Astronomy, University College London, London, United Kingdom

[78] Louisiana Tech University, Ruston LA, United States of America

[79] Laboratoire de Physique Nucléaire et de Hautes Energies, UPMC and Université Paris-Diderot and CNRS/IN2P3, Paris, France

[80] Fysiska institutionen, Lunds universitet, Lund, Sweden

[81] Departamento de Fisica Teorica C-15, Universidad Autonoma de Madrid, Madrid, Spain

[82] Institut für Physik, Universität Mainz, Mainz, Germany

[83] School of Physics and Astronomy, University of Manchester, Manchester, United Kingdom

[84] CPPM, Aix-Marseille Université and CNRS/IN2P3, Marseille, France

[85] Department of Physics, University of Massachusetts, Amherst MA, United States of America

[86] Department of Physics, McGill University, Montreal QC, Canada

[87] School of Physics, University of Melbourne, Victoria, Australia

[88] Department of Physics, The University of Michigan, Ann Arbor MI, United States of America

[89] Department of Physics and Astronomy, Michigan State University, East Lansing MI, United States of America

90 (a)INFN Sezione di Milano; (b)Dipartimento di Fisica, Università di Milano, Milano, Italy

91 B.I. Stepanov Institute of Physics, National Academy of Sciences of Belarus, Minsk, Republic of Belarus

92 National Scientific and Educational Centre for Particle and High Energy Physics, Minsk, Republic of Belarus

93 Department of Physics, Massachusetts Institute of Technology, Cambridge MA, United States of America

94 Group of Particle Physics, University of Montreal, Montreal QC, Canada

95 P.N. Lebedev Institute of Physics, Academy of Sciences, Moscow, Russia

96 Institute for Theoretical and Experimental Physics (ITEP), Moscow, Russia

97 Moscow Engineering and Physics Institute (MEPhI), Moscow, Russia

98 D.V.Skobeltsyn Institute of Nuclear Physics, M.V.Lomonosov Moscow State University, Moscow, Russia

99 Fakultät für Physik, Ludwig-Maximilians-Universität München, München, Germany

100 Max-Planck-Institut für Physik (Werner-Heisenberg-Institut), München, Germany

101 Nagasaki Institute of Applied Science, Nagasaki, Japan

102 Graduate School of Science and Kobayashi-Maskawa Institute, Nagoya University, Nagoya, Japan

103 (a)INFN Sezione di Napoli; (b)Dipartimento di Scienze Fisiche, Università di Napoli, Napoli, Italy

104 Department of Physics and Astronomy, University of New Mexico, Albuquerque NM, United States of America

105 Institute for Mathematics, Astrophysics and Particle Physics, Radboud University Nijmegen/Nikhef, Nijmegen, Netherlands

106 Nikhef National Institute for Subatomic Physics and University of Amsterdam, Amsterdam, Netherlands

107 Department of Physics, Northern Illinois University, DeKalb IL, United States of America

108 Budker Institute of Nuclear Physics, SB RAS, Novosibirsk, Russia

109 Department of Physics, New York University, New York NY, United States of America

110 Ohio State University, Columbus OH, United States of America

111 Faculty of Science, Okayama University, Okayama, Japan

112 Homer L. Dodge Department of Physics and Astronomy, University of Oklahoma, Norman OK, United States of America

113 Department of Physics, Oklahoma State University, Stillwater OK, United States of America

114 Palacký University, RCPTM, Olomouc, Czech Republic

115 Center for High Energy Physics, University of Oregon, Eugene OR, United States of America

116 LAL, Université Paris-Sud and CNRS/IN2P3, Orsay, France

117 Graduate School of Science, Osaka University, Osaka, Japan

118 Department of Physics, University of Oslo, Oslo, Norway

119 Department of Physics, Oxford University, Oxford, United Kingdom

120 (a)INFN Sezione di Pavia; (b)Dipartimento di Fisica, Università di Pavia, Pavia, Italy

121 Department of Physics, University of Pennsylvania, Philadelphia PA, United States of America

122 Petersburg Nuclear Physics Institute, Gatchina, Russia

123 (a)INFN Sezione di Pisa; (b)Dipartimento di Fisica E. Fermi, Università di Pisa, Pisa, Italy

124 Department of Physics and Astronomy, University of Pittsburgh, Pittsburgh PA, United States of America

125 (a)Laboratorio de Instrumentacao e Fisica Experimental de Particulas - LIP, Lisboa, Portugal; (b)Departamento de Fisica Teorica y del Cosmos and CAFPE, Universidad de Granada, Granada, Spain

126 Institute of Physics, Academy of Sciences of the Czech Republic, Praha, Czech Republic

127 Czech Technical University in Prague, Praha, Czech Republic

128 Faculty of Mathematics and Physics, Charles University in Prague, Praha, Czech Republic

129 State Research Center Institute for High Energy Physics, Protvino, Russia

130 Particle Physics Department, Rutherford Appleton Laboratory, Didcot, United Kingdom

131   Physics Department, University of Regina, Regina SK, Canada

132   Ritsumeikan University, Kusatsu, Shiga, Japan

133   [a]INFN Sezione di Roma I; [b]Dipartimento di Fisica, Università La Sapienza, Roma, Italy

134   [a]INFN Sezione di Roma Tor Vergata; [b]Dipartimento di Fisica, Università di Roma Tor Vergata, Roma, Italy

135   [a]INFN Sezione di Roma Tre; [b]Dipartimento di Matematica e Fisica, Università Roma Tre, Roma, Italy

136   [a]Faculté des Sciences Ain Chock, Réseau Universitaire de Physique des Hautes Energies - Université Hassan II, Casablanca; [b]Centre National de l'Energie des Sciences Techniques Nucleaires, Rabat; [c]Faculté des Sciences Semlalia, Université Cadi Ayyad, LPHEA-Marrakech; [d]Faculté des Sciences, Université Mohamed Premier and LPTPM, Oujda; [e]Faculté des sciences, Université Mohammed V-Agdal, Rabat, Morocco

137   DSM/IRFU (Institut de Recherches sur les Lois Fondamentales de l'Univers), CEA Saclay (Commissariat à l'Energie Atomique et aux Energies Alternatives), Gif-sur-Yvette, France

138   Santa Cruz Institute for Particle Physics, University of California Santa Cruz, Santa Cruz CA, United States of America

139   Department of Physics, University of Washington, Seattle WA, United States of America

140   Department of Physics and Astronomy, University of Sheffield, Sheffield, United Kingdom

141   Department of Physics, Shinshu University, Nagano, Japan

142   Fachbereich Physik, Universität Siegen, Siegen, Germany

143   Department of Physics, Simon Fraser University, Burnaby BC, Canada

144   SLAC National Accelerator Laboratory, Stanford CA, United States of America

145   [a]Faculty of Mathematics, Physics & Informatics, Comenius University, Bratislava; [b]Department of Subnuclear Physics, Institute of Experimental Physics of the Slovak Academy of Sciences, Kosice, Slovak Republic

146   [a]Department of Physics, University of Cape Town, Cape Town; [b]Department of Physics, University of Johannesburg, Johannesburg; [c]School of Physics, University of the Witwatersrand, Johannesburg, South Africa

147   [a]Department of Physics, Stockholm University; [b]The Oskar Klein Centre, Stockholm, Sweden

148   Physics Department, Royal Institute of Technology, Stockholm, Sweden

149   Departments of Physics & Astronomy and Chemistry, Stony Brook University, Stony Brook NY, United States of America

150   Department of Physics and Astronomy, University of Sussex, Brighton, United Kingdom

151   School of Physics, University of Sydney, Sydney, Australia

152   Institute of Physics, Academia Sinica, Taipei, Taiwan

153   Department of Physics, Technion: Israel Institute of Technology, Haifa, Israel

154   Raymond and Beverly Sackler School of Physics and Astronomy, Tel Aviv University, Tel Aviv, Israel

155   Department of Physics, Aristotle University of Thessaloniki, Thessaloniki, Greece

156   International Center for Elementary Particle Physics and Department of Physics, The University of Tokyo, Tokyo, Japan

157   Graduate School of Science and Technology, Tokyo Metropolitan University, Tokyo, Japan

158   Department of Physics, Tokyo Institute of Technology, Tokyo, Japan

159   Department of Physics, University of Toronto, Toronto ON, Canada

160   [a]TRIUMF, Vancouver BC; [b]Department of Physics and Astronomy, York University, Toronto ON, Canada

161   Faculty of Pure and Applied Sciences, University of Tsukuba, Tsukuba, Japan

162   Department of Physics and Astronomy, Tufts University, Medford MA, United States of America

163   Centro de Investigaciones, Universidad Antonio Narino, Bogota, Colombia

164   Department of Physics and Astronomy, University of California Irvine, Irvine CA, United States of America

165   [a]INFN Gruppo Collegato di Udine; [b]ICTP, Trieste; [c]Dipartimento di Chimica, Fisica e Ambiente, Università di Udine, Udine, Italy

166 Department of Physics, University of Illinois, Urbana IL, United States of America
167 Department of Physics and Astronomy, University of Uppsala, Uppsala, Sweden
168 Instituto de Física Corpuscular (IFIC) and Departamento de Física Atómica, Molecular y Nuclear and Departamento de Ingeniería Electrónica and Instituto de Microelectrónica de Barcelona (IMB-CNM), University of Valencia and CSIC, Valencia, Spain
169 Department of Physics, University of British Columbia, Vancouver BC, Canada
170 Department of Physics and Astronomy, University of Victoria, Victoria BC, Canada
171 Department of Physics, University of Warwick, Coventry, United Kingdom
172 Waseda University, Tokyo, Japan
173 Department of Particle Physics, The Weizmann Institute of Science, Rehovot, Israel
174 Department of Physics, University of Wisconsin, Madison WI, United States of America
175 Fakultät für Physik und Astronomie, Julius-Maximilians-Universität, Würzburg, Germany
176 Fachbereich C Physik, Bergische Universität Wuppertal, Wuppertal, Germany
177 Department of Physics, Yale University, New Haven CT, United States of America
178 Yerevan Physics Institute, Yerevan, Armenia
179 Centre de Calcul de l'Institut National de Physique Nucléaire et de Physique des Particules (IN2P3), Villeurbanne, France

a Also at Department of Physics, King's College London, London, United Kingdom
b Also at Laboratorio de Instrumentacao e Fisica Experimental de Particulas - LIP, Lisboa, Portugal
c Also at Faculdade de Ciencias and CFNUL, Universidade de Lisboa, Lisboa, Portugal
d Also at Particle Physics Department, Rutherford Appleton Laboratory, Didcot, United Kingdom
e Also at TRIUMF, Vancouver BC, Canada
f Also at Department of Physics, California State University, Fresno CA, United States of America
g Also at Novosibirsk State University, Novosibirsk, Russia
h Also at Department of Physics, University of Coimbra, Coimbra, Portugal
i Also at Università di Napoli Parthenope, Napoli, Italy
j Also at Institute of Particle Physics (IPP), Canada
k Also at Department of Physics, Middle East Technical University, Ankara, Turkey
l Also at Louisiana Tech University, Ruston LA, United States of America
m Also at Dep Fisica and CEFITEC of Faculdade de Ciencias e Tecnologia, Universidade Nova de Lisboa, Caparica, Portugal
n Also at Department of Physics and Astronomy, Michigan State University, East Lansing MI, United States of America
o Also at Department of Financial and Management Engineering, University of the Aegean, Chios, Greece
p Also at Department of Physics, University of Cape Town, Cape Town, South Africa
q Also at Institute of Physics, Azerbaijan Academy of Sciences, Baku, Azerbaijan
r Also at Institut für Experimentalphysik, Universität Hamburg, Hamburg, Germany
s Also at Manhattan College, New York NY, United States of America
t Also at CPPM, Aix-Marseille Université and CNRS/IN2P3, Marseille, France
u Also at School of Physics and Engineering, Sun Yat-sen University, Guanzhou, China
v Also at Academia Sinica Grid Computing, Institute of Physics, Academia Sinica, Taipei, Taiwan
w Also at Laboratoire de Physique Nucléaire et de Hautes Energies, UPMC and Université Paris-Diderot and CNRS/IN2P3, Paris, France
x Also at School of Physical Sciences, National Institute of Science Education and Research, Bhubaneswar, India
y Also at Dipartimento di Fisica, Università La Sapienza, Roma, Italy
z Also at DSM/IRFU (Institut de Recherches sur les Lois Fondamentales de l'Univers), CEA Saclay (Commissariat à l'Energie Atomique et aux Energies Alternatives), Gif-sur-Yvette, France
aa Also at Moscow Institute of Physics and Technology State University, Dolgoprudny, Russia
ab Also at section de Physique, Université de Genève, Geneva, Switzerland

[ac] Also at Departamento de Fisica, Universidade de Minho, Braga, Portugal
[ad] Also at Department of Physics, The University of Texas at Austin, Austin TX, United States of America
[ae] Also at Department of Physics and Astronomy, University of South Carolina, Columbia SC, United States of America
[af] Also at Institute for Particle and Nuclear Physics, Wigner Research Centre for Physics, Budapest, Hungary
[ag] Also at DESY, Hamburg and Zeuthen, Germany
[ah] Also at International School for Advanced Studies (SISSA), Trieste, Italy
[ai] Also at Faculty of Physics, M.V.Lomonosov Moscow State University, Moscow, Russia
[aj] Also at Nevis Laboratory, Columbia University, Irvington NY, United States of America
[ak] Also at Physics Department, Brookhaven National Laboratory, Upton NY, United States of America
[al] Also at Department of Physics, Oxford University, Oxford, United Kingdom
[am] Also at Discipline of Physics, University of KwaZulu-Natal, Durban, South Africa
[*] Deceased